

# COMPLEX CRUSTAL STRAIN APPROXIMATION

DIETER SCHNEIDER

September 1982



TECHNICAL REPORT  
NO. 91

## PREFACE

In order to make our extensive series of technical reports more readily available, we have scanned the old master copies and produced electronic versions in Portable Document Format. The quality of the images varies depending on the quality of the originals. The images have not been converted to searchable text.

THE COMPLEX STRAIN APPROXIMATION IN SPACE AND TIME  
APPLIED TO THE KINEMATICAL ANALYSIS OF RELATIVE  
HORIZONTAL CRUSTAL MOVEMENTS

by

Dieter Schneider

Dipl. Ing. , Federal Institute of Technology (ETH),

Zürich, 1977

A thesis submitted in partial fulfilment of the  
requirements for the degree of  
Doctor of Philosophy in Engineering  
in the Department  
of  
Surveying Engineering

This thesis is accepted

- - - - -

Dean of Graduate Studies

THE UNIVERSITY OF NEW BRUNSWICK

September, 1982

© Dieter Schneider, 1982

## ABSTRACT

The analysis of repeated geodetic observations has become an important tool for the investigation of the kinematics of tectonic plate boundary zones. The most appropriate analytical method for such investigations of contemporary crustal deformation is the strain analysis, a method of differential geometry.

In attempting to find an elegant mathematical formulation to describe plane strain, the use of complex analysis proves to be very advantageous. The analytical modeling of spatially and temporally continuous and discontinuous displacement fields is developed using least-squares approximation of generalized polynomials. Algebraic polynomials are proposed for the continuous approximation, whereas specifically designed step functions are used to model the discontinuities in space and time.

A mathematical model of simultaneous network adjustment and strain approximation is elaborated. It yields a general analytical method which enables strain-rates, or accumulated strain and fault-slip, to be determined from various types of geodetic measurements. In contrast to the widely used observation method (Frank's method), this approach does not rely on repeated observations of the same observables. Repeatedly observed networks of non-identical design can be analyzed. The constraints incorporated by the approximation model allow strain estimation even when the network of some observation epochs suffer from

formulation or configuration defects with respect to positions.

Experiments with various graphical representations of strain are carried out. Strain pedal-curves and shear-rosettes expressing extension and shear in a given direction, plotted at equally spaced grid points, provide a comprehensive display of non-homogeneous strain-fields in space. Confidence regions associated with extension and shear in a given direction are plotted together with these strain figures.

A software package 'CRUSTRAIN' is developed for the simultaneous adjustment and strain approximation and for the display of the estimated strain parameters. The method is first tested with synthetic data and then with a real kinematic network.

The method is applied to the 1970-80 Hollister network, which had been observed by the U.S. Geological Survey. This application reveals the strength as well as the limitations of the proposed technique. An approximation model is evaluated which incorporates third-degree complex algebraic polynomials with four block translation terms in space and fifth-degree algebraic polynomials with three episodic terms in time. This approximation estimates co-seismic fault-slip and strain release associated with three moderate earthquakes which occurred in the Hollister area within the time interval in question.

TABLE OF CONTENTS

Abstract.....i

List of Tables.....vii

List of Figures.....viii

Acknowledgements.....xi

SECTION 1: INTRODUCTION.....1

    1.1 Geodesy, Crustal Dynamics and Earthquake Research.....1

    1.2 Geophysical Background.....3

    1.3 Geodetic Techniques for Detecting Contemporary Horizontal  
        Crustal Movements.....12

    1.4 Recent Development of the Crustal Strain Analysis Technique....17

    1.5 Contribution of this Research.....20

SECTION 2: KINEMATIC NETWORKS.....23

    2.1 Definitions and Assumptions.....23

    2.2 Determinacy Problems.....25

        2.2.1 Formulation and Configuration Defects in Horizontal  
            Geodetic Networks.....25

        2.2.2 Determinacy Defects in Kinematic Networks.....29

    2.3 Kinematic Functional Models.....32

        2.3.1 Displacement Models.....32

        2.3.2 Constrained Models.....35

        2.3.3 Models using Differential Geometry.....37

    2.4 Stochastic Models.....37

SECTION 3: DEFORMATION OF A CONTINUUM.....39

    3.1 Deformation of Bodies.....39

        3.1.1 Deformation and Displacement Gradients.....39

        3.1.2 Progressive Deformation.....43

    3.2 Temporal Variation of Strain.....46

SECTION 4: TWO-DIMENSIONAL STRAIN ANALYSIS.....47

    4.1 Infinitesimal Strain Tensor-Field in Two Dimensions.....47

        4.1.1 Decomposition into Symmetrical and Anti-Symmetrical  
            Parts.....48

|   |   |     |
|---|---|-----|
| 4.1.2   | Decomposition into Conformal and Anti-Conformal Parts.... | 50  |
| 4.2   | Strain Components as Complex Variables.....               | 51  |
| 4.2.1   | Elements of Complex Analysis.....                         | 51  |
| 4.2.2   | Complex Strain Elements.....                              | 54  |
| 4.3   | Geometry of Two-Dimensional Strain.....                   | 55  |
| 4.3.1   | Strain and Affine Transformation.....                     | 55  |
| 4.3.2   | Non-homogeneous Strain Fields.....                        | 59  |
| 4.3.3   | Further Expressions for Incremental Strain.....           | 60  |
| SECTION 5: GRAPHICAL REPRESENTATION OF STRAIN-TENSOR FIELDS.....      |   | 64  |
| 5.1   | General Considerations.....                               | 64  |
| 5.2   | Principal Axes Diagram.....                               | 65  |
| 5.3   | Strain Ellipse and Strain Pedal Curve.....                | 66  |
| 5.4   | Shear Rosette.....  | 69  |
| 5.5   | Dilation Circle and Rotation Sector.....                  | 70  |
| 5.6   | Scalar Strain Quantities.....                             | 70  |
| 5.7   | Confidence Regions of Strain Quantities.....              | 71  |
| SECTION 6: LEAST-SQUARES APPROXIMATION.....                           |   | 78  |
| 6.1   | General Considerations.....                               | 78  |
| 6.2   | Complex Approximation Function.....                       | 80  |
| 6.2.1   | Approximation Function in Space.....                      | 81  |
| 6.2.2   | Modeling the Time Variation.....                          | 83  |
| 6.3   | Functions in Space.....                                   | 84  |
| 6.3.1   | Continuous Functions.....                                 | 84  |
| 6.3.2   | Modeling Discontinuities Along Known Faults.....          | 85  |
| 6.4   | Time Functions.....                                       | 88  |
| 6.4.1   | Linear and Piecewise Linear Time Functions.....           | 88  |
| 6.4.2   | Continuous Time Functions.....                            | 89  |
| 6.4.3   | Episodic Time Functions.....                              | 90  |
| SECTION 7: SIMULTANEOUS NETWORK ADJUSTMENT AND STRAIN APPROXIMATION.. |   | 91  |
| 7.1   | General Concept.....                                      | 91  |
| 7.2   | Network Adjustment of Individual Epochs.....              | 92  |
| 7.3   | Model for the Approximation.....                          | 93  |
| 7.4   | Combined Model.....                                       | 96  |
| 7.5   | Ortho-Normalization.....                                  | 99  |
| 7.6   | Statistical Testing.....                                  | 100 |
| 7.6.1   | Confidence Region of the Coefficient Vector.....          | 100 |
| 7.6.2   | Null Hypothesis.....                                      | 101 |
| 7.6.3   | Statistical Filtering Procedure.....                      | 102 |
| 7.6.4   | Test on the Quadratic Form $\lambda_0^T \lambda_0$ .....  | 103 |
| 7.7   | Back-Transformation into Original Solution Space.....     | 103 |

|  |  |     |
|--|--|-----|
| 7.8  | Additional Nuisance Parameters.....                        | 105 |
| 7.9  | Prediction in Space and Time.....                          | 105 |
| 7.9.1  | Relative Displacements and Strain.....                     | 105 |
| 7.9.2  | Statistical Estimates.....                                 | 106 |
| SECTION 8: TEST COMPUTATIONS.....                    |  | 107 |
| 8.1  | Concept of Numerical Testing and General Experience.....   | 107 |
| 8.2  | Test with Simulated Networks.....                          | 108 |
| 8.3  | Practical Test with a Quadrilateral in the Swiss Jura..... | 111 |
| 8.3.1  | Introduction to the Jura Tectonics.....                    | 111 |
| 8.3.2  | Precise Geodetic Observations.....                         | 113 |
| 8.3.3  | Crustal Strain Analysis of the Network 'LE PONT'.....      | 115 |
| 8.3.4  | Statistical Testing.....                                   | 119 |
| 8.3.5  | Interpretation.....  | 121 |
| 8.3.6  | Conclusions and Recommendations.....                       | 122 |
| SECTION 9: APPLICATION TO THE HOLLISTER NETWORK..... |  | 133 |
| 9.1  | Tectonics and Seismicity of the Hollister Area.....        | 133 |
| 9.1.1  | Junction of Two Active Strike-Slip Faults.....             | 133 |
| 9.1.2  | Local Seismicity.....                                      | 134 |
| 9.2  | Geodetic Data.....   | 139 |
| 9.2.1  | Precise EDM Observations.....                              | 139 |
| 9.2.2  | Station Elevations and Approximate Coordinates.....        | 141 |
| 9.2.3  | Reduced Observations.....                                  | 142 |
| 9.2.4  | Distribution of the Observations in Time.....              | 143 |
| 9.3  | Preceding Analyses.....                                    | 145 |
| 9.4  | Separate Network Adjustments.....                          | 147 |
| 9.5  | Simultaneous Adjustments and Approximations.....           | 152 |
| 9.5.1  | Assumptions.....   | 152 |
| 9.5.2  | Concept of Model Evaluation.....                           | 153 |
| 9.5.3  | Strain from Models Continuous in Space.....                | 156 |
| 9.5.4  | Relative Rigid Block Translation.....                      | 158 |
| 9.5.5  | Strain and Fault Slip from Combined Models.....            | 161 |
| 9.5.6  | Piecewise Linear Time Functions.....                       | 163 |
| 9.5.7  | Episodic Time Functions.....                               | 165 |
| 9.5.8  | Additional Experiments.....                                | 166 |
| 9.5.9  | Final Approximation Model.....                             | 168 |
| 9.6  | Interpretation.....  | 188 |
| SECTION 10: CONCLUSIONS AND RECOMMENDATIONS.....     |  | 192 |
| References.....                                      |  | 197 |



|               |  |     |
|---------------|--|-----|
| APPENDIX I:   | NOTATIONS USED FOR STRAIN PARAMETERS.....  | 204 |
| APPENDIX II:  | OUTLINE OF THE LEAST-SQUARES APPROXIMATION THEORY....  | 205 |
| APPENDIX III: | PROGRAM PACKAGE 'CRUSTRAIN'.....   | 212 |
|               | 1. General Concept.....  | 212 |
|               | 2. Program GEOPAN-C.....   | 214 |
|               | 3. Program CRUSTRAIN.....  | 215 |
|               | 4. Program STRAINPLOT.....   | 218 |
|               | 5. Program ISOLIN.....   | 219 |
| APPENDIX IV:  | A PROOF FOR THE DERIVATION OF THE NORMAL EQUATIONS<br>USING GENERALIZED MATRIX INVERSION TECHNIQUES..... | 221 |

Vita

## LIST OF TABLES

| TABLE |   | PAGE |
|-------|---|------|
| 8.1   | Tests with simulated kinematic networks . . . . .           | 110  |
| 8.2   | Statistical results of network adjustments . . . . .        | 116  |
| 8.3   | LE PONT: Predicted uniform tensor shear-rates . . . . .     | 124  |
| 8.4   | LE PONT: Statistical testing . . . . .                      | 125  |
| 8.5   | Legend to Figures 8.2 to 8.7 . . . . .                      | 126  |
| 9.1   | The largest seismic events in the Hollister area, 1970-80 . | 135  |
| 9.2   | Constraints for three-dimensional network adjustments . . . | 151  |
| 9.3   | Abbreviations used in the table of approximations . . . . . | 154  |
| 9.4   | Table of approximations . . . . .                           | 155  |
| 9.5   | Comparison of uniform strain-rates . . . . .                | 157  |
| 9.6   | Comparison of fault slip-rates . . . . .                    | 159  |
| 9.7   | Intervals of the piecewise linear time function . . . . .   | 163  |
| 9.8   | Co-seismic episodes . . . . .                               | 166  |
| A.1   | Specifications of Program GEOPAN-C . . . . .                | 215  |
| A.2   | Specifications of Program CRUSTRAIN . . . . .               | 217  |
| A.3   | Specifications of Program STRAINPLOT . . . . .              | 219  |
| A.4   | Specifications of Program ISOLIN . . . . .                  | 220  |

LIST OF FIGURES

| FIGURE   | PAGE |
|--|------|
| 1.1 Interactions between tectonic plates . . . . .   | 6    |
| 1.2 Tectonic faults . . . . .  | 7    |
| 1.3 Reid's Elastic Rebound Model . . . . .   | 10   |
| 3.1 Deformation of a body . . . . .  | 41   |
| 4.1 General affine transformation decomposed into a sequence of<br>rotations and stretches . . . . . | 56   |
| 5.1 Neighborhood transformation of a unit circle . . . . .   | 68   |
| 5.2 Principal axes of strain . . . . .   | 72   |
| 5.3 Axes of maximum shear . . . . .  | 73   |
| 5.4 Strain ellipses and principal axes of strain . . . . .   | 74   |
| 5.5 Dilation circles and rotation sectors . . . . .  | 75   |
| 5.6 Strain pedal-curves and principal axes of strain . . . . .                                       | 76   |
| 5.7 Shear-rosettes, axes of maximum shear and principal axes<br>of strain . . . . .                  | 77   |
| 6.1 Model for block translations using complex masking functions                                     | 87   |
| 8.1 Section of tectonic map of Switzerland . . . . .   | 112  |
| 8.2 LE PONT: uniform tensor shear-rate 1973-74 . . . . .   | 127  |
| 8.3 LE PONT: uniform tensor shear-rate 1973-78 . . . . .   | 128  |
| 8.4 LE PONT: uniform tensor shear-rate 1974-78 . . . . .   | 129  |
| 8.5 LE PONT: uniform tensor shear-rate 1973-78 . . . . .   | 130  |
| 8.6 LE PONT: uniform tensor shear-rate 1973-78 . . . . .   | 131  |
| 8.7 LE PONT: velocity of rigid block translation 1973-78 . . . . .                                   | 132  |
| 9.1 Fault locations and actual seismicity (1969-70) in the<br>Hollister area . . . . .               | 136  |

| FIGURE  | PAGE |
|---|------|
| 9.2 Detailed map of the junction of two faults near Hollister .                                     | 137  |
| 9.3 Kinematic network Hollister 1970-80 . . . . .   | 138  |
| 9.4 Histogram displaying the distribution of observations in<br>time . . . . .                      | 144  |
| 9.5 Network configuration of observation epoch No. 26<br>(1979.335-376) . . . . .                   | 149  |
| 9.6 Average spatially uniform tensor shear-rate (Mod. No.2) . .                                     | 170  |
| 9.7 Velocity of average rigid block translation (Mod. No. 21) .                                     | 171  |
| 9.8 Velocity of average block translation and over-all tensor<br>shear-rate (Mod. No. 31) . . . . . | 172  |
| 9.9 Calaveras fault-slip as estimated from the piecewise linear<br>model No. 82 . . . . .           | 173  |
| 9.10 San Andreas fault-slip as estimated from the piecewise<br>linear model No. 82 . . . . .        | 174  |
| 9.11 Tensor shear-rate component in the direction normal to the<br>San Andreas fault . . . . .      | 175  |
| 9.12 Calaveras fault-slip and its standard deviation (Mod. No.91)                                   | 176  |
| 9.13 San Andreas fault-slip and its standard deviation<br>(Mod. No.91) . . . . .                    | 177  |
| 9.14 Fault slip-rates and tensor shear-rates (Mod. No.91,<br>t=1972.0) . . . . .                    | 178  |
| 9.15 Co-seismic fault-slip and tensor shear (Mod. No.91,<br>t=1972.76) . . . . .                    | 179  |
| 9.16 Fault slip-rates and tensor shear-rates (Mod. No.91,<br>t=1974.0) . . . . .                    | 180  |
| 9.17 Co-seismic fault-slip and tensor shear (Mod. No.91,<br>t=1974.91) . . . . .                    | 181  |
| 9.18 Fault slip-rates and tensor shear-rates (Mod. No.91,<br>t=1975.0) . . . . .                    | 182  |
| 9.19 Fault slip-rates and tensor shear-rates (Mod. No.91,<br>t=1977.0) . . . . .                    | 183  |

| FIGURE  | PAGE |
|---|------|
| 9.20 Fault slip-rates and tensor shear-rates (Mod. No.91,<br>t=1979.0) . . . . .  | 184  |
| 9.21 Co-seismic fault-slip and tensor shear (Mod No.91,<br>t=1979.60) . . . . .   | 185  |
| 9.22 Fault slip-rates and tensor shear-rates (Mod. No.91,<br>t=1980.0) . . . . .  | 186  |
| 9.23 Rosettes showing the tensor shear-rate and its standard<br>deviation in a given direction (Mod. No.91, t=1970.0) . . . | 187  |
| A.1 Program Package 'CRUSTRAIN': Data Flow Diagram . . . . .  | 213  |

## ACKNOWLEDGMENTS

A substantial part of this research was carried out at the Institute of Geodesy and Photogrammetry of the Swiss Federal Institute of Technology (ETHZ) in Zürich. Prof. H.-G. Kahle of the above mentioned institute not only showed a keen interest in this study, but also made a part-time research assistantship available. I extend my gratitude to the Swiss Federal Office of Topography and the Swiss Federal Administration for granting an educational leave. Their generous offer of almost unlimited computer time on their computer facilities permitted me to complete this work.

I am sincerely thankful to Dr. Petr Vaníček, my research supervisor and teacher, for his supportive guidance, his constant encouragement and never-ending patience which were of great help even over the distance of several thousand kilometres. I profitted greatly from many of his ideas which he had developed in attempting to model vertical crustal velocities, and from his sound experience in the field of numerical analysis.

Dr. Savage's help (U.S. Geological Survey) in providing all the required data of the Hollister network and in critically discussing our preliminary results is greatly acknowledged. I also benefitted from the earlier investigations, done by Dr. N. Pavoni from the Institute of Geophysics of the ETH Zürich, on the geological structure and seismotectonics of the Hollister area. Computer software was provided by the following authors: Dr. E. Klingelé (ETH-Zürich), Dr. R.R. Steeves and

K. Thapa (both previously at UNB).

I owe special thanks to Thomas Wray of the Surveys and Mapping Branch (E.M.R.) in Ottawa, who during a long night's discussion convinced me of the elegance of the complex formulation of plane strain. I would like to extend my appreciation to my colleagues of the Department of Surveying Engineering at UNB, at the ETH in Zürich and, last but not least, at the Federal Office of Topography in Wabern for their stimulating discussions and constant support.

This work is dedicated to my wife, Claudia, to whom I am greatly indebted for her patience and invaluable encouragement.

## SECTION 1

## INTRODUCTION

1.1 Geodesy, Crustal Dynamics and Earthquake Research

The determination of the earth's shape and its gravity field were the main aims of geodesy for many centuries. With only few exceptions, the theory and methods applied were based on the model of a rigid earth body. At the time when geodetic networks were established all over the continents, the positions of the monumented network stations, once determined, were regarded as time invariant for decades or centuries.

Only twenty years ago the introduction of new terrestrial, as well as extra-terrestrial geodetic observation techniques, increased the ease and the accuracy of geodetic positioning (Vaníček and Krakiwsky, 1982). In the same decade, the revolutionary hypothesis of plate tectonics finally gained universal acceptance (Kahle, 1980). The rate of relative tectonic movement estimated from geological evidence is so large at some places that its determination with modern geodetic means seems feasible. Today, there is no doubt that the old assumptions of a rigid earth's crust are no longer acceptable in light of the new dynamic concept of plate tectonics.

Geodesy of the modern era is characterized by a systematic treatment of all dynamic phenomena that change the shape and the gravity field of



the earth and, consequently, influence the positions of points on it. Reductions which account for the different temporal variations have to be considered in geodetic positioning. Information that geodesy can offer on the earth's temporal deformation is also most welcome in contemporary geodynamics research.

Earthquakes are among the most destructive of all natural catastrophes. They are feared in seismic active areas because they occur suddenly and often without warning. Until recently, one would not have considered earthquake prediction a serious scientific topic. In the 1960's, prediction oriented earthquake research programs were started in countries with high seismic activity, such as Japan and the U.S. (Rikitake,1976; Kisslinger et al.,1978).

Geodesy plays an important role in this interdisciplinary research as it provides the geometrical information on the temporal deformation of the earth's crust. Repeated surveys of horizontal and vertical geodetic networks and of special monitoring configurations are carried out in order to detect deformations of the crust associated with seismic events. Recently developed geodetic space techniques will increasingly be used in this decade for the investigation of tectonic motions and crustal deformations (Committee on Geodesy,1978). The symbiotic relation with modern geophysics and its challenging problems is one of the main reasons for the recent impulse in geodetic science.

As geodesists are concerned with the treatment of observations of geometrical quantities in three-dimensional space, the kinematical

analysis of repeatedly observed networks is clearly one of their domains.

## 1.2 Geophysical Background

The following introduction to plate tectonics, seismology and earthquake processes provides a brief review of terms and definitions relevant to the geodetic crustal movement analysis.

The origin of the theory of global plate tectonics goes back to 1910, when the geophysicist Alfred Wegener noticed the astonishing congruency of the Atlantic coasts of America and Africa (Wegener, 1929) on a world map. It took almost 50 years from the time when he first published his ideas on the 'Continental Drift' until the plate tectonics hypothesis found universal acceptance by earth scientists. The modern model of global plate tectonics convincingly explains various geological and geophysical phenomena. According to this hypothesis, the earth's crust and uppermost mantle form the lithosphere, the solid upper layer of the earth of variable thickness (25 to 90 km for the oceanic and 50 to 150 km for the continental lithosphere). The lithosphere is divided into 6 main plates: the American, Eurasian, Indo-Australian, African, Pacific and Antarctic plates. The limits of the global lithospheric plates are defined by narrow zones of high seismic activity.

Extensive geomagnetic investigations of the phenomenon of sea floor spreading revealed the motion of the tectonic plates through geological history. Magmatic material from the mantle rises and accretes onto the

plates. Symmetrical patterns of magnetic anomalies on the sea floor centered about the mid-oceanic ridges have been explored in all major oceans. The plates spread in opposite directions along the worldwide mid-ocean ridge system (extrusion zones). Beneath continents or island arcs, the oceanic plates are thrust under the continental plates, the descending slab moving down into the mantle to be melted and recycled (subduction zones).

The combination of mechanisms which drive the plates, and the way the plates respond to these forces, are not perfectly understood at present. Current hypothesis involve three possible mechanisms :

- 1) coupling of the plates to convective flow in the mantle,
- 2) negative buoyancy of subducted slabs,
- 3) gravitational sliding down from the slopes of the oceanic ridges.

Modern plate tectonics distinguishes four principal modes of interaction between lithospheric plates (Lomnitz, 1975) :

a) Subduction boundaries:

Where an oceanic plate converges with a continental plate, the oceanic plate is thrust under the continental plate (cf. Figure 1.1a). Typical subduction boundaries can be found along the Pacific island arcs. The trace of the boundary is located offshore in a deep trench filled with sediments. The subduction process is associated with intermediate and deep-focus earthquakes. Their foci are located on the surface or in the thrusting slab (Benioff zones).

b) Transcurrent, or Strike-Slip, Plate Boundaries:

Transcursion occurs either between two oceanic plates, or between an oceanic plate and a continent. The plates slide horizontally in opposite directions, neither creating nor destroying crustal material. Horizontal shear across the strike-slip faults (cf. Figure 1.1b) characterizes these zones.

c) Extrusion Zones or Spreading Centers

Along the mid-ocean ridges, two thin lithospheric plates grow apart as mantle material is added to create new crust (cf. Figure 1.1c). The spreading rates are estimated to vary between 2 - 5 cm/yr.

d) Accretion Zones and Zones of Orogenic Collisions

Accretion is defined as a slow collision between an oceanic plate and a continental plate, the latter growing at the expense of the former (cf. Figure 1.1d). Where two continental plates are being pushed together, an upheaval of crustal material resulting in mountain building takes place (orogenic collision).

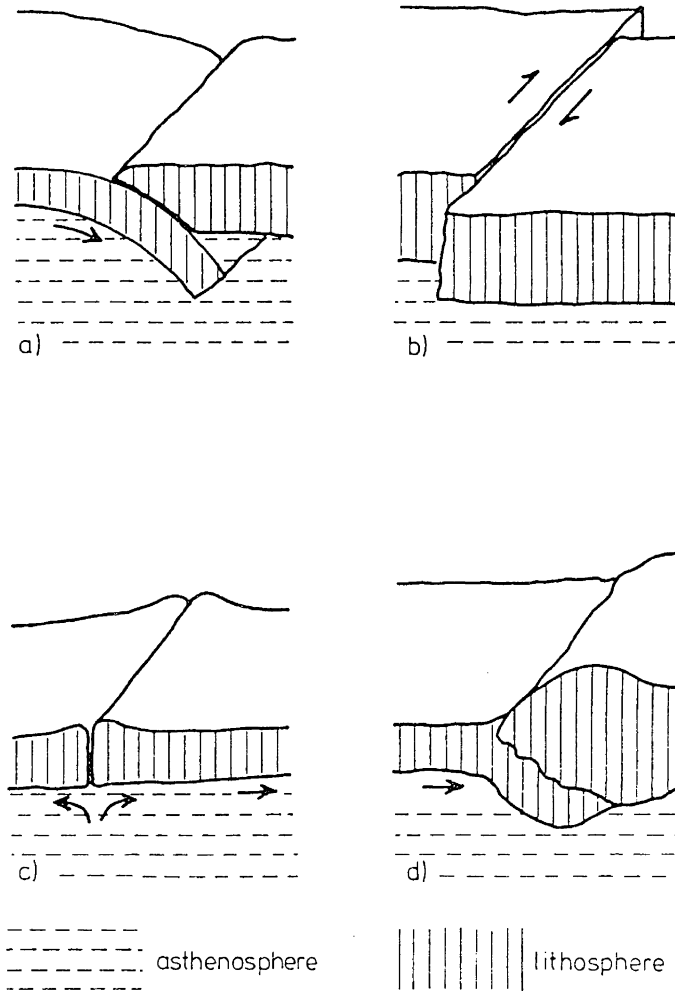


Figure 1.1

Interaction between tectonic plates

a) subduction boundary, b) strike-slip boundary, c) extrusion zone, d) accretion zone

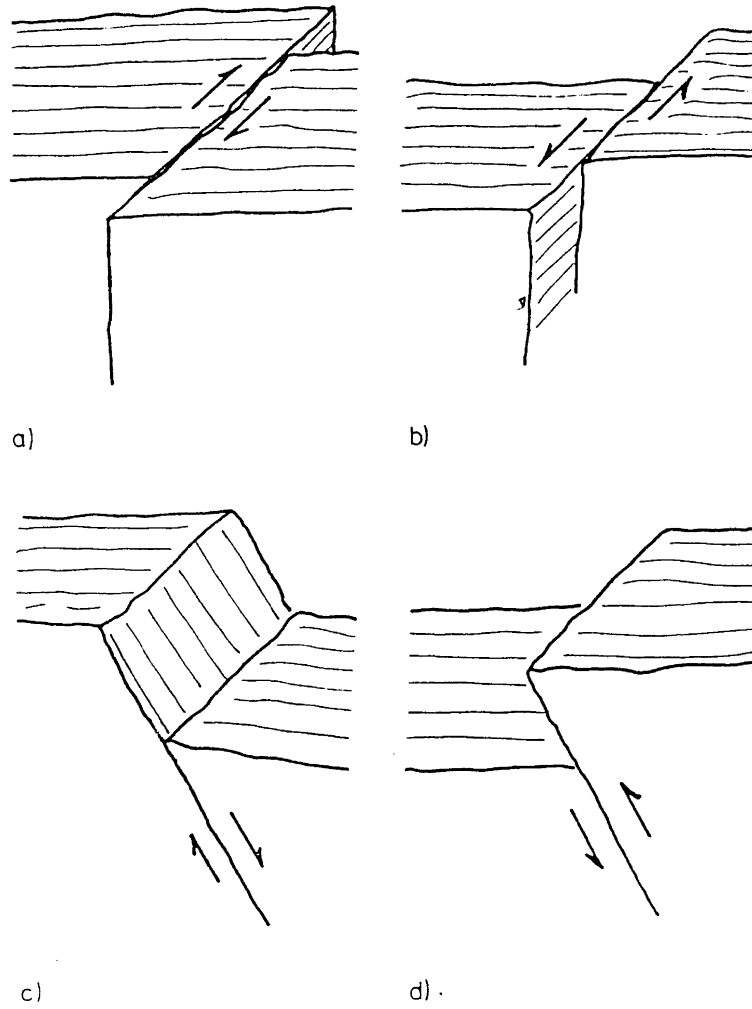


Figure 1.2

Tectonic faults

a) right-lateral, b) left-lateral strike-slip faults; c) normal, d) reverse dip-slip faults

All plate boundaries are marked by different kinds of faults and trenches. The strike-slip, or transcurrent, faults (cf. Figure 1.2 ) are designated as right or left lateral (dextral or sinistral), depending on their sense of relative displacement. If the relative displacement of a fault is perpendicular to the line formed by the intersection of the fault plane with the horizontal surface, the fault is called a dip-slip fault (cf. Figure 1.2c and d). Combinations of dip-slip and strike-slip faulting also occur.

The occurrence of most earthquakes is a result of the interaction of plates at their boundaries. 98 percent of the energy released in shallow earthquakes is released in the areas of tectonic plate boundaries (Lomnitz,1975).

Seismic events can be defined in terms of three different aspects:

- mechanical rupture in the lithosphere,
- energy released from the earth's interior,
- radiation of elastic waves.

When a seismic event takes place in the earth's crust, two kinds of waves propagate through the body of the earth: P-waves (dilatational waves) and S-waves (shear waves). Two other kinds of waves travel along the earth's surface: Rayleigh-waves and Love-waves (Jeffrey,1970).

Seismic events are described by their position, depth, time and energy

released. Instead of energy measures, measures of earthquake size are also used. Richter's magnitude  $M$  is the most common measure.  $M$  is a logarithmic function of the observed maximum amplitude on a standard type of seismograph corrected for the distance.

The focus, or hypocenter, is the point within the earth where the movement is initiated, whereas the epicenter is the vertical projection of the focus on the earth's surface. Earthquakes are classified as shallow, intermediate or deep, depending on their focal depths.

| Type:        | Depth:       |
|--------------|--------------|
| shallow      | 0 - 60 km    |
| intermediate | 60 - 150 km  |
| deep         | 150 - 700 km |

The seismic process in the earth's crust can be summarized as follows:

- 1) A non-hydrostatic stress field is being generated in a finite region of the crust around the fault. Elastic energy is being accumulated.
- 2) A rupture occurs along the fault and a part of the accumulated energy is suddenly released by radiation of seismic waves. Another part of the energy is transformed into heat and potential energy.
- 3) The medium tends to reach a state of equilibrium by means of aftershocks and fault-creep.



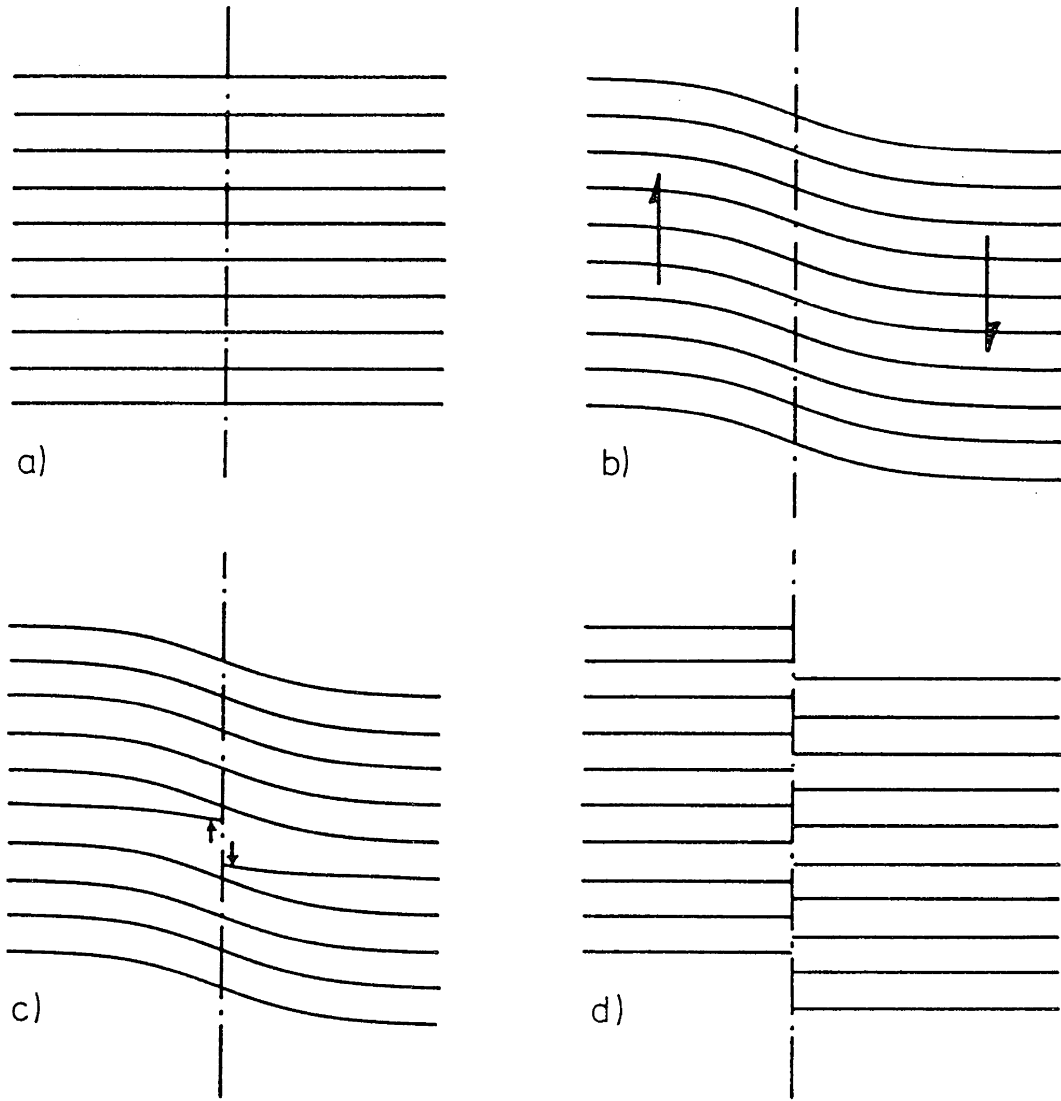


Figure 1.3

Reid's Elastic Rebound Model

Reid analyzed the relative horizontal crustal movements along the San Andreas Fault associated with the 1906 San Francisco earthquake (Benioff, 1964). In order to interpret the data from repeatedly observed geodetic networks, he set up the elastic rebound model, a theoretical model for the strike-slip faulting process.

According to his theory, the blocks on either side of the fault begin to move laterally, relative to each other, some time after an earthquake. Because of the friction at the fault surfaces, the blocks are locked together and become strained. (cf. Figure 1.2b).

As the movement continues and strain is accumulated, there comes a time when at some point the stress exceeds the restraints. At that point, the surface suddenly slips or rebounds (cf. Figure 1.2c). The slip increases the stress at adjacent points where the surface slips as well, with the result that the slip is propagated along the fault. The sudden movement of the rocks in opposite directions on both sides of the fault generates seismic waves. During the earthquake most of the stress is released and the accumulation of strain starts again (cf. Figure 1.2d).

The source mechanism can be investigated from the observed relative displacements at the fault trace and from the seismic waves recorded from local and remote seismographs. The co-seismic slip displacements observed vary from a few centimeters in small earthquakes to more than 10 m in large ones. The duration of the slip is estimated to be a fraction of a second up to 10 seconds.

An insight into the source mechanism of earthquakes can be found by determining the direction of initial wave motion from the seismograms at different stations. The result of this seismo-tectonic analysis is the so called fault plane solution which provides the orientation of the fault plane at the focus in space.

### 1.3 Geodetic Techniques for Detecting Contemporary Horizontal Crustal Movements

In investigating the deformation of a section of the crust within a certain interval of time, the ideal data should be of an areal nature and continuous in space and time. Unfortunately, geodetic methods do not provide such data. Only a finite number of points suitable for network stations can usually be found on a solid crustal formation. The observations between these points are repeated a limited number of times. Typical geodetic observables are therefore discrete functions in space as well as in time. Provided that a sufficient number of appropriately distributed discrete data is available, continuous information in space and time may, however, be estimated by computing best approximations of continuous models on the given discretizations. This method will be extensively used in the present work.

Local relative movements of the earth's crust have to be regarded in a three-dimensional Cartesian coordinate system. Purely horizontal or purely vertical movements do not exist in reality. Despite this fact, it has been common practice to investigate the horizontal and vertical components of the relative displacements separately.

There is little that distinguishes the two components of movement other than their directions. The horizontal components are, in general, expected to be much larger than the vertical ones. In addition, there is theoretically a difference as far as the driving forces are concerned. If crustal masses are displaced vertically, gravitational potential energy is accumulated or released. The gravitational forces, however, are not relevant (except for second order effects) for the horizontal components of the motion.

The main reason for the separate treatment of the two components is the separately available horizontal and vertical observation data. It is a traditional geodetic practice to observe horizontal and vertical networks separately, as they require different kinds of field observations (triangulation or levelling).

In mountainous regions the situation is different, levelling being often replaced by trigonometric height difference determination. Three-dimensional networks (Schneider, 1979) may be a preferable alternative in this case. Three-dimensional networks are also the most natural configurations if extra-terrestrial geodetic observations are to be used for crustal movement analyses in the future. If three-dimensional configurations are observed, in which the horizontal and the vertical components of the displacement vectors are determined with approximately the same accuracy, the analysis of relative movements in three-dimensional space is clearly preferable.

As three-dimensional data are not available to date, the conventional,

separate treatment is adopted in this work. Horizontal components of relative crustal movements will then be the only concern in this study.

Geometrical configurations in which geodetic observations are repeatedly being collected, will be called kinematic networks in this study. A more comprehensive definition of this term will be provided in Section 3.

The following three types of horizontal kinematic networks can be distinguished:

a) Resurveyed Horizontal Geodetic Networks:

These networks are established for horizontal position control, thus being of regional character and covering large areas. Their advantage is that their observation epochs stretch back for decades or even for more than a century. These networks, however, are not designed for the investigation of crustal movements, and it is thus uncertain if the kinematical questions can be answered through their analysis. The network design at the observation epochs may differ considerably: Pure triangulation networks from the beginning of this century may be resurveyed using modern EDM-techniques. Possible effects of incompleteness in the mathematical model of the network adjustment have to be considered carefully in this case, as they may cause network distortions which could be misinterpreted. Resurveyed horizontal geodetic networks are the largest source of data presently available for crustal kinematics investigations.

b) Horizontal Monitoring Configurations:

In regions of special interest, where horizontal movements are suspected, local horizontal networks or simple configurations, such as quadrilaterals or base lines, are established. These networks are optimally designed for crustal kinematics investigations. Monitoring configurations are frequently resurveyed using accurate observation techniques. The operations of the observation campaigns usually follow standard observation programs. In this way, the most straight-forward case of an invariant network design for the epochs of reobservation is obtained.

c) Repeated Relative Positioning:

High relative position accuracies over distances of a few kilometres can be achieved with classical terrestrial geodetic methods. If geodetic networks are designed over distances of hundreds or thousands of kilometres as would be required in geodynamic projects (e.g. for measurements of mean relative interplate motions), the accumulated relative position errors exceed the expected relative displacements. Besides this, the cost of resurveying extended high accuracy networks is prohibitive.

Repeated point positioning by means of space geodesy techniques is the best suited approach to detect relative motions of widely separated points of the earth's surface. Present VLBI-techniques allow the precise determination of three-dimensional position differences between points on different tectonic plates (NASA, 1979). Accuracies of a few

centimetres can be achieved over long distances of intercontinental scale.

Unfortunately, the accuracy of the point positioning technique for regional or local investigations is at present not high enough. However, various space techniques are under development and are expected to be operational within this decade.

As point positioning data will not be used in this study, we will conclude this discussion on point positioning techniques by just mentioning the most promising space techniques under development:

- Observatory VLBI:

These systems are suitable for the detection of mean relative velocities of global tectonic plates. The current precision of VLBI systems for the measurement of three-dimensional position differences is 3 to 6 cm. It is planned to upgrade the VLBI technique by using water vapor radiometers to achieve precisions of 1 to 3 cm (NASA,1981).

- Mobile Station VLBI:

A mobile astronomical VLBI unit specifically designed for field operations is being developed (NASA,1981). Measurement precision of 5 cm are expected from the ARIES project by using an observatory antenna as a base station (CSTG,1980).

- Mobile Laser Ranging to Satellites:

The systems are designed for regional crustal kinematics

investigations. The following ranging accuracies are claimed for the different systems: NASA-Stalpas: 1-2 cm ; Mobals: 3-5 cm ; TLRS: 1-2 cm (NASA,1981).

- Satellite Emission Systems:

Satellites of the NAVSTAR Global Positioning System (GPS) will be used for range difference determinations by simultaneous satellite microwave measurements for regional crustal kinematics investigations. Prototypes of receivers under development are either based on the interferometric mode of operation, or on the reconstruction of the GPS carrier phase (NASA,1981). Relative position accuracies of 2 cm over a distance of 100 - 200 km are expected from the SERIES project of the Jet Propulsion Laboratory (CSTG,1980).

1.4 Recent Development of the Crustal Strain Analysis Technique

Earliest reports on the analysis of crustal strain from repeated geodetic observations were published in the Bulletin of the Institute for Earthquake Research of the University of Tokyo at least 50 years ago. Pope (1966) compiled the history of the method and outlined the traditional computational techniques.

Japanese seismologists, Terada and Miyabe (1929) and Tsuboi (1930), developed computational and graphical methods of strain determination based on the coordinate approach. According to Terada's and Miyabe's method, separate network adjustments by variation of coordinates are



performed. The strain in each triangle is then assumed to be homogeneous, or uniform in space. Displacement gradients, and subsequently strain components, are computed from the displacement differences at the three points of each triangle of the network. The derived strain components are then associated with the centroid of each triangle.

Kasahara and Sugimura (1964) made an attempt to get a smoother approximation to the relative displacement field than the fit of piece-wise linear functions. Two second-degree algebraic polynomials of two variables are fitted to the discrete fields representing both horizontal displacement components. Whitten (1968) suggested a time varying model from which components of strain could be computed over the entire area for each location and instant of time.

Frank (1966) formulated the observation method. Differences of 'raw' observations, rather than adjusted values, are used to compute the strain without first having to evaluate station coordinates and displacements. The preference for 'raw' observation data is a sign of the apparent distrust in the geodetic least-squares model which is wide-spread among geophysicists. A large number of successful applications of this method by the investigation of horizontal crustal movements in California are reported by researchers of the USGS: Savage and Burford (1970), Savage and Prescott (1976), Thatcher (1979), Savage et al. (1979), King et al. (1980) and Prescott et al. (1981).

Applications of the coordinate method are reported by geodesists of the

USNGS. Pope (1969) analyzed relative co-seismic movements associated with the 1964 Alaska earthquake. An interesting comparison of results from coordinate and observation (using 'raw' observations) approaches is given by Miller et al. (1969) of their investigations in the Taft - Mojave area in California. The results from the observation method with 'raw' data show higher and more random shear, but do not differ significantly from the results of the coordinate method.

Brunner (1979, I) uses the 'inner coordinate' approach to derive unique displacement vectors for the least-squares estimation of the homogeneous strain components. As any method based on the coordinate approach, this method allows the analysis of networks with different designs in both epochs. The method is only developed for the two-epoch case and for the approximation of strain uniform in space. A theoretical comparison of the observation method with the (inner) coordinate method reveals that under certain conditions (invariant design) both methods yield identical results (Brunner, 1979, II; Brunner, 1980).

Margrave and Nyland (1980) utilize two-dimensional polynomials of low order to model the displacement field. It is assumed that the state of strain over the network can be represented as a spatially continuous tensor field. Observation equations relating the observation differences to the unknown polynomial coefficients are solved directly by generalized matrix inversion techniques. This method is only developed for the two-epoch case with invariant design.

Snay and Cline (1980) describe a method of simultaneous adjustment of station coordinates and velocities from multiple repeated surveys with non-identical network design. By introducing an arbitrary set of minimal-constraints, strain-rates uniform in space and constant in time are derived. A very similar method of simultaneous reduction of multiple surveys is proposed by Bibby (1982). He shows that any incorporation of appropriate minimal-constraints yields the same solution for the strain coefficients. These coefficients can be estimated free of bias. He concludes that the use of 'inner coordinate' solutions (station coordinates) for the analysis of strain from repeated surveys is not justified.

Dermanis (1981) investigated the geodetic estimability of crustal deformation parameters as computed by the coordinate method. A finite element strain analysis technique, with which the area of investigation is dissected into finite elements, is proposed and practically tested by Welsch (1982). Chrzanowski et al. (1982,I and II) present a general approach to the deformation analysis, using polynomial fitting and strain estimation based on the coordinate method.

#### 1.5 Contribution of this Research

Among the developed ideas concerning the mathematical modeling of displacement fields and strain fields and their interpretation, the following findings are considered to be contributions to the present state of crustal strain research:

- 1) Complex analysis is applied to the theory of plane strain. This mathematical formulation considerably simplifies the analytical treatment.
- 2) A comprehensive geometrical interpretation of the components of strain is found by relating the components of strain to the general affine transformation.
- 3) A compact complex approximation function is proposed for the approximation of displacement fields continuous in space. Strain can easily be derived from this function. An extension of this function which takes into account temporal variations is provided for the approximation of deformations in space and time.
- 4) Solutions are found for the problem of modeling the discontinuities of the displacement field in space and time.
- 5) A new method of simultaneous network adjustment and strain approximation is developed. It estimates the most significant trend of the deformation and simultaneously filters out the noise from the observations.
- 6) Various possibilities for graphically displaying the estimated strain quantities and their confidence regions are tested and compared.
- 7) A software package 'CRUSTRAIN' is developed containing computer programs for the simultaneous network adjustment and strain approximation and the graphical display of the estimated strain quantities and their confidence regions.

- 8) The pre-analysis of kinematic network projects is advocated and practically tested. This is considered a useful tool for optimal design studies of kinematic networks.

## SECTION 2

## KINEMATIC NETWORKS

2.1 Definitions and Assumptions

The presently available geodetic techniques for detecting relative horizontal crustal movements were described in 1.2 from a general point of view. In this section, the kinematic aspects of horizontal geodetic networks will be treated in a more systematic manner. The techniques of repeated geodetic observations can be used for various purposes. This work will be limited to the tectonic crustal movement analysis, although some considerations in this section may also be valid for kinematic networks in engineering surveying.

Let us first look at the object of our investigation, the uppermost layer of the earth's crust. No assumptions are made at this point as to the physical properties (rheology) of this continuum. It is only assumed that there is repeated access to a set of well defined material points of the continuum. Each point is represented by one monument, or better by a whole group of monuments, which defines the points (stations) of a network configuration in a three-dimensional Euclidean space. Monumentation will not be discussed in this work, although it should be emphasized that monumentation is one of the practical problems in kinematic networks which is to be considered with great care. For the present case, it is assumed that each station of the network coincides at any instant of time with the same material point

of the crust.

The traditional geodetic concept of a separate treatment of horizontal and vertical networks (cf. 1.3) is adopted. The horizontal network is to be understood as a two-dimensional mapping of the original configuration in space. The following types of geodetic observations will be considered: angles or directions, distances, azimuths and relative positions — all being observed at a well defined (measured) instant of time.

A configuration which is compatible with the assumptions above and in which such geodetic observations have repeatedly been collected will be called a kinematic network. No difference will be made between the different types of kinematic networks, such as repeated relative positioning networks, resurveyed geodetic networks or monitoring configurations. The distribution of the observations in space and time and their stochastic model define the accuracy with which the parameters of the deformation can be determined.

It is further assumed that all observations collected in three-dimensional physical space have been properly reduced to a conformal mapping plane. Euclidean plane geometry can thus be applied to formulate the functional model of the network adjustments.

As a consequence of the time dependence of the observations, the kinematic network is not only defined by its geometry in space, but also by the distribution of the observations in the time domain. It is

common geodetic practice to carry out surveys during relatively short observation campaigns. Groups of observations collected at the same time, or within a short span of time, are called simultaneous or near-simultaneous. In seismically active areas, the question of simultaneity has to be considered with care, as the relative movements may be relatively fast and non-linear in time.

## 2.2 Determinacy Problems

### 2.2.1 Formulation and Configuration Defects in Horizontal Geodetic Networks

Let us consider a local, horizontal geodetic network with  $n_p$  stations in which  $n$  geodetic observations  $\underline{l}$  with regular covariance matrix  $\underline{C}_l$  have been collected. After linearization and elimination of the orientation unknowns from the observation equations, the well-known linear model for the network adjustment on the mapping plane (by the variation of coordinates) reads

$$\underline{v} = \underline{A} \underline{d} - \underline{l} \quad (2.1)$$

where:  $\underline{A}$  ... design matrix

$\underline{d} = \underline{x} - \underline{x}_0$  ...  $u$  - dimensional parameter vector

$\underline{x}, \underline{x}_0$  ... vector of unknown and approximate coordinates

$\underline{v}$  ... residual vector

which, by applying the least-squares principle, yields the system of normal equations



$$\underline{N} \hat{\underline{d}} - \underline{u} = \underline{0} \quad (2.2)$$

where  $\underline{N} = \underline{A}^T \underline{C}_1^{-1} \underline{A}$

and  $\underline{u} = \underline{A}^T \underline{C}_1^{-1} \underline{1}$ .

Up to this point, no constraint among the coordinates has been incorporated. The matrix of the normal equations  $\underline{N}$  is thus singular

$$\det(\underline{N}) = 0 \quad (2.3)$$

with a rank defect

$$\begin{aligned} \text{def}(\underline{N}) &= \text{def}(\underline{A}) \\ &= u - \text{rank}(\underline{A}) \quad ; u = \text{dim}(\text{row}(\underline{A})) \end{aligned} \quad (2.4)$$

even if all stations of the network are sufficiently related to their neighbors by geodetic observations. This is not surprising if one considers that the geodetic observations provide only relative information on the positions of the connected stations; yet absolute positions are introduced as unknown parameters in the model. A suitable set of constraints is missing which relates the configuration to the coordinate frame. The network is said to suffer from a formulation defect (called datum defect by other authors; (Pelzer,1980)). The rank defect  $\text{def}(\underline{A})$  depends on the type of network. The design matrix of a pure triangulation network, without any constraint among the coordinates, which contains only direction observations will, for example, have the rank defect  $\text{def}(\underline{A}) = 4$  with 2 indeterminable translations, 1 rotation and 1 scale factor. Formulation defects  $\text{def}(\underline{A}) = 3$  and  $\text{def}(\underline{A}) = 2$  are encountered with pure trilateration networks and combined networks containing azimuth, direction and distance observations respectively.

By selecting an appropriate set of constraints, one particular solution among the infinite set of possible solutions is chosen. This is done by augmenting the deficient design matrix in the following manner (Vaníček and Krakiwsky, 1982)

$$\underline{A} \rightarrow \begin{bmatrix} \underline{A} \\ \underline{D} \end{bmatrix} . \quad (2.5)$$

Any set of constraints  $\underline{D}_m$ , satisfying the equation

$$\text{rank} \begin{bmatrix} \underline{A} \\ \underline{D}_m \end{bmatrix} = \text{rank}(\underline{A}) + \text{rank}(\underline{D}_m) = u \quad (2.6)$$

is called minimal-constraints. In the example above, of a combined network with two indeterminable translations, fixing the position of one station would be sufficient. For each selection of minimal-constraints, a different solution  $\hat{\underline{x}}$  with a different covariance matrix  $\underline{C}_{\hat{\underline{x}}}$  is obtained.

One particularly appealing choice among the minimal-constraints, fulfilling the condition

$$\underline{A} \cdot \underline{D}_1^T = \underline{0} \quad (2.7)$$

which leads to the property of the covariance matrix of the solution vector

$$\min_{\underline{D}_m} (\text{tr}(\underline{C}_{\hat{\underline{x}}})) \quad (2.8)$$

is the inner constraints solution. It can also be expressed by the pseudo-inverse (Moore-Penrose g-inverse) of  $\underline{N}$ :  $\underline{N}^+$ ,

$$\hat{\underline{d}}_1 = \underline{N}^+ \underline{u} \quad (2.9)$$

$$\underline{C}_{\hat{\underline{d}}_1} = \underline{N}^+ . \quad (2.10)$$

In addition to (2.8) this solution has the property

$$\min_{\hat{\underline{d}}} (\hat{\underline{d}}^T \hat{\underline{d}}) \quad (2.11)$$

The complete set of minimal-constraint solutions is obtained from a particular minimal constraints solution by applying a similarity transformation which reads in complex notation

$$\begin{aligned} \hat{z}_j^{(c)} &= z_\tau + m \cdot \exp(i\omega) \cdot \hat{z}_j^{(p)} & (2.12) \\ &= z_\tau + a \cdot \hat{z}_j^{(p)} \\ &= z_\tau + (1 + \mathcal{P}) \cdot \hat{z}_j^{(p)} \\ &= \hat{z}_j^{(p)} + z_\tau + \mathcal{P} \cdot \hat{z}_j^{(p)} \\ &= \hat{z}_j^{(p)} + f(x_\tau, y_\tau, m, \omega) \end{aligned}$$

where:  $j = 1, 2, \dots, n_p$

$$\begin{aligned} \hat{z}_j^{(p)} &= (\hat{x}_j^{(p)} + i\hat{y}_j^{(p)}) \in \mathbb{C} \dots \text{particular solution} \\ \hat{z}_j^{(c)} &= (\hat{x}_j^{(c)} + i\hat{y}_j^{(c)}) \in \mathbb{C} \dots \text{complete solutions} \\ z_\tau &= (x_\tau + iy_\tau) \in \mathbb{C} \dots \text{translation parameter} \\ m &= |a| \in \mathbb{R} \dots \text{scale factor} \\ \omega &= \arg(a) \in \mathbb{R} \dots \text{rotation angle} \\ a, \mathcal{P} &\in \mathbb{C} \dots \text{conformal parameters.} \end{aligned}$$

Note: For networks with scale control (if  $\underline{l}$  contains at least 1 distance):  $m = 1$ ; for networks with orientation control (if  $\underline{l}$  contains at least 1 azimuth):  $\omega = 0$ .

It is obvious from eqn. (2.12) that the adjusted point coordinates depend on the parameters  $x_\tau, y_\tau, m$  and  $\omega$ , which are indeterminable from  $\underline{l}$  of the network.

We insist that the coordinate systems used to describe the different

solutions do not greatly depart from each other. Then the four parameters  $m-1, \omega, x_T$  and  $y_T$  are small quantities which fulfil the inequalities:

$$m - 1 \ll 1 \quad (2.13)$$

$$\omega \ll 1$$

$$x_T < \epsilon$$

$$y_T < \epsilon$$

where  $\epsilon$  is a small distance (e.g.  $\epsilon < 0.1\text{m}$ ).

If, after selecting a set of minimal-constraints, the position of some individual network stations can still not be determined geometrically from the observations  $\underline{l}$ , the network is said to suffer from a configuration defect (Pelzer, 1980). The rank defect  $\text{def}(\underline{A}) = \text{def}(\underline{N})$  depends on the number of indeterminable coordinates of the configuration.

### 2.2.2 Determinacy Defects in Kinematic Networks

Let us consider a two-epoch horizontal kinematic network, surveyed twice at the instants of time  $t_1$  and  $t_2$  with the observations

$$\underline{l}^{(k)} = \underline{l}^{(k)}(t_k) \quad ; k=1,2 \quad (2.14)$$

and their covariance matrices

$$\underline{C}_l^{(k)} \quad ; k=1,2$$

(Note: The observations of different observation epochs are assumed to be uncorrelated; problems concerning possible cross-correlations between the sets of observations will be discussed in 2.4).

Let  $\hat{z}_{(k)}^{(P)}$ ;  $k=1,2$  be a vector of particular solutions of separate minimal-constraints adjustments. The difference of these complex positions is a particular solution of the complex displacement field associated with the time interval  $[t_1, t_2]$

$$\Delta \hat{z}^{(P)} = \hat{z}_{(2)}^{(P)} - \hat{z}_{(1)}^{(P)}. \quad (2.15)$$

The complete solution follows from eqn. (2.12)

$$\Delta \hat{z}^{(C)} = \hat{z}_{(2)}^{(C)} - \hat{z}_{(1)}^{(C)} \quad (2.16a)$$

$$\begin{aligned} \Delta \hat{z}_j^{(C)} &= \hat{z}_{(2)j}^{(P)} + z_{\tau}^{(2)} + \mathcal{G}_2 \hat{z}_{(2)j}^{(P)} - \hat{z}_{(1)j}^{(P)} - z_{\tau}^{(1)} - \mathcal{G}_1 \hat{z}_{(1)j}^{(P)} \\ &= \Delta \hat{z}_j^{(P)} + \Delta z_{\tau} + \mathcal{G}_2 \hat{z}_{(2)j}^{(P)} - \mathcal{G}_1 \hat{z}_{(1)j}^{(P)}, \end{aligned} \quad (2.16b)$$

where:  $j = 1, 2, \dots, n_p$

$$\Delta \hat{z}^{(P)} = \hat{z}_{(2)}^{(P)} - \hat{z}_{(1)}^{(P)}$$

$$\Delta z_{\tau} = z_{\tau}^{(2)} - z_{\tau}^{(1)}.$$

Denoting  $\mathcal{G}_2 - \mathcal{G}_1$  by  $\Delta \mathcal{G}$  yields

$$\begin{aligned} \Delta \hat{z}_j^{(C)} &= \Delta \hat{z}_j^{(P)} + \Delta z_{\tau} + (\mathcal{G}_1 + \Delta \mathcal{G}) (\hat{z}_{(1)j}^{(P)} + \Delta \hat{z}_j^{(P)}) - \mathcal{G}_1 \hat{z}_{(1)j}^{(P)} \\ &= \Delta \hat{z}_j^{(P)} + \Delta z_{\tau} + \Delta \mathcal{G} \cdot \hat{z}_{(1)j}^{(P)} + \mathcal{G}_2 \Delta \hat{z}_j^{(P)}; \quad j=1, 2, \dots, n_p. \end{aligned} \quad (2.17)$$

This relationship expresses the dependence of the complete set of displacement fields on the indeterminable parameters

$$\Delta z_{\tau}, \Delta \mathcal{G} \text{ and } \mathcal{G}_2.$$

If one considers the expected displacements to be small, i.e.

$$|\Delta \hat{z}_j^{(P)}| < \varepsilon \quad \text{and} \quad |\Delta \hat{z}_j^{(C)}| < \varepsilon \quad ; \quad j=1, 2, \dots, n \quad (2.18)$$

with  $\varepsilon$  being a small distance (e.g.  $\varepsilon < 0.5\text{m}$ ) and the inequalities (2.13), the last term in eqn. (2.17), being a product of small numbers, can be neglected

$$\Delta \hat{z}_j^{(C)} \doteq \Delta \hat{z}_j^{(P)} + \Delta z_{\tau} + \Delta \mathcal{G} \cdot z_j^{\circ} \quad ; \quad j=1, 2, \dots, n_p \quad (2.19)$$

where  $z_j^{\circ} = (x_o + iy_o)_j$  are approximate positions.

If we further realize that

$$\Delta\varphi = \varphi_2 - \varphi_1 \doteq m_2 - m_1 + i(\omega_2 - \omega_1) = \Delta m + i\Delta\omega \quad (2.20)$$

it follows

$$\begin{aligned} \Delta\hat{z}_j^{(c)} &\doteq \Delta\hat{z}_j^{(p)} + \Delta z_\tau + (\Delta m + i\Delta\omega) \cdot z_j^o ; j=1,2,\dots,n_p \quad (2.21) \\ &\doteq \Delta\hat{z}_j^{(p)} + f(\Delta x, \Delta y, \Delta m, \Delta\omega) \quad ; j=1,2,\dots,n_p. \end{aligned}$$

In the first approximation, the displacement field depends on indeterminable translation  $\Delta z$ , scale difference  $\Delta m$  and rotation difference parameter  $\Delta\omega$ . It is interesting to note that the indeterminable parameters of geodetic networks in eqn. (2.12) are replaced by new indeterminacies in eqn. (2.21), the latter being differences of the former. Consequently, the displacement field does not depend on the choice of the minimal constraints if the same set of constraints is introduced in the adjustment of both epochs. If the networks of both epochs each contain at least one distance (scale control), the parameter:  $\Delta m = 0$ . Analogously, if both sets of observations  $\underline{l}^{(k)}$  each contain at least one azimuth, the parameter  $\Delta\omega = 0$ .

In the case of tectonic crustal movement analysis, the object (the crust) is to be monitored by resurveyed geodetic networks which are, as a whole, established on the deformable body without any external reference. Therefore, it is not possible, in general to make any assumption about the movement of an individual point or a group of points.

## 2.3 Kinematic Functional Models

### 2.3.1 Displacement Models

A general mathematical model for kinematic networks is obtained from the generalization of the model

$$\underline{l} = \underline{A} \underline{d} + \underline{\xi} \quad (2.22)$$

(Note: Eqn. (2.22) is called Gauss-Markoff model in German literature (Niemeier, 1979))

where:  $\underline{l}$  ... observation vector

$\underline{A}$  ... design matrix

$\underline{d} = \underline{x} - \underline{x}_0$  ... parameter vector

$\underline{\xi}$  ... error vector ,

taking into account the time dependency

$$\underline{l}(t) = \underline{A} \underline{d}(t) + \underline{\xi}(t) . \quad (2.23)$$

Present geodetic techniques provide only a discrete series of observations in time. The continuous time functions in eqn. (2.23) are therefore replaced by their discretizations

$$\underline{l}(t_i) = \underline{A} \underline{d}(t_i) + \underline{\xi}(t_i) \quad ; i=1,2,\dots,n_e. \quad (2.24)$$

The re-observations of the network usually take place during short observation campaigns. This procedure is not only favorable for operational and economical reasons, it also provides reliability checks of the redundant observations. The observations of one campaign, belonging to the same epoch of time  $[t-\Delta\tau/2, t+\Delta\tau/2]$ , are treated as

simultaneous. A separate least-squares adjustment by variation of coordinates yields a unique solution if the design of the re-observed network does not suffer from formulation or configuration defects.

In seismically very active areas, the length of the observation epochs  $\Delta T$  has to be kept as short as possible. The maximum length  $\Delta T$  which can be tolerated without danger of biasing the results depends on the expected maximum rate of change of the observables.

a) Two-Epoch Case with Invariant Design:

In the ideal case of a two-epoch kinematic network, the configuration which was observed at time  $t_1$ , is being reobserved at time  $t_2$  according to the same observation program. This is expressed by the following mathematical model, with both the design and covariance matrices remaining invariant,

$$(\underline{l}^{(1)}, \underline{l}^{(2)}) + (\underline{v}^{(1)}, \underline{v}^{(2)}) = \underline{A} \cdot (\underline{d}^{(1)}, \underline{d}^{(2)}) . \quad (2.25)$$

If the first subvectors in eqn. (2.25) are subtracted from the second, it follows that

$$\underline{l}^{(2)} - \underline{l}^{(1)} + \underline{v}^{(2)} - \underline{v}^{(1)} = \underline{A} \cdot (\underline{d}^{(2)} - \underline{d}^{(1)}) . \quad (2.26)$$

This is the simple displacement model (Vaníček and Krakiwsky, 1982)

$$\Delta \underline{l} + \underline{v}_{\Delta l} = \underline{A} \cdot \Delta \underline{x} \quad (2.26a)$$

where:  $\Delta \underline{l} = \underline{l}^{(2)} - \underline{l}^{(1)}$  ... vector of observation differences

$\Delta \underline{x} = \underline{d}^{(2)} - \underline{d}^{(1)}$  ... vector of relative displacements.



## b) Multi-Epoch Case with Invariant Design:

The observation equations (2.25) extended to the multi-epoch case read

$$(\underline{l}^{(1)}, \underline{l}^{(2)}, \dots, \underline{l}^{(n_e)}) + (\underline{v}^{(1)}, \underline{v}^{(2)}, \dots, \underline{v}^{(n_e)}) = \underline{A}(\underline{d}^{(1)}, \underline{d}^{(2)}, \dots, \underline{d}^{(n_e)}) \quad (2.27)$$

$$\underline{l} + \underline{v} = \underline{A} \cdot \underline{d}$$

with

$$\underline{C}_l^{(1)} = \underline{C}_l^{(2)} = \dots = \underline{C}_l^{(n_e)}. \quad (2.28)$$

The observation vectors  $\underline{l}^{(i)}$  are said to belong to the same observation space

$$\underline{l}^{(1)}, \underline{l}^{(2)}, \dots, \underline{l}^{(n_e)} \in L. \quad (2.29)$$

Particular effects of line-dependent systematic errors, such as effects of erroneous station heights in EDM-networks, are eliminated to a large degree if this ideal, invariant design model is applied. As a consequence of the changing environment and the development of geodetic observation techniques, the design, as well as the stochastic model of the repeatedly observed networks, is invariant only in exceptional cases.

## c) Multi-Epoch Case with Varying Design:

If individual design matrices  $\underline{A}_{ii}$  are introduced, a more general functional model is obtained

$$\begin{bmatrix} \underline{l}^{(1)} \\ \underline{l}^{(2)} \\ \cdot \\ \cdot \\ \cdot \\ \underline{l}^{(n_e)} \end{bmatrix} + \begin{bmatrix} \underline{v}^{(1)} \\ \underline{v}^{(2)} \\ \cdot \\ \cdot \\ \cdot \\ \underline{v}^{(n_e)} \end{bmatrix} = \begin{bmatrix} \underline{A}_{11} & \underline{A}_{12} & \underline{A}_{13} & \cdots & \underline{A}_{1n_e} \\ \underline{A}_{21} & \underline{A}_{22} & \underline{A}_{23} & \cdots & \underline{A}_{2n_e} \\ \cdot & \cdot & & & \cdot \\ \cdot & \cdot & & & \cdot \\ \cdot & \cdot & & & \cdot \\ \underline{A}_{n_e1} & \underline{A}_{n_e2} & \underline{A}_{n_e3} & \cdots & \underline{A}_{n_en_e} \end{bmatrix} \begin{bmatrix} \underline{d}^{(1)} \\ \underline{d}^{(2)} \\ \cdot \\ \cdot \\ \cdot \\ \underline{d}^{(n_e)} \end{bmatrix} \quad (2.30)$$

$$\underline{A}_{ik} = 0 \quad ; \quad i \neq k \quad (2.31)$$

A further extension of the model (2.30, 2.31) with

$$\underline{A}_{ik} \neq 0 \quad ; \quad i \neq k \quad (2.32)$$

allows the introduction of unknown parameters common to different epochs. Examples of such parameters are unknown instrument scale factors or zero errors of EDM instruments.

### 2.3.2 Constrained Models

In all the functional models which were discussed above, no assumptions were made concerning the kind of relative movement of the individual points. No constraints were introduced among the individual positions  $\underline{x}^{(i)}$  of each epoch of observation. If we reliably know the physical laws that govern the movements, the movements can be restricted by introducing an appropriate set of constraints among the unknown displacements. The models

$$\dot{\underline{l}} + \underline{v}_i = \underline{A}' \dot{\underline{x}} \quad (2.33)$$

or

$$\ddot{\underline{l}} + \underline{v}_i = \underline{A}'' \ddot{\underline{x}} \quad (2.34)$$

where:  $\dot{\underline{l}}, \ddot{\underline{l}}$  ... vector of time derivatives of the observables

$\dot{\underline{x}}, \ddot{\underline{x}}$  ... vector of point velocity or acceleration

$\underline{A}' , \underline{A}''$  ... design matrices, relating point velocity or acceleration to changes in the observables. are examples of temporally constrained models in which a constant velocity or acceleration in time is being assumed.

An alternative selection of constrained models are the spatially constrained models. The slip displacement model, for example, postulates that motion consists of pure translation in a prescribed direction. The introduction of this particular type of constraint will be discussed in Section 4. Other spatially constrained models could be based on mathematical models of the fault displacement (e.g. the dislocation theory; (Chinnery, 1961)).

A special class of spatially constrained models is the spatially continuous or piecewise continuous displacement model. According to this approach, the sought relative displacement field is assumed to be a continuous function in space

$$\Delta z : z \rightarrow \Delta z(z) = f(z) . \quad (2.35)$$

This assumption, which will be adopted in this study, will be further discussed with the following strain models.

### 2.3.3 Models using Differential Geometry

None of the models discussed above is free of the problem of indeterminacy. Even if the resurveyed configurations all have scale and orientation control, the indeterminacy in translation still remains. The problem is inherently associated with displacements; these are not the most appropriate quantities to seek. The introduction of the strain tensor (cf. Section 3), is the most elegant approach, as it circumvents the indeterminacy problem if second order effects are excluded.

What assumptions have to be made for these differential models? The only condition is that the field of displacement vectors must be once differentiable almost everywhere. If the investigated section of the earth's crust were an ideal elastic continuum, the deformation it would undergo by stresses applied to it would simply be governed by the generalized Hooke's law. This means the strain would always be proportional to the stress induced by the driving tectonic forces. The assumption of continuity and differentiability would, in this case, be based on the physics of continuum. The assumption of differentiability can, however, be made without knowledge about the rheology of the crustal material.

### 2.4 Stochastic Models

The most general covariance matrix of the entire set of observations is given by

$$\underline{C} = \begin{bmatrix} C_{11} & C_{12} & C_{13} & \dots & C_{1n_e} \\ & C_{22} & C_{23} & \dots & C_{2n_e} \\ & & \cdot & & \cdot \\ & & & \cdot & \cdot \\ & & & & \cdot \\ & & & & C_{n_en_e} \end{bmatrix} \quad (2.36)$$

The off-diagonal submatrices express the cross-covariances between observations of different observation epochs. One reason for such non-zero cross-correlations could be, for example, line dependent systematic errors. The neglect of these off-diagonal sub-matrices leads to an underestimation of the accuracy of the estimated relative displacements (Vaníček and Krakiwsky, 1982). It should, however, be noted that it is very difficult to find reliable estimates for these cross-correlations. Well knowing that the cross-correlations have an effect on the statistical estimates of the deformation parameters, we are going to neglect them.

## SECTION 3

## DEFORMATION OF A CONTINUUM

The basic terms relevant to strain analysis, starting with the kinematics of a deformable body, will be defined in this section. The theory of the deformation of continua is to be treated in three-dimensional space. The analytical treatment of crustal kinematics is definitely a three-dimensional problem. Only particular problems of plane deformation are formulated in two-dimensional subspaces. Mainly for operational reasons discussed in Sub-section 1.3, it is, however, common geodetic practice to investigate horizontal and vertical relative crustal movements separately. This study follows the traditional geodetic concept, even though this separation is rather artificial. The theory of two-dimensional strain will be presented in Section 4.

### 3.1 Deformation of Bodies

-----

#### 3.1.1 Deformation and Displacement Gradients

Let  $\underline{r} = (x,y,z)$  denote the initial coordinates of the material point  $P_i$  (cf. Figure 3.1) of a deformable body with respect to a fixed Cartesian frame. (Note: A Lagrangean coordinate frame, defining 'material coordinates' is being used here; (Fraeijs de Veubeke,1979).)

Each vector  $\underline{r}_i$ ;  $i=1,2,\dots,n$  identifies a material point of the body at a state  $t_0$  of evolution (where  $\underline{r}$  belongs to the initial position vector space,  $\underline{r} \in P$ ). Let  $\underline{r}' = (x',y',z')$  denote the final coordinates of the same material point in a deformed or final configuration at time  $t_1$  (where  $\underline{r}'$  belongs to the final position vector space,  $\underline{r}' \in P'$ ). The displacement vector of  $P_i$  in the time interval  $[t_0, t_1]$  is denoted by

$$\underline{d} = (u,v,w) = \underline{r}' - \underline{r} \quad (3.1)$$

(where  $\underline{d}$  belongs to the displacement vector space,  $\underline{d} \in D$ ).

The displacements, and therefore also the final coordinates, may be expressed as functions of the initial coordinates

$$\underline{d} = \underline{d}(\underline{r}) \quad (3.2)$$

$$\underline{r}' = \underline{r} + \underline{d}(\underline{r}) = \underline{r}'(\underline{r}) . \quad (3.3)$$

The functions (3.2) and (3.3) define two transformations:  $P \rightarrow P'$  from initial to final position vector space, and  $P \rightarrow D$  from position into displacement space.

Let the field  $\underline{d}(\underline{r})$  be once differentiable almost everywhere. Let point  $P_2$  be another material point in the infinitesimal neighborhood of  $P_1$ . Figure 3.1 shows the displacement which the material points in the neighborhood of  $P_1$  experience if the body is deformed.

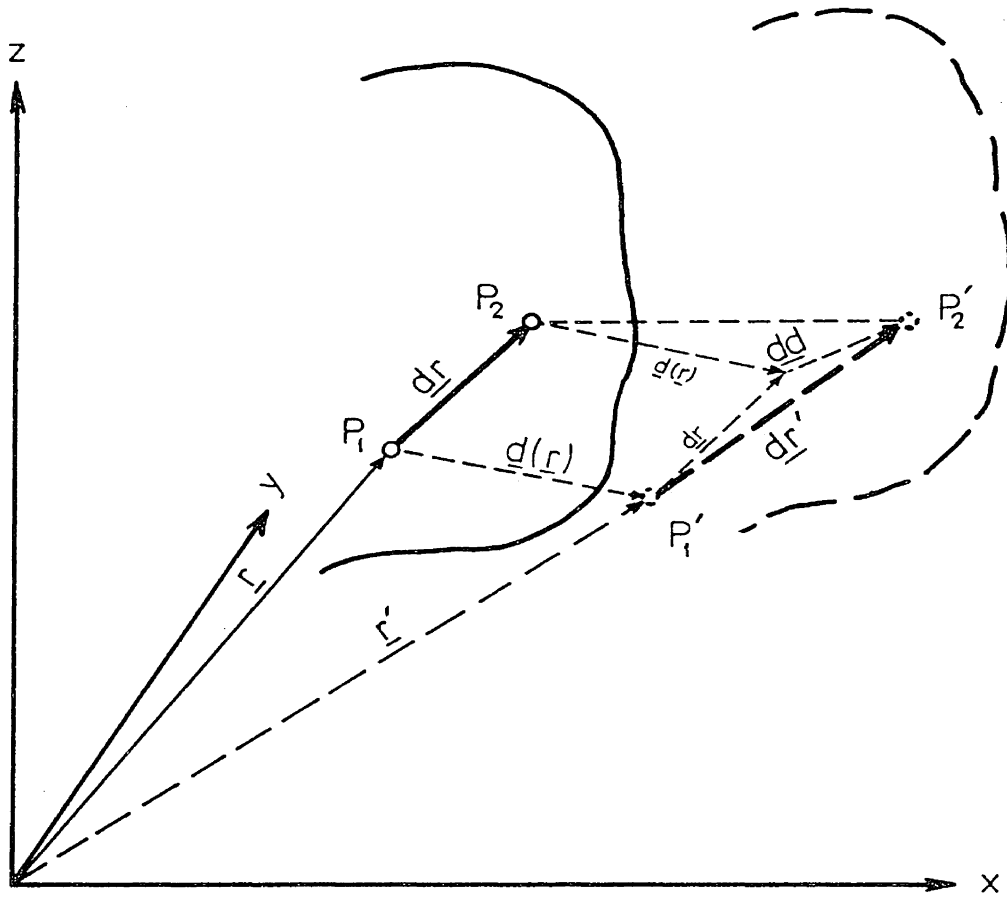


Figure 3.1

Deformation of a body



The relative position vector  $\underline{dr}$  of the original configuration is deformed into  $\underline{dr}'$  at the final state. This change of neighborhood is characterized by the linear neighborhood transformation (Fraeijs de Veubeke, 1979)

$$\underline{dr}' = \underline{\nabla r}'^T \cdot \underline{dr} = \underline{F} \cdot \underline{dr} \quad (3.4)$$

where:  $\underline{\nabla} = \left( \frac{\partial}{\partial x}, \frac{\partial}{\partial y}, \frac{\partial}{\partial z} \right)^T$  ... gradient operator

$\underline{\nabla r}'^T$  ... dyadic product of two vectors

$$\underline{F} = \begin{bmatrix} \frac{\partial x'}{\partial x} & \frac{\partial x'}{\partial y} & \frac{\partial x'}{\partial z} \\ \frac{\partial y'}{\partial x} & \frac{\partial y'}{\partial y} & \frac{\partial y'}{\partial z} \\ \frac{\partial z'}{\partial x} & \frac{\partial z'}{\partial y} & \frac{\partial z'}{\partial z} \end{bmatrix} \quad \dots \text{deformation matrix or} \quad (3.5)$$

Jacobian matrix of the  
transformation:  $\underline{r} \rightarrow \underline{r}'$

The differential displacement  $\underline{dd}$  is the difference

$$\begin{aligned} \underline{dd} &= \underline{dr}' - \underline{dr} & (3.6) \\ &= \underline{\nabla r}'^T \cdot \underline{dr} - \underline{dr} \\ &= \underline{F} \cdot \underline{dr} - \underline{dr} \\ &= (\underline{F} - \underline{I}) \cdot \underline{dr} . \end{aligned}$$

If one realizes that  $\underline{\nabla r}'^T = \underline{\nabla}(\underline{r} + \underline{d})^T = \underline{I} + \underline{\nabla d}^T$  it follows that

$$\begin{aligned} \underline{dd} &= (\underline{I} + \underline{\nabla d}^T) \underline{dr} - \underline{dr} & (3.7) \\ &= \underline{\nabla d}^T \cdot \underline{dr} \\ &= \underline{E} \cdot \underline{dr} \end{aligned}$$

where

$$\begin{aligned} \underline{E} &= \underline{F} - \underline{I} = \begin{bmatrix} \frac{\partial u}{\partial x} & \frac{\partial u}{\partial y} & \frac{\partial u}{\partial z} \\ \frac{\partial v}{\partial x} & \frac{\partial v}{\partial y} & \frac{\partial v}{\partial z} \\ \frac{\partial w}{\partial x} & \frac{\partial w}{\partial y} & \frac{\partial w}{\partial z} \end{bmatrix} \\ &= \begin{bmatrix} e_{xx} & e_{xy} & e_{xz} \\ e_{yx} & e_{yy} & e_{yz} \\ e_{zx} & e_{zy} & e_{zz} \end{bmatrix} \end{aligned} \quad (3.8)$$

is the strain matrix, or displacement gradient matrix (Fraeijs de Veubeke, 1979).

The strain matrix  $\underline{E}$  is the Jacobian matrix of the transformation  $\underline{r} \rightarrow \underline{d}$  (3.2) from the position into the displacement vector space  $P \rightarrow D$ .

### 3.1.2 Progressive Deformation

Figure 3.1 describes a deformation of a deformable body by instantaneous position vectors of its material points at two successive instants of time. The deformation is understood as the change in configuration between the initial (undeformed) state and the final (deformed) state.

In reality a body can pass through various intermediate stages before it arrives from its initial state at its final state of deformation.

This evolution of the configuration of material points, called progressive deformation, can be described either by finite or by infinitesimal strain. The finite deformation expressed by finite strain relates the instantaneous configuration to the initial (undeformed) state. Incremental (or infinitesimal) strain, on the other hand, relates instantaneous changes in configuration to the instantaneous configuration (Means, 1967). In incremental strain theory the distortions and the parameters describing them are considered so small that their products and squares can be neglected without any influence on the results. Considerable simplifications of the formulation result from these considerations.

In crustal strain analysis (from re-surveyed geodetic networks), the relative displacements are always very small compared to the position differences. The incremental strain theory is thus applicable without restriction.

Progressive deformation can be described by a succession of changes in the configuration. Let the deformation  $\underline{r} \rightarrow \underline{r}'$  (cf. Figure 3.1) in the interval  $[t_0, t_1]$  be followed by a second change of configuration  $\underline{r}' \rightarrow \underline{r}''$  between the instants  $t_1$  and  $t_2$ . The sequence of deformation  $\underline{r} \rightarrow \underline{r}' \rightarrow \underline{r}''$  is expressed by the functions  $\underline{r}' = \underline{r}'(\underline{r})$  followed by  $\underline{r}'' = \underline{r}''(\underline{r}')$ , or for the displacements  $\underline{d} = \underline{d}(\underline{r})$  followed by  $\underline{d}'' = \underline{d}''(\underline{r}')$ . The combined deformation is described by

$$\begin{aligned} \underline{r}'' &= \underline{r}''(\underline{r}'(\underline{r})) & (3.9) \\ &= \underline{r} + \underline{d}(\underline{r}) + \underline{d}''(\underline{r} + \underline{d}(\underline{r})) \end{aligned}$$

and its displacements by

$$\begin{aligned}\underline{d}'' &= \underline{r}'' - \underline{r} & (3.10) \\ &= \underline{d}(\underline{r}) + \underline{d}'(\underline{r} + \underline{d}(\underline{r})) .\end{aligned}$$

Let us now consider the neighborhood transformation (3.4) corresponding to the sequence  $\underline{r} \rightarrow \underline{r}' \rightarrow \underline{r}''$ :  $d\underline{r}' = \underline{F} \cdot d\underline{r}$  followed by  $d\underline{r}'' = \underline{F}' \cdot d\underline{r}'$ , where the deformation matrices are defined according to eqn. (3.5). The resulting deformation matrix  $\underline{F}''$  of the composed transformation  $\underline{r} \rightarrow \underline{r}''$  is the product of the component Jacobian matrices taken in the appropriate order

$$\begin{aligned}d\underline{r}'' &= \underline{F}' \cdot \underline{F} \cdot d\underline{r} & (3.11) \\ &= \underline{F}'' \cdot d\underline{r} .\end{aligned}$$

The same sequence of deformations expressed by the differential displacements is found if the deformation matrix  $\underline{F}$  is replaced by the strain matrix  $\underline{E}$

$$\begin{aligned}d\underline{d} &= \underline{E} \cdot d\underline{r} & (3.12) \\ &= (\underline{F} - \underline{I}) d\underline{r} \text{ followed by}\end{aligned}$$

$$\begin{aligned}d\underline{d}' &= \underline{E}' \cdot d\underline{r}' & (3.13) \\ &= (\underline{F}' - \underline{I}) d\underline{r}'\end{aligned}$$

and for the composed transformation

$$\begin{aligned}d\underline{d}'' &= \underline{E}'' \cdot d\underline{r} = (\underline{F}'' - \underline{I}) \cdot d\underline{r} = (\underline{F}' \cdot \underline{F} - \underline{I}) d\underline{r} & (3.14) \\ &= (\underline{E}' + \underline{I}) \cdot (\underline{E} + \underline{I}) \cdot d\underline{r} - \underline{I} \cdot d\underline{r} \\ &= (\underline{E}' \underline{E} + \underline{E}' + \underline{E}) d\underline{r} .\end{aligned}$$

For incremental deformations, the relative displacements are small compared to the relative positions. Thus the elements of the displacement gradient matrices  $\underline{E}$  and  $\underline{E}'$  satisfy the following condition

$$e_{ik} \ll 1 \quad ; \quad i, k = 1, 2, 3 . \quad (3.15)$$

In this case the field  $\underline{d}(\underline{r})$  is said to satisfy the condition of geometric linearity (Fraeijs de Veubeke, 1979). If the product  $\underline{E}' \cdot \underline{E}$  is neglected, the strain matrix of the total change of configuration  $\underline{E}''$  is simply found as the sum of the component gradient matrices

$$\underline{E}'' = \underline{E} + \underline{E}' . \quad (3.16)$$

For the displacement, follows the linearized law of superposition for incremental deformations

$$d\underline{d}'' = d\underline{d} + d\underline{d}' . \quad (3.17)$$

### 3.2 Temporal Variation of Strain

The strain tensor of the earth's crust is not only a function of the position vector  $\underline{r}$ , but also varies in time. According to the law of superposition of incremental deformations (3.16 and 3.17), the progressive deformation can be considered as a summation of infinitesimal deformations.

Let the relative velocity field  $d\underline{v}(\underline{r}, t)$  be a continuously varying function in space and time. The relative displacement in the time interval  $[t_0, t_1]$  is then obtained from the integral

$$d\underline{d}^{[t_0, t_1]} = \int_{t_0}^{t_1} d\underline{v}(\underline{r}, t) dt . \quad (3.18)$$

From eqn. (3.16) it follows analogously for the strain matrix

$$\underline{E}^{[t_0, t_1]} = \int_{t_0}^{t_1} \dot{\underline{E}}(\underline{r}, t) dt \quad (3.19)$$

where  $\dot{\underline{E}}$  is the gradient of velocity matrix, which is generally time dependent.

## SECTION 4

## TWO-DIMENSIONAL STRAIN ANALYSIS

In an attempt to find a compact and elegant mathematical formulation of the horizontal components of relative crustal motion, the use of complex analysis was studied. In the theory of plane stress and strain, the use of complex functions of complex variables is clearly indicated because of the ease with which the solution can be formed and manipulated. The advantages of this treatment are comparable to those achieved when complex analysis is applied to conformal mapping.

The basic definitions, as well as the mathematical relations among the complex components of plane strain, are hardly found in recent literature of the mechanics of continua (Sokolnikoff,1956; Jaeger,1961; Ramsay,1967; Means,1967; Fraeijs de Veubeke,1979). The basic theory of plane strain will therefore be outlined in this section.

#### 4.1 Infinitesimal Strain Tensor-Field in Two Dimensions

As we are only concerned with the horizontal components of the relative displacements in the  $x$ - $y$  mapping plane in this study, the three-dimensional formulation of strain presented in Section 3 can be reduced to a two-dimensional one. In this section, the vectors  $\underline{r}$  and  $\underline{d}$  represent the two-dimensional projections of the position and

displacement vectors onto the mapping plane. The three-dimensional gradient operator  $\underline{\nabla}$  is to be replaced by the two-dimensional operator

$$\underline{\nabla}' = \left( \frac{\partial}{\partial x}, \frac{\partial}{\partial y} \right)^T. \quad (4.1)$$

The infinitesimal strain matrix  $\underline{E}$  (3.8), containing 9 elements, is to be replaced by a two-dimensional matrix with 4 elements

$$\underline{E} = \begin{bmatrix} \frac{\partial u}{\partial x} & \frac{\partial u}{\partial y} \\ \frac{\partial v}{\partial x} & \frac{\partial v}{\partial y} \end{bmatrix} = \begin{bmatrix} e_{xx} & e_{xy} \\ e_{yx} & e_{yy} \end{bmatrix}. \quad (4.2)$$

There are different possibilities for splitting the strain matrix  $\underline{E}$  into parts. We shall introduce two kinds of decompositions which are particularly useful for the deformation analysis.

#### 4.1.1 Decomposition into Symmetrical and Anti-Symmetrical Parts

The general neighborhood transformation (3.4) can be accomplished in two steps. The first step is a pure deformation, whereas the second is an infinitesimal rotation. Analytically this is achieved by the decomposition of the strain matrix (Jacobian matrix) into a symmetrical and a anti-symmetrical (skew-symmetrical) part

$$\begin{aligned}\underline{E} &= 1/2(\underline{E} + \underline{E}^T) + 1/2(\underline{E} - \underline{E}^T) & (4.3) \\ &= \underline{\mathcal{E}} + \underline{\Omega}\end{aligned}$$

$$= \begin{bmatrix} e_{xx} & \frac{1}{2}(e_{xy} + e_{yx}) \\ \frac{1}{2}(e_{xy} + e_{yx}) & e_{yy} \end{bmatrix} + \begin{bmatrix} 0 & -\frac{1}{2}(e_{yx} - e_{xy}) \\ \frac{1}{2}(e_{yx} - e_{xy}) & 0 \end{bmatrix}$$

symmetric                  anti-symmetric .

The matrix  $\underline{\mathcal{E}}$ , called symmetric strain tensor (Jaeger, 1961), is a tensor of order two which expresses the pure deformation which remains after separating any rigid block motion (translation or rotation).

The symmetric strain tensor  $\underline{\mathcal{E}}$  can be transformed into a diagonal form by solving the two-dimensional eigenvalue problem. The eigenvalues  $\mathcal{E}_1$  and  $\mathcal{E}_2$  represent the maximum and minimum extensions in the direction of the eigenvectors  $(\cos\theta, \sin\theta)$  and  $(-\sin\theta, \cos\theta)$ . The eigenvalues  $\mathcal{E}_1$  and  $\mathcal{E}_2$  are called principal strains; the eigendirections, principal strain directions.

The transformation into the system of principal strain axes is expressed by the following spectral decomposition of the symmetric strain tensor

$$\begin{aligned}\underline{\mathcal{E}} &= \underline{S} \cdot \underline{D} \cdot \underline{S}^T & (4.7) \\ &= \begin{bmatrix} \cos\theta & -\sin\theta \\ \sin\theta & \cos\theta \end{bmatrix} \begin{bmatrix} \mathcal{E}_1 & 0 \\ 0 & \mathcal{E}_2 \end{bmatrix} \begin{bmatrix} \cos\theta & \sin\theta \\ -\sin\theta & \cos\theta \end{bmatrix}\end{aligned}$$

where:  $\underline{D}$  ... diagonal strain tensor (spectral matrix)

$\underline{S}$  ... modal matrix



$\theta$  ... orientation of the principal axes system .

#### 4.1.2 Decomposition into Conformal and Anti-Conformal Parts

The neighborhood transformation  $\underline{dr} \rightarrow \underline{dr}'$  (3.4) is conformal if the Cauchy-Riemann equations are satisfied by the components of the Jacobian matrix:

$$\left. \begin{array}{l} e_{xx} = e_{yy} \\ e_{xy} = -e_{yx} \end{array} \right\} \text{ (conformal) .} \quad (4.8)$$

Conversly,  $\underline{dr} \rightarrow \underline{dr}'$  is anti-conformal (Grove and Ladas,1974) if:

$$\left. \begin{array}{l} e_{xx} = -e_{yy} \\ e_{xy} = e_{yx} \end{array} \right\} \text{ (anti-conformal) .} \quad (4.9)$$

In eqn. (4.3) the deformation tensor was decomposed into a symmetrical and an anti-symmetrical part. It can just as well be decomposed into a conformal and an anti-conformal part

$$\begin{aligned} \underline{E} &= \begin{bmatrix} \sigma + \tau & \nu - \omega \\ \nu + \omega & \sigma - \tau \end{bmatrix} = \begin{bmatrix} \sigma & -\omega \\ \omega & \sigma \end{bmatrix} + \begin{bmatrix} \tau & \nu \\ \nu & -\tau \end{bmatrix} \quad (4.10) \\ &= \underline{J}_c + \underline{J}_a \\ &\quad \text{conformal} \quad \quad \quad \text{anti-conformal .} \end{aligned}$$

The elements  $\sigma, \omega, \tau$  and  $\nu$  introduced in eqn. (4.10) are linear combinations of the gradients of displacement; their interpretation is:

$$\begin{aligned}
 \zeta &= 1/2 (e_{xx} + e_{yy}) && \dots \text{dilation or average extension} \\
 \omega &= 1/2 (e_{yx} - e_{xy}) && \dots \text{average differential rotation} \\
 \tau &= 1/2 (e_{xx} - e_{yy}) && \dots \text{tensor shear components.} \\
 \nu &= 1/2 (e_{yx} + e_{xy}) &&
 \end{aligned}
 \tag{4.11}$$

Their geometrical meaning will be discussed in Sub-section 4.3. The matrices  $\underline{J}_c$  and  $\underline{J}_a$  in eqn. (4.10) can be interpreted as the Jacobian matrices of two successive transformations. The differential of the total transformation is then

$$d\underline{d} = \underline{J}_c \cdot d\underline{r} + \underline{J}_a \cdot d\underline{r}, \tag{4.12}$$

where the first term expresses a conformal and the second an anti-conformal transformation.

## 4.2 Strain Components as Complex Variables

### 4.2.1 Elements of Complex Analysis

A brief introduction into complex analysis is presented in this chapter. This theory is required for the derivation of the complex equivalent of the functional relationship between position and displacement vector space.

Let  $z = x + iy$  be a complex variable,  $z(x,y) \in \mathbb{C}$ , and let the complex function

$$w : z \rightarrow w(z) \quad ; \quad w(z) \in \mathbb{C} \tag{4.13}$$

have the real and imaginary parts

$$w = u(z) + i \cdot v(z) \quad ; \quad u(x,y), v(x,y) \in \mathbb{R} \quad (4.14)$$

where  $u(x,y)$  and  $v(x,y)$  are real functions

$$w = u(x,y) + i \cdot v(x,y) \quad ; \quad x,y \in \mathbb{R} \quad (4.15)$$

which are continuously differentiable with respect to  $x$  and  $y$  in the neighborhood of  $x_0, y_0$ . In this case, the differentials

$du, dv$  of  $u$  and  $v$  exist in  $x_0, y_0$ :

$$du = u_x(x_0, y_0) dx + u_y(x_0, y_0) dy \quad (4.16)$$

$$dv = v_x(x_0, y_0) dx + v_y(x_0, y_0) dy$$

where  $dx = x - x_0$  and  $dy = y - y_0$ .

(Note: The notation  $u_x(x_0, y_0)$  is used for the partial derivative

$$\left. \frac{\partial u}{\partial x} \right|_{\substack{x=x_0 \\ y=y_0}}$$

in this study.)

The differential of  $w = w(z)$  at  $z_0 = (x_0 + i y_0)$  is the linear function

$$dw = du + i dv \quad (4.17)$$

$$= [u_x(x_0, y_0) + i v_x(x_0, y_0)] dx + [u_y(x_0, y_0) + i v_y(x_0, y_0)] dy$$

$$= w_x(x_0, y_0) \cdot dx + w_y(x_0, y_0) \cdot dy,$$

where:  $w_x(x_0, y_0) = u_x(x_0, y_0) + i v_x(x_0, y_0)$

$$w_y(x_0, y_0) = u_y(x_0, y_0) + i v_y(x_0, y_0).$$

The complex increments  $dz$  and  $\bar{dz}$  (complex conjugate) are defined as follows:

$$dz = z - z_0 = (x + iy) - (x_0 + i y_0) = dx + i dy \quad ; \quad dz \in \mathbb{C}$$

$$\bar{dz} = \bar{z} - \bar{z}_0 = (x - iy) - (x_0 - i y_0) = dx - i dy \quad ; \quad \bar{dz} \in \mathbb{C} \quad (4.18)$$

and the real increments are inversely given by

$$dx = 1/2 (dz + \bar{dz}) \quad ; \quad dy = 1/2i (dz - \bar{dz}). \quad (4.19)$$

The differential expressed by the complex increment and its conjugate

follows from eqns. (4.17) and (4.19). It has the form

$$dw = \mathcal{F}(z_0) dz + \Psi(z_0) \bar{dz}, \tag{4.20}$$

where:  $\mathcal{F}(z_0) = 1/2 [w_x(z_0) - i w_y(z_0)]$  ;  $\mathcal{F}(z) \in \mathbb{C}$  (4.21)

$$\Psi(z_0) = 1/2 [w_x(z_0) + i w_y(z_0)] ; \Psi(z) \in \mathbb{C} .$$

The complex function  $w(z)$  is said to be complex differentiable at  $z_0$  if, and only if,  $\Psi(z_0) = 0$ ,

or  $w_x(z_0) + i w_y(z_0) = 0$  (4.22)

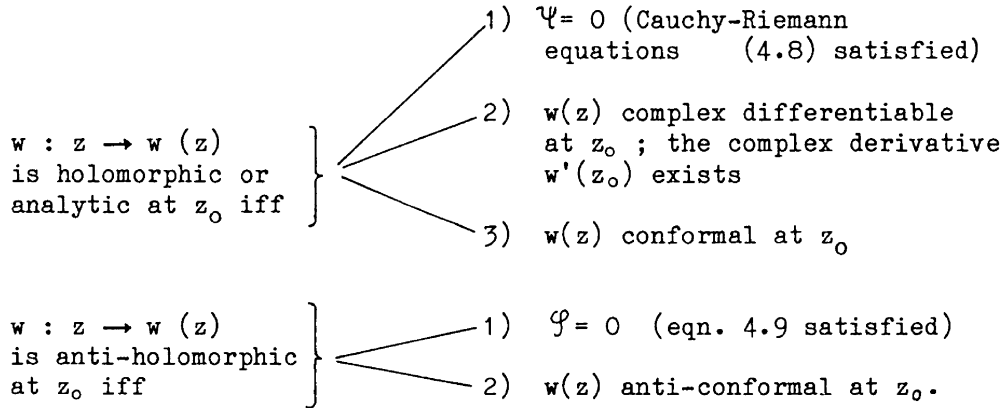
$$u_x(z_0) - v_x(z_0) + i [u_y(z_0) + v_y(z_0)] = 0$$

which is the complex equivalent to the Cauchy - Riemann differential equations (4.8). Only in this case does the complex derivative

$$w'(z) = dw/dz \Big|_{z_0} = \lim_{\Delta z \rightarrow 0} \frac{w(z_0 + \Delta z) - w(z_0)}{\Delta z} = \mathcal{F}(z_0) \tag{4.23}$$

exist and  $w(z)$  is said to be analytic or holomorphic (Henrici,1974).

The properties of holomorphic (anti-holomorphic) functions are recapitulated as follows:



Holomorphic and anti-holomorphic functions possess precisely the property of conformality and anti-conformality which is prescribed for the two Jacobian matrices  $\underline{J}_c$  and  $\underline{J}_a$  by the eqns. (4.8) to (4.10), (Grove and Ladas,1974).

## 4.2.2 Complex Strain Elements

The equivalence between the real differential of the total transformation (4.12) and the complex differential (4.20) will be shown in this chapter. The real vector space  $R^2$  is said to be isomorphic to the complex space  $C$ . Any mapping  $C \rightarrow C$  can therefore be redefined by a real vector transformation  $R^2 \rightarrow R^2$ . The matrix form

$$\begin{bmatrix} a \\ b \end{bmatrix} = \begin{bmatrix} x & -y \\ y & x \end{bmatrix} \cdot \begin{bmatrix} c \\ d \end{bmatrix} \quad (4.24)$$

is equivalent to the product of two complex numbers (Budden, 1968)

$$(a + i b) = (x + i y) \cdot (c + i d) . \quad (4.25)$$

If one realizes that the products

$$\begin{bmatrix} \sigma & -\omega \\ \omega & \sigma \end{bmatrix} \begin{bmatrix} dx \\ dy \end{bmatrix} \quad \text{and} \quad \begin{bmatrix} \tau & \nu \\ \nu & -\tau \end{bmatrix} \begin{bmatrix} dx \\ dy \end{bmatrix}$$

$$\underline{J}_c \quad \underline{d}\underline{r} \qquad \qquad \underline{J}_a \quad \underline{d}\underline{r}$$

are equivalent to the complex products

$$(\sigma + i\omega) \underbrace{(dx + i dy)}_{dz} \quad \text{and} \quad (\tau + i\nu) \underbrace{(dx - i dy)}_{\bar{d}z} ,$$

it is clear that the differential (4.12)

$$d\underline{d} = \underline{J}_c \underline{d}\underline{r} + \underline{J}_a \underline{d}\underline{r}$$

can be replaced by the complex differential

$$dw = (\sigma + i\omega) dz + (\tau + i\nu) \bar{d}z . \quad (4.26)$$

It follows for the complex variables  $\mathcal{G}$  and  $\mathcal{P}$  in eqn. (4.20) that

$$\mathcal{G} = (\sigma + i\omega) \quad (4.27)$$

$$\mathcal{P} = (\tau + i\nu) . \quad (4.28)$$

These two terms will be called conformal and anti-conformal complex strain elements.

### 4.3 Geometry of Two-Dimensional Strain

#### 4.3.1 Strain and Affine Transformation

The strain matrix  $\underline{E}$  (4.2) contains all the information needed for describing the distortions of a configuration by means of incremental strain.  $\underline{E}(x,y)$  is a tensor field of second order which varies, in general, from point to point. An important special case discussed in theory of elasticity is the uniform (or homogeneous) strain field  $\underline{E}$ , invariant in  $x$  and  $y$ . This exceptional case occurs theoretically with ideal, homogeneous elastic bodies which possess spatially uniform moduli of elasticity.

An attempt will be made in this chapter to relate the components of homogeneous strain to the parameters of a general affine transformation. The geometrical meaning of the components of strain can easily be understood in this way.

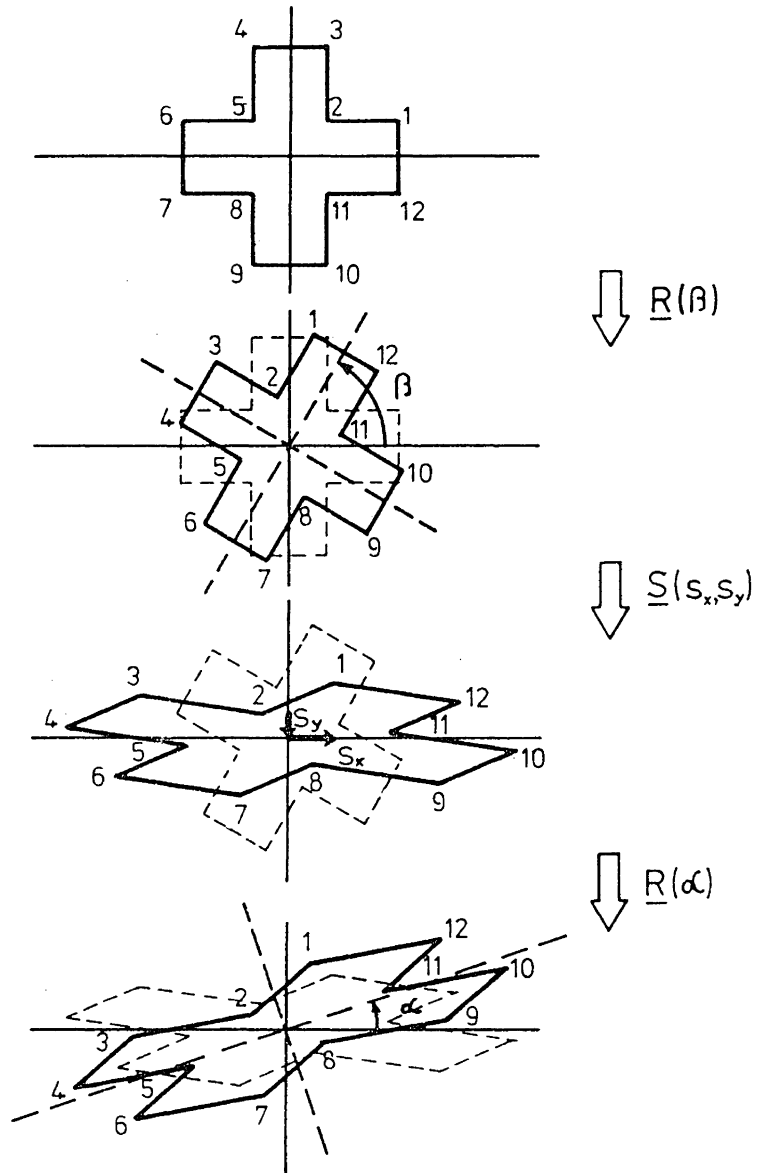


Figure 4.1

General affine transformation

decomposed into a sequence of rotations and stretches

In the case of a homogeneous strain field, the transformation  $\underline{r} \rightarrow \underline{r}'$ , analytically expressed by eqn. (3.4) is uniform (or constant) in space. The transformation equation has the same form as the linear expressions for the real (3.4), or for the complex differentials (4.20)

$$\underline{r}' = \underline{F} \cdot \underline{r} \quad (4.29)$$

$$z' = (1 + \mathcal{C}) \cdot z + \Psi \bar{z} \quad (4.30)$$

where the differentials  $d\underline{r}$ ,  $d\underline{r}'$ ,  $dz$  and  $d\bar{z}$  are replaced by the vectors  $\underline{r}$ ,  $\underline{r}'$  and by the complex variables  $z$  and  $\bar{z}$ . The deformation matrix  $\underline{F}$  (3.5) consists of 4 constants and  $\mathcal{C}$  and  $\Psi$  are two complex constants.

The linear form (4.29) is analogous to the transformation

$$\begin{bmatrix} x' \\ y' \end{bmatrix} = \begin{bmatrix} a_0 \\ b_0 \end{bmatrix} + \begin{bmatrix} a_1 & a_2 \\ b_1 & b_2 \end{bmatrix} \cdot \begin{bmatrix} x \\ y \end{bmatrix} \quad (4.31)$$

$$\underline{r}' = \underline{r}_0 + \underline{A} \cdot \underline{r}$$

with six parameters:  $a_i, b_i$ ;  $i=0,1,2$ , which is known as the equation of a general affine transformation (Wolfrum, 1978). The only difference is the additional translation vector  $\underline{r}_0$  in eqn. (4.31).

Figure 4.1 depicts a comprehensive geometrical description of the general affine transformation. The transformation is decomposed into a sequence of rotations and stretches

$$\underline{r}' = \underline{R}(\mathcal{L}) \cdot \underline{S}(s_x, s_y) \cdot \underline{R}(\beta) \cdot \underline{r} \quad (4.32)$$

where:  $\underline{R}$  ... rotation matrix

$\underline{S}$  ... diagonal matrix with the scale factors  $s_x$  and  $s_y$

(Note: The translation  $\underline{r}_0$  has been omitted in eqn. (4.32).)



With the substitution

$$s_x = s + \delta \quad \text{and} \quad s_y = s - \delta$$

where:  $s = 1/2 (s_x + s_y)$  ... average scale factor

$$\delta = 1/2 (s_x - s_y) \quad \dots \text{ differential scale factor} \\ \text{(see also 4.3.3) ,}$$

eqn. (4.32) can be decomposed into a conformal and an anti-conformal part

$$\begin{aligned} \underline{r}' &= \underline{R}(\alpha) \cdot [s \cdot \underline{I} + \delta \cdot \underline{Z}] \cdot \underline{R}(\beta) \cdot \underline{r} \\ &= s \cdot \underline{R}(\alpha + \beta) \cdot \underline{r} + \delta \underline{R}(\alpha) \cdot \underline{Z} \cdot \underline{R}(\beta) \cdot \underline{r} \end{aligned} \quad (4.33)$$

where

$$\underline{Z} = \begin{bmatrix} 1 & 0 \\ 0 & -1 \end{bmatrix} \quad \dots \text{ reflection matrix expressing} \\ \text{the reflection at the x-axis.}$$

Realizing that

$$\underline{Z} \cdot \underline{R} \begin{bmatrix} x \\ y \end{bmatrix} = \underline{R} \begin{bmatrix} x \\ -y \end{bmatrix} \quad (4.34)$$

yields

$$\begin{bmatrix} x' \\ y' \end{bmatrix} = s \cdot \underline{R}(\alpha + \beta) \begin{bmatrix} x \\ y \end{bmatrix} + \delta \underline{R}(\alpha - \beta) \begin{bmatrix} x \\ -y \end{bmatrix}. \quad (4.35)$$

This is the description of the general affine transformation (without translation) by the four geometrically meaningful parameters  $\alpha, \beta, s$  and  $\delta$ . In complex notation, the same transformation is given by

$$z' = s \cdot \exp i(\alpha + \beta) \cdot z + \delta \cdot \exp i(\alpha - \beta) \cdot \bar{z} \quad (4.36)$$

where  $\alpha, \beta, s, \delta \in \mathbb{R}$ .

From eqn. (4.30) and (4.36) it follows for the complex strain components

$$(1 + \varphi) z + \psi \bar{z} = s \cdot \exp i(\alpha + \beta) z + \delta \cdot \exp i(\alpha - \beta) \bar{z} \quad (4.37)$$

$$\varphi = s \cdot \exp i(\alpha + \beta) - 1 \quad (4.38)$$

$$\Psi = \delta \cdot \exp i(\alpha - \beta) \quad (4.39)$$

and for the real strain components

$$\begin{aligned} \sigma &= \operatorname{Re}(\mathcal{F}) = s \cdot \cos(\alpha + \beta) - 1 \\ \omega &= \operatorname{Im}(\mathcal{F}) = s \cdot \sin(\alpha + \beta) \\ \tau &= \operatorname{Re}(\Psi) = \delta \cos(\alpha - \beta) \\ \nu &= \operatorname{Im}(\Psi) = \delta \sin(\alpha - \beta) . \end{aligned} \quad (4.40)$$

For small relative displacements  $|\underline{d}| \ll |\underline{r}|$  it is

$$\begin{aligned} s &\doteq 1 \\ \alpha + \beta &\ll 1 \\ \alpha &\doteq -\beta \end{aligned} \quad (4.41)$$

which yields the approximate relationship

$$\begin{aligned} \sigma &\doteq s - 1 \\ \omega &\doteq \alpha + \beta \\ \tau &\doteq \delta \cos 2\beta \\ \nu &\doteq -\delta \sin 2\beta . \end{aligned} \quad (4.42)$$

#### 4.3.2 Non-Homogeneous Strain Fields

In the general case of a spatially non-homogeneous strain field, the transformation  $\underline{dr} \rightarrow \underline{dr}'$  is not constant in space. Therefore, it can not be interpreted geometrically by a general affine transformation. The deformation, and thus the strain matrix  $\underline{E}(x,y)$ , varies in space. However, for infinitesimal relative positions and displacements, in the neighborhood of any point, the linear representation of the distortion (incremental strain), and thus the analogy to the affine

transformation, is valid.

### 4.3.3 Further Expressions for Incremental Strain

Unfortunately the definitions, conventions and notations for strain quantities are not used consistently in the literature of the theory of elasticity. For non-specialists, this makes the method of strain analysis and the interpretation of its results difficult to understand. The gradients of displacement  $e_{xx}$ ,  $e_{xy}$ ,  $e_{yx}$  and  $e_{yy}$  defined in eqn. (3.8) are intrinsically easily understood. They depend, however, on the choice of the coordinate system. The strain components (4.11), as they were derived from the decomposed strain matrix, are felt to be the most natural choice of geometrically intelligible measures of strain. It is their symmetry in the definition (4.11) and the coincidence of the real with the complex formulation (4.26-4.28) which is the most appealing from the analysis point of view. All interpretations in this study will therefore be based on these quantities.

The four strain components are dimensionless quantities. It is common practice in the field of crustal strain analysis to express them in units of microstrain [ $\mu$ strain], which is defined identically to parts per million [ppm].

In this chapter a series of derived measures of strain which are frequently used in the field of strain analysis will be introduced.

## a) Linear Extension:

The linear extension of a distance  $ds$  between two neighboring points  $P_1$  and  $P_2$  (cf. Figure 3.1) is defined as

$$e = \frac{ds' - ds}{ds} \quad (4.43)$$

where:  $ds$  ... distance  $\overline{P_1 P_2}$  before the deformation

$ds'$  ... distance  $\overline{P'_1 P'_2}$  after the deformation .

The elements  $e_{xx}$ ,  $e_{yy}$  (and  $e_{zz}$ ) of the gradient of deformation matrix are called extensional strains. They express the linear extension of lines which were parallel to the axes of the coordinate system before the deformation.

## b) Scale Factor:

The scale factor (also called stretch)

$$m = ds'/ds = 1 + e \quad (4.44)$$

is obtained from the linear extension.

## c) Dilatation:

(Note: Dilatation is not to be confused with 'dilation' as defined by eqn. (4.11), cf. (4.50)). The dilatation is defined as the relative change of an infinitesimal area analogously to the linear extension

$$\Delta = \frac{dA' - dA}{dA} \quad , \quad (4.45)$$

where:  $dA$  ... area of undeformed configuration

$dA'$  ... area of deformed configuration

and

$$m_A = dA'/dA = 1 + \Delta \quad (4.46)$$

is the ratio of the deformed and the original area.

The scale factors in the principal directions are found from the principal strains

$$m_1 = 1 + \varepsilon_1 \quad (4.47)$$

$$m_2 = 1 + \varepsilon_2 .$$

The infinitesimal dilatation is obtained from the product

$$m_A = m_1 \cdot m_2 = (1 + \varepsilon_1) (1 + \varepsilon_2) \doteq 1 + \varepsilon_1 + \varepsilon_2 \quad (4.48)$$

if products of small quantities are neglected. For the dilatation it follows

$$\Delta \doteq \varepsilon_1 + \varepsilon_2 . \quad (4.49)$$

The dilation, or average extension, is equal to the dilatation divided by two

$$\sigma = \Delta / 2 . \quad (4.50)$$

d) Total Shear:

Total shear is defined as

$$\gamma_T = (\tau^2 + \nu^2)^{\frac{1}{2}} . \quad (4.51)$$

In contrast to the shear components (4.11), this quantity does not depend on the choice of the coordinate system. As will be shown in Section 5, total shear is equal to the maximum of the amount of shear as a function of the direction. It is interesting to note that total shear is equal to the differential scale factor  $\sigma$  of the general affine transformation (4.32), which follows from eqn. (4.42).

The shearing measures stated so far are all measures of tensor shear. This definition will be used without exception in this study. It

should, however, be noted that some authors use the measure of engineering shear, which is twice the tensor shear.

e) Strain-Rate Components

In analogy to the derivation of the symmetric strain tensor and the strain components, a strain-rate tensor and strain-rate components:

$$\begin{aligned} \dot{\hat{C}} &= \frac{d\hat{C}}{dt} & \dot{\hat{\omega}} &= \frac{d\hat{\omega}}{dt} & (4.52) \\ \dot{\hat{\tau}} &= \frac{d\hat{\tau}}{dt} & \dot{\hat{\nu}} &= \frac{d\hat{\nu}}{dt} \end{aligned}$$

can be derived from  $\dot{\underline{E}}$ . All strain-rate quantities have the physical dimension  $t^{-1}$  and are measured in micro-strain per year [ $\mu\text{strain/yr}$ ].

## SECTION 5

GRAPHICAL REPRESENTATION OF STRAIN-TENSOR FIELDS  
AND THEIR CONFIDENCE REGIONS5.1 General Considerations

In any attempt to interpret the computed numerical values of strain-tensor fields, there is a demand for graphical display. Modern graphical computer facilities, such as automatic plotters and CRT-terminals, provide the possibility of displaying graphical representations of computed strain.

Various graphical representation techniques for strain quantities have been studied and tested. Those methods which were found to be appropriate for crustal strain investigations will be discussed in this section. As strain is a tensorial rather than a scalar quantity, its visualization by a three-dimensional surface is not possible. Only scalar components of strain could be separately displayed in this way. If one single component is to be investigated, its lines of equal values (iso-lines) can be plotted in the x-y-plane. In general, plotting of meaningful strain figures at grid points was found to provide a more geometrically intuitive description of the strain field.

The strain quantities as they are estimated from the least-squares approximation are random variables. In any attempt to draw conclusions from these results, the interpreter has to consider the statistical

confidence of these estimates. For this reason techniques which graphically depict the statistical quantities associated with the strain values are finally presented.

## 5.2 Principal Axes Diagram

The elements  $\epsilon_1$ ,  $\epsilon_2$  and  $\theta_s$ , which result from the diagonalization of the symmetric strain tensor (4.3), can be visualized in a very simple way by the principal axes diagram of strain (cf. Figure 5.2). This diagram depicts the direction and magnitude of maximum and minimum extension in a geometrically intuitive way. The size of the axes is a measure of the magnitude of the principal strains. Positive values (extensions) are plotted by solid lines, negative values (contractions) by broken lines. Additional small arrows, pointing towards the centre of the diagram for contractions and in the opposite direction for extensions, were found to enhance the visual impact of these diagrams.

The principal axes of strain diagram also expresses shear in an indirect way. The magnitude of shear can be visualized from the difference of the principal strains. The directions of maximum shear form angles of  $45^\circ$  with the two principal strain axes.

Similar to the principal axes of strain diagram, maximum shear can be shown by an axes of maximum shear diagram (cf. Figure 5.3). The length of any of the two equal axes expresses total shear  $\gamma_r$  (4.51).

As far as numerical computation and plotting of large numbers of



diagrams are concerned, the principal axes diagrams turned out to be the most economical.

### 5.3 Strain Ellipse and Strain Pedal-Curve

The symmetric strain tensor  $\underline{\underline{\epsilon}}(x,y)$  (cf. (4.3)) describes the non-translational, non-rotational linear deformation at any point  $P(x,y)$ , relating the vectors of position space  $\underline{dr}$  with those of the displacement space  $\underline{dd}$  by

$$\underline{dd} = \underline{\underline{\epsilon}} \underline{dr} . \quad (5.1)$$

Defining  $\underline{q}$  as a unit position vector

$$\underline{q}(\alpha) = \begin{bmatrix} \cos \alpha \\ \sin \alpha \end{bmatrix}, \quad (5.2)$$

where  $\alpha$  denotes the angle, measured anti-clockwise from the x-axis,

$$\underline{dd}(\alpha) = \underline{\underline{\epsilon}} \underline{q}(\alpha) = \begin{bmatrix} (\sigma + \tau) \cos \alpha + \nu \sin \alpha \\ \nu \cos \alpha + (\sigma - \tau) \sin \alpha \end{bmatrix} \quad (5.3)$$

represents the mapping of a unit circle in position space into displacement space. Eqn. (5.3) is the parametric vector equation of the strain ellipse, which is one possible graphical representation of the local deformation at  $P(x,y)$ .

Replacing the real strain components by its complex expressions  $\mathcal{P}, \mathcal{Q}$  and the unit vector  $\underline{q}(\alpha)$  by its complex equivalent

$$\exp(i\alpha) = \cos \alpha + i \sin \alpha , \quad (5.4)$$

the complex parametric equation for the strain ellipse can easily be found from

$$v(\alpha) = \mathcal{P} \exp(i\alpha) + \mathcal{Q} \exp(-i\alpha) - i\omega \exp(i\alpha) ; v(\alpha) \in \mathbb{C} \quad (5.5)$$

$$\begin{aligned}
 v(\alpha) &= (\varphi - i\omega) \exp(i\alpha) + \psi \exp(-i\alpha) \\
 &= \operatorname{Re}(\varphi) \cdot \exp(i\alpha) + \psi \exp(-i\alpha) .
 \end{aligned}$$

The strain conic is an ellipse only when both eigenvalues of the strain tensor are positive. If one is positive and the other negative, the conic is theoretically a two branch hyperbola. If both are negative, it is an imaginary ellipse. A graphical representation of the latter two cases may make some intuitive sense. Some authors connect the ends of the positive or negative semiaxes by ellipses in all cases (Thapa,1980), (cf. Figure 5.4).

Another interesting quantity to be graphically represented is the extension (or contraction) in a certain direction. Extension, as a function of the direction (or azimuth), can be derived from the expression for the strain conic (5.3). The projection

$$\begin{aligned}
 b_1(\alpha) &= \underline{q}^T(\alpha) \underline{d} \underline{d} = \underline{q}^T(\alpha) \underline{\mathcal{E}} \underline{q}(\alpha) \\
 &= \sigma + \tau \cos 2\alpha + \nu \sin 2\alpha .
 \end{aligned} \tag{5.6}$$

of the vector  $\underline{d} \underline{d}$  onto  $\underline{q}$  is exactly the component which we are looking for (cf. Figure 5.1). The expression (5.6) is the parametric equation of a pedal-curve which is called the strain pedal-curve (Pope,1966). This reads in complex notation

$$\begin{aligned}
 b_1(\alpha) &= \operatorname{Re}(\exp(-i\alpha) \cdot v) \quad ; \quad b_1(\alpha) \in \mathbb{R} \\
 &= \operatorname{Re}(\varphi \exp(i\alpha) \cdot \exp(-i\alpha) + \psi \exp(-2i\alpha)) \\
 &= \operatorname{Re}(\varphi + \psi \exp(-2i\alpha)) .
 \end{aligned} \tag{5.7}$$

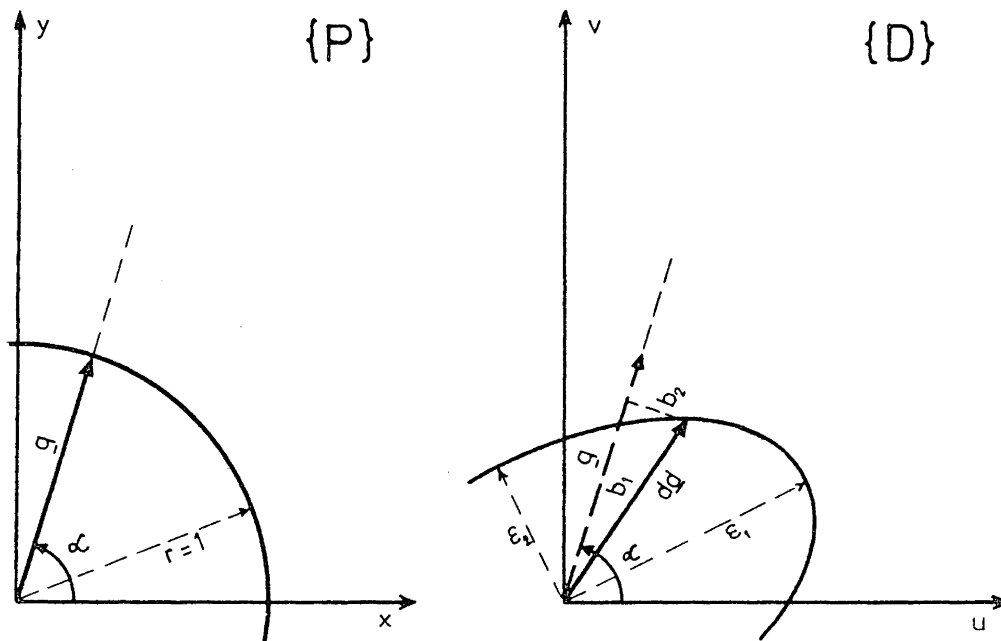


Figure 5.1

Neighborhood transformation of a unit circle

#### 5.4 Shear Rosette

Shear can be described as the change in a  $90^\circ$  angle. Shear at any point in a certain direction can be computed similarly as extension in a given direction. It is simply the component  $b_2$  in Figure 5.1 ,

$$\begin{aligned} b_2(\alpha) &= \text{Im} (\exp(-i\alpha) \cdot v) & ; b_2(\alpha) \in \mathbb{R} & \quad (5.8) \\ &= \text{Im} (\Psi \exp(-2i\alpha)) \end{aligned}$$

or in real notation

$$b_2(\alpha) = v \cdot \cos 2\alpha - \tau \cdot \sin 2\alpha . \quad (5.9)$$

It should be noted that eqn. (5.9) defines a four-petal rosette called the shear rosette (Pope, 1966). The directions of zero shear correspond with the directions of the principal strain axes. The latter form angles of  $45^\circ$  with the directions of maximum shear. An optional confidence region of shear (cf. Sub-section 5.7) is also plotted in the graphical example which depicts shear-rosettes (cf. Figure 5.7). The shear  $b_2$  in (5.8) does not depend on the conformal complex strain component  $\varphi$ . Thus the shear-rosette is invariant to infinitesimal rotations and scale changes.

Extension and shear in a given direction can both be expressed by the complex matrix equation

$$c = b_1 + i b_2 = [1, \exp(-2i\alpha)] \begin{bmatrix} \text{Re}(\varphi) \\ \Psi \end{bmatrix} \quad (5.10)$$

which is equivalent to the real matrix equation

$$\begin{bmatrix} b_1 \\ b_2 \end{bmatrix} = \begin{bmatrix} 1, 0, \cos 2\alpha, \sin 2\alpha \\ 0, 0, -\sin 2\alpha, \cos 2\alpha \end{bmatrix} \cdot \begin{bmatrix} \text{Re } \varphi \\ \text{Im } \varphi \\ \text{Re } \psi \\ \text{Im } \psi \end{bmatrix} \quad (5.11)$$

$$\underline{b} = \underline{A} \cdot \underline{f}.$$

### 5.5 Dilation Circle and Rotation Sector

Dilation  $\varphi$  and average differential rotation  $\omega$  are scalar strain quantities. Dilation at discrete points is best described graphically by a circle with variable radius (solid circle for extension, broken circle for contraction). The average differential rotation  $\omega$  is preferably represented by a small sector with variable central angle (plotted with solid lines for positive rotations, broken lines for negative rotations, cf. Figure 5.5). The values of the average differential rotation  $\omega$  are, in general, so small ( $<10^{-5}$  rad) that it would be impossible to plot them to scale as an angle. Therefore  $\omega$  has to be multiplied by an appropriate scale factor (e.g.  $10^6$ ).

### 5.6 Scalar Strain Quantities

The least-squares approximation of the strain-field provides continuous numerical functions in space. Dilation, average differential rotation, total shear or shear in a prescribed direction are examples of scalar strain functions. The most appropriate way to represent these scalar functions graphically is by plotting their lines of equal functional value (iso-lines, i.e. by displaying their three-dimensional surfaces over the x-y-plane).

### 5.7 Confidence Regions of Strain Quantities

The covariance matrix  $\hat{C}_{\lambda}$  is computed together with the solution vector for the polynomial coefficients of the approximation function. Applying the covariance law to the approximation function (cf. Section 6), covariance matrices  $\hat{C}_{\phi, \psi}$  of the strain components are found at any prediction point. Applying the covariance law to eqn. (5.11) yields the covariance matrix of the radial distances of the strain pedal-curve and the shear-rosette

$$\hat{C}_{\underline{b}} = \underline{A} \cdot \hat{C}_{\phi, \psi} \underline{A}^T. \quad (5.12)$$

The 68.3 percent confidence interval of the extension and shear in a certain direction is found, if covariances are neglected, from

$$\hat{C}_{\underline{b}_i} = (\hat{c}_{\underline{b}_{ii}})^{\frac{1}{2}} \quad ; \quad i=1,2. \quad (5.13)$$

The confidence intervals of the radial distances describe two curves similar to the strain pedal-curves and the shear-rosettes. They can be computed as parametric functions of  $\mathcal{L}$  and be plotted together with the strain figures in a different color or with a different line type (cf. Figures 5.6 and 5.7).

The confidence intervals of the dilation and the average differential rotation are found directly from their variances in  $\hat{C}_{\phi, \lambda}$ . The confidence interval to any level of confidence of the dilation at a certain prediction point are graphically displayed by circles concentric to the dilation circles (cf. Figure 5.5). The confidence interval of the rotation sector is depicted by a small arc, concentric to the sector arc (cf. Figure 5.5).

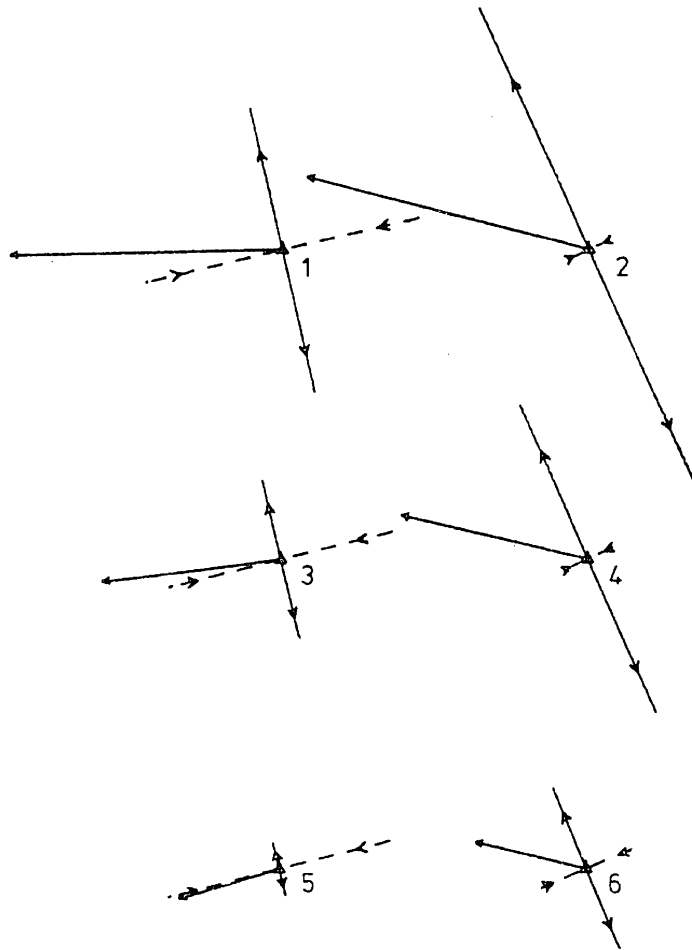


Figure 5.2

Principal axes of strain

Map scale: 1:400000. Relative displacements: arrows (1:20).  
 Extension/contraction: solid/broken lines (5mm<sup>2</sup>=1μstrain).

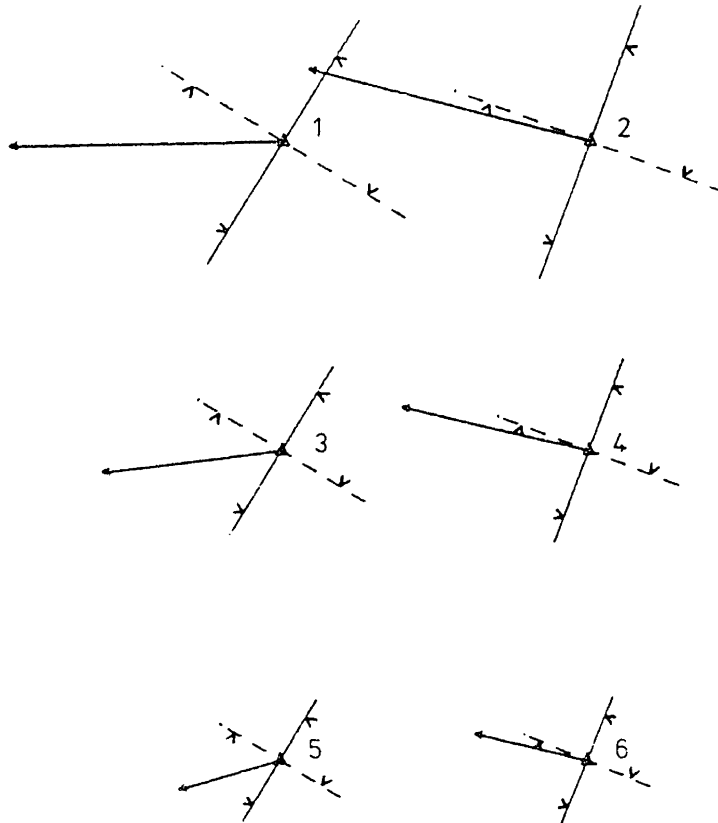


Figure 5.3

Axes of maximum shear

Map scale: 1:400000. Relative displacements: arrows (1:20).  
 Left/right lateral tensor shear: solid/broken lines ( $5\text{mm}^2 = 1\mu\text{strain}$ ).



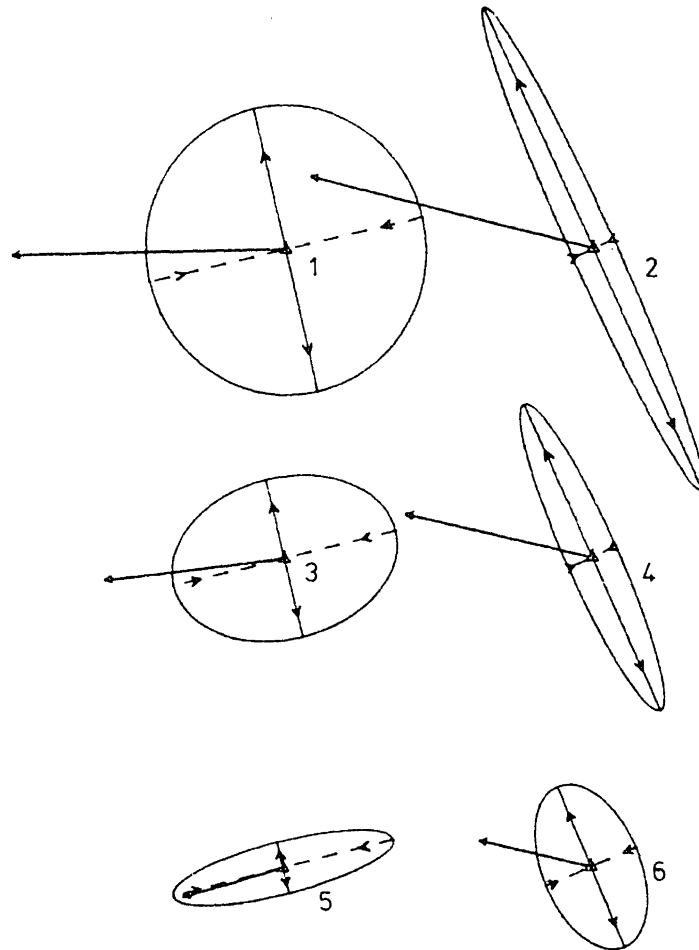


Figure 5.4

Strain ellipses and principal axes of strain

Map scale: 1:400000. Relative displacements: arrows (1:20).  
 Extension/contraction: solid/broken lines ( $5\text{mm}^2 = 1\mu\text{strain}$ ).

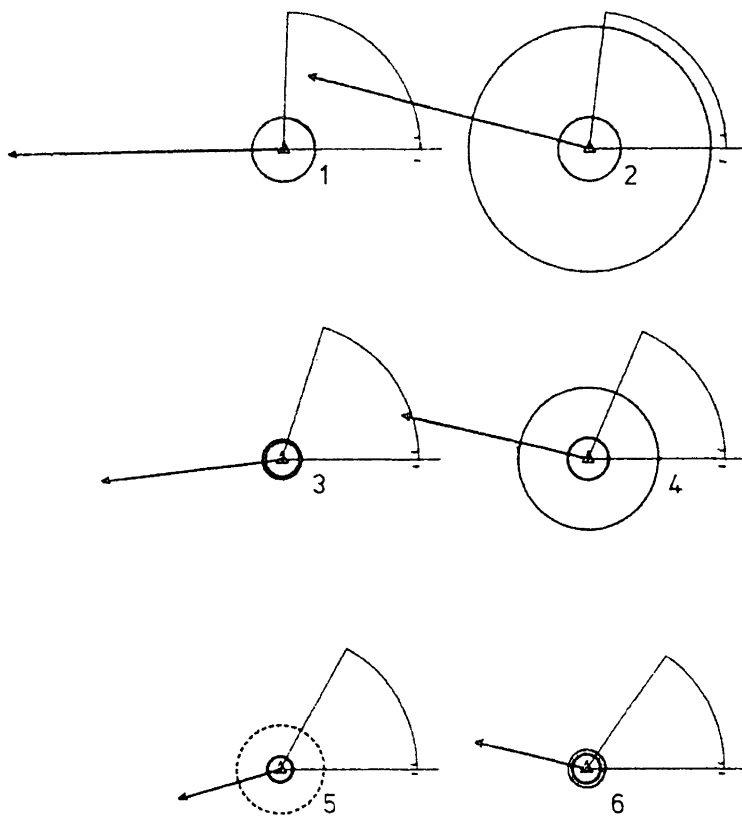


Figure 5.5

## Dilation circles and rotation sectors

Map scale: 1:400000. Relative displacements: arrows (1:20).  
 Positive/negative dilation: radius of solid/broken circles  
 ( $5\text{mm} \hat{=} 1\mu\text{strain}$ ). Average differential rotation: angle of sectors  
 ( $1\text{gon} \hat{=} 10\mu\text{gon}$ ). Std.dev. of dilation: heavy circles. Std.dev. of  
 rotation: marks at sector arcs.

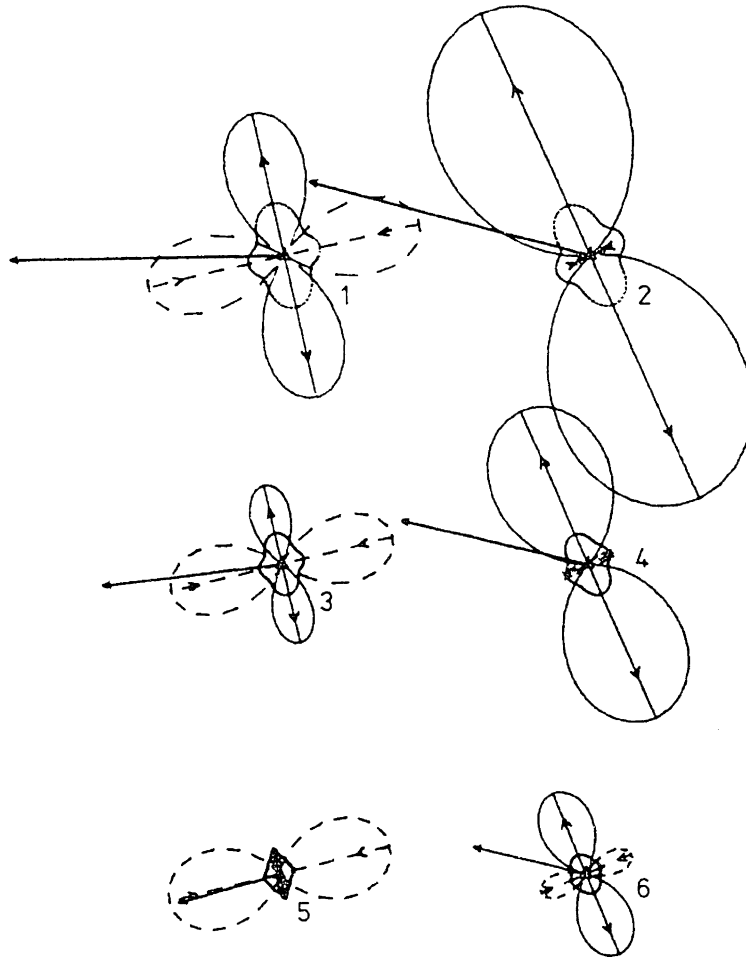


Figure 5.6

Strain pedal-curves and principal axes of strain

Map scale: 1:400000. Relative displacements: arrows (1:20).  
 Extension/contraction as a function of the azimuth: radial distance to  
 the solid/broken curve ( $5\text{mm} \hat{=} 1\mu\text{strain}$ ). Std.dev. of  
 Extension/contraction: radial distance to heavy curve.

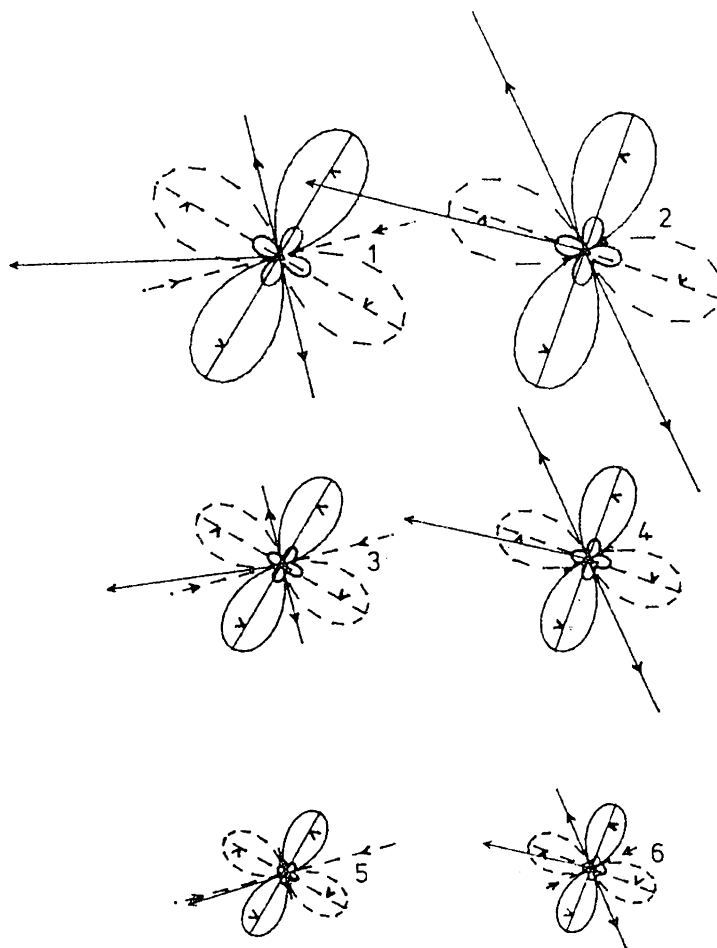


Figure 5.7

Shear-rosettes, axes of maximum shear and principal axes of strain .

Map scale: 1:400000. Relative displacements: arrows (1:20).  
 Left/right lateral tensor shear as a function of the azimuth: radial  
 distance to solid/broken curve ( $5\text{mm} \hat{=} 1\mu\text{strain}$ ). Std.dev. of shear:  
 radial distance to heavy curve.

## SECTION 6

## LEAST-SQUARES APPROXIMATION

6.1 General Considerations

The method of repeated observation of kinematic horizontal networks provides information on relative displacements associated with a limited number of material points (stations) and with a finite number of instants of time (observation epochs). Let us assume that the deformation of the crust can be represented by an approximation function in space and time which is continuous and continuously differentiable with respect to the coordinates as well as with respect to time. Limited discontinuities in space (along fault lines) and in time (at instants of seismic events) will, in some cases, be considered by extending the approximation function. The strain tensor field varying in space and time is considered the basic representation of the sought crustal deformation.

The problem of least-squares approximation to be solved can be defined as follows:

Given a discrete, time varying vector-field at a number of points and at a finite series of time, find another function of prescribed general form in space and time which approximates the given function in the least-squares sense. Predict the gradient matrix of the approximating vector function at a number of prescribed points and instants of time.

The choice of the approximation functions will first be discussed in this section. Based on the theory of Hilbert space optimization, linear forms, or generalized polynomials, are used in the general formulation of the approximation problem. No choice of the analytical shape of the space and time functions is made at this stage of mathematical formulation. Any set of linearly independent base functions of continuous or discontinuous kind may be chosen. The selection may be arbitrary, or may ideally reflect the physical behaviour of the crustal material.

The main objective of the present method of polynomial modeling is to discover the most significant trend (signal) in the time varying, relative displacement field. At the same time, local irregularities in space and small fluctuations in time (noise), which are likely to be caused by random observation errors, have to be filtered out. A statistical test procedure is applied to test whether or not a determined coefficient is statistically different enough from zero to be included in the model. Such a test is best performed in an orthogonal or orthonormal solution space. The main advantage of orthogonal coefficient spaces is that the normal equations are no longer interdependent; they can each be solved separately. The resulting coefficients are statistically independent and can thus be tested individually.

In general, the selected system of base functions is not orthogonal. Any such system can, however, be transformed into an orthogonal or orthonormal system through an orthogonalization process, such as the

Gram-Schmidt process (Schwarz et al.,1972). After rejecting the non-significant orthonormal coefficients, the remaining set of coefficients is transformed back to the original coefficient space.

The real model of the kinematic network adjustment, as it is discussed in Section 3, provides the functional, as well as the statistical relationship between the original geodetic observations and the discrete, relative displacement field. This model is to be combined with the approximation model formulated in complex vector spaces. Least-squares adjustment models with complex observation, function and parameter spaces can be solved either directly, using the least-squares norm (6.3) defined in complex vector space, or conventionally, after re-defining the model in real vector spaces. If linear constraints among the real or imaginary parts of the parameters have to be introduced, as in the present approximation model, the second approach is clearly advantageous. The straight-forward combination of the network model with the re-defined real approximation model is presented in Section 7.

## 6.2 Complex Approximation Function

The model of the least-squares approximation of a time varying vector field is best developed in the following two steps:

- 1) First an approximation function linear in time is chosen, which approximates a discrete vector field linear in time.

- 2) The approximation function in space is then extended, taking into account the time variations.

### 6.2.1 Approximation Function in Space

We adopt a complex valued approximation function, piecewise continuous within certain regions delimited by active fault lines

$$h : z \rightarrow h(z) \in \mathbb{C} \quad (6.1)$$

Let the discrete displacement field be given by the discrete, complex function

$$w_k : z_k \rightarrow w_k(z_k) \quad ; \quad k = 1, 2, \dots, n_p \quad (6.2)$$

where:  $z_k \in \mathbb{C}$  ... complex coordinates of point  $P_k$

$w_k \in \mathbb{C}$  ... complex displacement of point  $P_k$ .

The function  $h(z)$  is to be found so that it approximates  $w_k(z_k)$  in the least-squares sense.

A function  $h(z)$  is said to be the best approximating one, in the least-squares sense, if its coefficients are such that the distance

$$\rho^2(w, h) = [w_k(z_k) - h(z_k)] [\bar{w}_k(z_k) - \bar{h}(z_k)] \quad (6.3)$$

(where  $\rho \in \mathbb{R}^+$  is least-squares norm) is minimized (Vaníček and Wells, 1972).

A comprehensive outline of the theory of least-squares approximation is provided in Appendix II.

The approximation function (6.1) possesses the complex differential



(4.20)

$$dh = 1/2(h_x - ih_y) dz + 1/2(h_x + ih_y) \bar{dz} \quad (6.4)$$

knowing from eqn. (4.22) that the first term vanishes if  $h(z)$  is anti-holomorphic and the second term vanishes if  $h(z)$  is holomorphic,  $h(z)$  is chosen as follows:

$$h(z) = g_c(z) + g_a^*(z) \quad (6.5)$$

$$\text{or } h(z, \bar{z}) = g_c(z) + g_a(\bar{z}) \quad (6.6)$$

where  $g_c : c \rightarrow g_c(c) \in \mathbb{C}$

and  $g_a : c \rightarrow g_a(c) \in \mathbb{C}$  are both holomorphic.

It is to be noted that if

$g : c \rightarrow g(c)$  is holomorphic,

$g^* : c \rightarrow g^*(c) = g(\bar{c})$  is anti-holomorphic.

Function (6.5) is a non-analytic function composed of a holomorphic and an anti-holomorphic term. The first term describes the conformal mapping:  $z \rightarrow g_c(z)$ , whereas the second expresses the anti-conformal mapping:  $z \rightarrow g_a^*(z) = g_a(\bar{z})$ . In eqn. (6.6), the same function is re-written by using complex conjugate coordinates  $(z, \bar{z})$  (Spiegel, 1974).

The complex differential (4.20) of  $h(z)$  is

$$dh(z) = dg_c(z) + dg_a^*(z) \quad (6.8)$$

$$\text{where: } dg_c(z) = 1/2 \left( \frac{\partial g_c(z)}{\partial x} - i \frac{\partial g_c(z)}{\partial y} \right) dz + 0 \cdot \bar{dz} \quad (6.9a)$$

$$dg_a^*(z) = 0 \cdot dz + 1/2 \left( \frac{\partial g_a^*(z)}{\partial x} + i \frac{\partial g_a^*(z)}{\partial y} \right) \cdot \bar{dz} \quad (6.9b)$$

$$= dg_a(\bar{z}) = 0 \cdot dz + 1/2 \left( \frac{\partial g_a(\bar{z})}{\partial x} + i \frac{\partial g_a(\bar{z})}{\partial y} \right) \cdot \bar{dz} \quad (6.9c)$$

from which follows

$$\begin{aligned} dh(z, \bar{z}) &= dg_c(z) \cdot dz + dg_a(\bar{z}) \cdot \bar{dz} \quad (6.10) \\ &= \varphi(z) \cdot dz + \psi(\bar{z}) \cdot \bar{dz} . \end{aligned}$$

The following generalized complex polynomials are chosen instead of

$g_c(z)$  and  $g_a(\bar{z})$  for their computational advantages

$$g_c(z) = \sum_{i=1}^n a_i f_i(z) = \underline{\Phi}_{(n)}(z) \cdot \underline{a} \quad (6.11a)$$

$$g_a(\bar{z}) = \sum_{i=1}^m b_i f_i(\bar{z}) = \underline{\Phi}_{(m)}(\bar{z}) \cdot \underline{b} \quad (6.11b)$$

where:  $\underline{\Phi}_{(n)}(c) = \{f_1(c), f_2(c), \dots, f_n(c)\} \in \mathbb{C} \dots$  functional base (6.12)

$\underline{a} \in \mathbb{C}^n \dots$  coefficient vector  
 $\substack{n,1$

$\underline{b} \in \mathbb{C}^m \dots$  coefficient vector ,  
 $\substack{m,1$

which yields the complex, generalized approximation polynomial in space

$$h_{(n,m)}(z, \bar{z}) = \underline{\Phi}_{(n)}(z) \cdot \underline{a} + \underline{\Phi}_{(m)}(\bar{z}) \cdot \underline{b} \quad (6.13)$$

with its differential

$$\begin{aligned} dh_{(n,m)}(z, \bar{z}) &= 1/2 \left( \frac{\partial \underline{\Phi}_{(n)}(z)}{\partial x} - i \frac{\partial \underline{\Phi}_{(n)}(z)}{\partial y} \right) \underline{a} dz + 1/2 \left( \frac{\partial \underline{\Phi}_{(m)}(\bar{z})}{\partial x} + i \frac{\partial \underline{\Phi}_{(m)}(\bar{z})}{\partial y} \right) \underline{b} d\bar{z} \quad (6.14) \\ &= \frac{d \underline{\Phi}_{(n)}(z)}{dz} \underline{a} dz + \frac{d \underline{\Phi}_{(m)}(\bar{z})}{d\bar{z}} \underline{b} d\bar{z} \\ &= \underline{\Phi}'_{(n)}(z) \cdot \underline{a} dz + \underline{\Phi}'_{(m)}(\bar{z}) \cdot \underline{b} d\bar{z} . \end{aligned}$$

The complex strain components are found from:

$$\varphi(z) = \underline{\Phi}'_{(n)}(z) \underline{a} \quad (6.15a)$$

$$\psi(z) = \underline{\Phi}'_{(m)}(\bar{z}) \underline{b} . \quad (6.15b)$$

### 6.2.2 Modeling the Time Variation

The temporal variations of the displacement field are accounted for by the following approximation polynomial

$$h_{(n,m,l)}(z, \bar{z}, t) = \left\{ \underline{\Phi}_{(n)}(z) \underline{A} + \underline{\Phi}_{(m)}(\bar{z}) \underline{B} \right\} \cdot \underline{T}^T(t) \quad (6.16)$$

where:  $\underline{A} \dots$  coefficient matrix ;  $a_{ik} \in \mathbb{C}$   
 $\substack{n,1$

$\underline{B} \dots$  coefficient matrix ;  $b_{ik} \in \mathbb{C}$   
 $\substack{m,1$

and  $\underline{\Phi}$  is the spatial component as defined in eqn. (6.12) and

$$\underline{T}_{(l)}(t) = \{\tau_1(t), \tau_2(t), \dots, \tau_l(t)\} ; \underline{T}_{(l)} \in \{\mathbb{R} \rightarrow \mathbb{R}^l\} \quad (6.17)$$

is the temporal component of the functional base.

The choice of the temporal component  $\underline{T}(t)$  of the base functions implies the temporal behaviour of the deformation. Certain kinds of time functions suitable for the crustal analysis will be discussed in Sub-section 6.4 .

### 6.3 Functions in Space

Any set of functions  $\{f_1(c), f_2(c), \dots, f_n(c)\}$  , containing  $n$  linearly independent analytic functions:  $f_i : c \rightarrow f_i(c)$  in the complex functional space, can be chosen as the spatial component of the functional base of the generalized approximation polynomial.

#### 6.3.1 Continuous Functions

If the section of the earth's crust under consideration was an ideal elastic body, its relative displacement field would be continuous and continuously differentiable. Phenomena, such as fractures and fault creep, which are known to cause local discontinuities in the displacement field occur in seismically active areas. However, a continuous approximation function is used as the basic model in this study. Discontinuities at prescribed locations are being accounted for by additional terms of the generalized polynomial in space (cf. 6.3.2).

The spatial component of the functional base

$$\underline{\Phi}_{(n)} = \{1, c, c^2, \dots, c^n\} \quad ; \quad \underline{\Phi}_{(n)} \in \{C \rightarrow C^n\} \quad (6.18a)$$

defines the complex algebraic polynomial of degree n

$$p_{(n)}(c) = \sum_{i=0}^n a_i c^i = \underline{\Phi}_{(n)} \cdot \underline{a} \quad \in C \quad (6.18b)$$

which is chosen for its computational advantage.

### 6.3.2 Modeling Discontinuities Along Known Faults

In a kinematic network which straddles active tectonic faults, the discontinuous part of the relative displacement field may be mainly responsible for the network distortions. Continuous space functions are in this case not adequate to model the relative motion.

One straight-forward way to approximate such local discontinuities along known faults is to decompose the deformation into relative rigid block motions (relative translations and rotations). For this purpose, the crust under investigation has to be subdivided into a number of crustal blocks. Relative rigid block motion parameters are introduced for each pair of adjacent blocks.

In the case of actively moving transcurrent faults, relative rigid block translation seems to be by far the most predominant part in the relative discontinuous displacement field. There may also be discontinuities present in rotation, shear and other strain components. Individual, spatially homogeneous or non-homogeneous strain in each block can be taken into account in the same way as rigid block

translation. In order to keep the approximation model in this study as simple as possible, we assume, however, that all non-translational discontinuities can be adequately approximated by continuous space functions.

#### Masking Functions:

The approximation function in space (6.13) is extended by the following discontinuous, complex masking functions

$$f_j(z) = \begin{cases} 0 & \text{if } z \notin B_j \\ 1/2 \exp(i\alpha_j) & \text{if } z \in l_j ; j=n+1, n+2, \dots, n+n_B \\ \exp(i\alpha_j) & \text{if } z \in B_j \end{cases} \quad (6.19)$$

where:  $\underline{\Phi} = \{f_1, f_2, \dots, f_{n+n_B}\}$  ... spatial component of the base function

$B_j$  ... set of all  $z$  corresponding to points within block  $B_j$

$l_j$  ... set of all  $z$  corresponding to points on polygon  $l_j$

$\alpha_j$  ... bearing of fault line  $l_j$

$n$  ... number of continuous coefficients

$n_B$  ... number of crustal blocks

(cf. Figure 6.1).

The true faults, known from geological maps, have to be generalized by straight lines. The real part of the unknown coefficient corresponding to  $f_j$  expresses the component of the fault-slip in the fault direction  $\alpha_j$ , whereas the imaginary part describes the relative displacement perpendicular to the fault. This model allows the approximation of either unrestricted relative block translations, or relative block translations constrained to the fault strike.

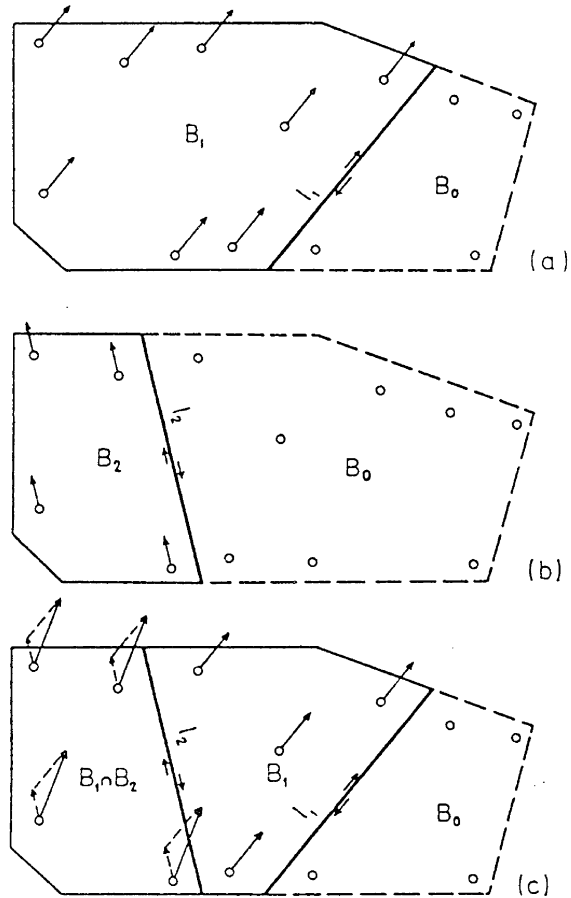


Figure 6.1

Model for block translations using complex masking functions

(a) Translation of block  $B_1$ , relative to to block  $B_0$ ; (b) Translation of block  $B_2$ , relative to block  $B_0$ ; (c) Superposition of two translations.

## 6.4 Time Functions

### 6.4.1 Linear and Piecewise Linear Time Functions

There are many cases in which a linear time function

$$p_{(1)}(t) = a_1 t \quad (6.20)$$

(with the temporal component of the base function

$$T_{(1)}(t) = \{\tau_1(t)\} = \{t\} )$$

is the only reasonable choice for the approximation model. If a kinematic network has been re-observed only two or three times, only a linear trend of the crustal deformation in time may be detectable. In the two-epoch case, this constant velocity model is obviously the sole choice.

The linear time model implies a time invariant velocity field and, subsequently, a time invariant strain-rate tensor field. In seismically active areas, the temporal behaviour of the deformation is too complex to be portrayed by a linear model. The linear time approximation provides only a general trend. The accumulation and release of strain associated with seismic events, which is one interesting phenomenon the seismologist is looking for, is obscured by this simple model.

In the multi-epoch case, a piecewise linear time function could be introduced. The piecewise linear temporal component of the base is composed of a series of linear functions

$$T_k(t) = \tau_k(t) = \begin{cases} t & ; t \in [t_{k-1}, t_k] \\ 0 & ; t \notin [t_{k-1}, t_k] \end{cases} ; k=1,2,\dots,l \quad (6.21)$$

where the domain of each is defined by the interval  $[t_{k-1}, t_k]$ ;  $k=1,2,\dots,l$ . The piecewise linear time function is treated as a special case of the episodic time function discussed in 6.4.3, with  $t_{k-1}$  and  $t_k$  defining the beginning and the end of the  $l$  episodes. If little is known a priori about the temporal behaviour of the deformation, the piecewise linear time model may be a helpful tool in detecting episodes of spasmodic motions.

#### 6.4.2 Continuous Time Functions

The temporal component of the functional base

$$\underline{T}_{(l)} = \{t, t^2, \dots, t^l\} \quad (6.22)$$

defines the real algebraic time polynomial

$$\underline{p}_{(l)} = \sum_{i=1}^l a_i t^i = \underline{T}_{(l)} \underline{a} \quad (6.23)$$

where  $\underline{a} \in R^l$  is a real coefficient vector.

The proper degree  $l$  of the time polynomial is difficult to select. There is a theoretical limit for  $l$  which follows from the theory of polynomial interpolation (Henrici and Huber, 1969)

$$l \leq n_e - 1 \quad (6.24)$$

where  $n_e$  is the number of (complete) epochs. In fact,  $l$  should always be much lower than  $n_e - 1$  to avoid spurious oscillations.



## 6.4.3 Episodic Time Functions

In order to model episodic motions which are expected to occur in relation to seismic events, the polynomial time function (6.23) is extended by the following episodic terms (Vaníček et al., 1979)

$$\tau_k(t) = \begin{cases} 0 & \text{if } t < b_k \\ (t-b_k)/(e_k-b_k) & \text{if } b_k \leq t < e_k ; k=1, 2, \dots, n_s \\ 1 & \text{if } t \geq e_k \end{cases} \quad (6.25)$$

where:  $b_k$  ... beginning of episode

$e_k$  ... end of episode (not to confuse with strains  $e_{xx}$ )

$n$  ... degree of algebraic polynomial

$n_s$  ... number of episodes.

The time intervals  $[b_k, e_k]$ ;  $k=1, 2, \dots, n_s$  of the expected episodic motions, in which eqn. (6.25) is assumed to be linear, have to be defined before the approximation. Eqn. (6.25) expresses the piecewise linear function (6.21) for a series of long intervals  $[b_k, e_k]$  and is similar to the Heaviside function (Henrici and Jeltsch, 1977) for

$$e_k - b_k \ll 1.$$

## SECTION 7

## SIMULTANEOUS NETWORK ADJUSTMENT AND STRAIN APPROXIMATION

7.1 General Concept

The possibilities of simultaneously combining the least-squares adjustment of kinematic networks with the complex strain approximation have been studied. A mathematical model will be derived in this section which directly relates the geodetic observations to the unknown coefficients of the strain approximation.

The observations of each epoch are introduced into separate network adjustments. If networks of some epochs suffer from formulation or configuration defects, their singular normal equation matrices are computed, but no least-squares solution is sought. Taking advantage of the redundancy in the networks of each epoch, the observations are screened for blunders and outliers. The functional model, as well as the statistical model, and all residuals of the adjustment are statistically tested. The normal equations of each epoch are stored and subsequently used for the multi-epoch strain approximation.

An attempt is made in this chapter to provide a comprehensive outline of the mathematical model of the developed method. Details, such as options for the three-dimensional adjustment and for simultaneous estimation of additional nuisance parameters, will be omitted for the sake of a transparent description. A summary of the complete

mathematical formulation, on which the computer program CRUSTRAIN (cf. Appendix III) was based, is provided in the external Appendix.

## 7.2 Network Adjustment of Individual Epochs

### a) Geodetic Observations of Epoch $i$ :

Let us consider a set of  $n$  geodetic observations

$$\underline{l}_i(t_i) \text{ with the covariance matrix } \underline{C}_i^{(i)}$$

belonging to the observation epoch  $i$  of a  $n_e$ -epoch kinematic network. It is assumed that the observation campaign was carried out almost instantaneously at time  $t_i$  and that all observations have properly been reduced to a conformal mapping plane.

The set of observations  $\underline{l}_i$  defines a configuration which will be called 'network of epoch  $i$ '. No difference will be made between an extended network:  $n \gg 1$  or a configuration of only 2 or 3 stations:  $n = 1$ .

### b) Parameter Vector:

The vector  $\underline{d}_i(t_i)$  contains the instantaneous corrections to the approximate coordinates of all stations of the kinematic network at time  $t_i$ .

### c) Minimum Constraints:

By keeping the coordinates of one station (e.g. the 1st station) fixed at all times, an arbitrary set of minimum constraints is introduced

$$x_1^{(i)} = y_1^{(i)} = 0 \quad ; \quad i=1,2,\dots,n_e \quad (7.1)$$

d) Observation Equations:

The linearized mathematical model is given by the observation equations

(2.1)

$$\underline{v}_i = \underline{A}_i \underline{d}_i - \underline{l}_i \quad (7.2)$$

e) Normal Equations:

The least-squares principle yields the normal equations

$$\underline{N}_i \hat{\underline{d}}_i - \underline{u}_i = \underline{0} \quad (7.3)$$

where  $\underline{N}_i = \underline{A}_i^T \underline{C}_i^{(i)-1} \underline{A}_i$  and  $\underline{u}_i = \underline{A}_i^T \underline{C}_i^{(i)-1} \underline{l}_i$ .

f) Least-Squares Estimates of Positions of Epoch  $i$ :

If the network of epoch  $i$  does not suffer from formulation or configuration defects, the following least-squares estimates are found:

$$\hat{\underline{d}}_i = \underline{N}_i^{-1} \underline{u}_i \quad (7.4)$$

$$\hat{\sigma}_{o_i}^2 = \frac{\underline{v}_i^T \underline{C}_i^{(i)-1} \underline{v}_i}{df_i} \quad ; \quad df_i = \dim(\underline{l}_i) - \dim(\underline{d}_i) \quad (7.5)$$

$$\underline{C}_{\hat{\underline{d}}_i}^{(i)} = \underline{N}_i^{-1} \quad (\sigma_o^2 = 1, \text{ known}) \quad (7.6)$$

$$\text{and} \quad \hat{\underline{C}}_{\hat{\underline{d}}_i}^{(i)} = \hat{\sigma}_{o_i}^2 \underline{N}_i^{-1} \quad (\sigma_o^2 \text{ unknown}) \quad (7.7)$$

### 7.3 Model for the Approximation

Let us consider the horizontal kinematic network with  $n_p$  stations, of which the approximate complex coordinates are given by

$$\underline{z}^o{}^T = [z_1^o, z_2^o, \dots, z_{n_p}^o] \quad (7.8)$$

The network has been repeatedly observed at  $n_e$  epochs of observations at times

$$\underline{t}^T = [t_1, t_2, \dots, t_{n_e}] \quad (7.9)$$

Let us further assume that the observations at each epoch have been adjusted by using the least-squares model (7.1 to 7.7) and an arbitrarily chosen set of minimum constraints (the choice does not really matter). The equation

$$z_i^{(i)} = 0 \quad ; \quad i=1,2,\dots,n_e \quad (7.10)$$

could be a typical choice.

The resulting coordinates of each epoch  $i$  are denoted

$$\underline{z}_i^T = [z_i^{(i)}, z_2^{(i)}, \dots, z_{n_p}^{(i)}] \quad (7.11)$$

which may be regarded as a data series in space and time. With the unknown, initial positions

$$\underline{z}_0^T = [z_{0_1}, z_{0_2}, \dots, z_{0_{n_p}}] \quad (7.12)$$

(with respect to an arbitrary reference time  $t_0$ ) the set of relative complex displacements

$$\underline{w}_i(t_i) = \underline{z}_i(t_i) - \underline{z}_0(t_0) \quad (7.13)$$

follows.

After selecting a functional base, the approximation function in space and time (6.13) is re-arranged as follows:

$$h_{(n,m,l)}(z, \bar{z}, t) = \underline{f}(z, \bar{z}, t) \cdot \underline{\lambda}^* \quad (7.14)$$

where  $\underline{f}(z, \bar{z}, t) = \{ \tau_1(t) [\underline{\Phi}_{(n)}(z), \underline{\Phi}_{(m)}(\bar{z})], \tau_2(t) [\underline{\Phi}_{(n)}(z), \underline{\Phi}_{(m)}(\bar{z}), \dots$

$$\dots, \tau_l(t) [\underline{\Phi}_{(n)}(z), \underline{\Phi}_{(m)}(\bar{z})] \} \in C^u \quad (7.15)$$

$$\underline{\lambda}^* = [a_{11} \ a_{12} \dots \ a_{1l} \ b_{11} \ b_{12} \dots \ b_{1l} \ a_{21} \ a_{22} \dots \ b_{m1}] \in C^u$$

$$u = (n+m) \cdot l .$$

The function  $h(z, \bar{z}, t)$ , which is called an approximant, is a scalar product in the  $u$ -dimensional complex functional space;  $f(z, \bar{z}, t)$  is the

functional base and  $\underline{\lambda}^*$  is a complex coefficient vector.

The linear form

$$\underline{z}_i + \underline{y}_i^* = \underline{z}_0 + \underline{F}_i^{*\top} \underline{\lambda}^* \quad ; \quad i = 1, 2, \dots, n_e \quad (7.16)$$

where:

$$\underline{F}_i^{*\top} = \begin{bmatrix} \underline{f}_1^\top(z, \bar{z}, t_i) \\ \underline{f}_2^\top(z, \bar{z}, t_i) \\ \vdots \\ \underline{f}_{n_p}^\top(z, \bar{z}, t_i) \end{bmatrix} ; \quad i=1, 2, \dots, n_e \quad \dots \text{ Vandermonde's matrix} \quad (7.17)$$

$\underline{y}_i^*$  ... complex residual vector

is the complex model of the least-squares approximation.

For reasons discussed in Sub-section 6.1, the linear form (7.16) is reformulated in real vector notation

$$\underline{d}_i + \underline{y}_i = \underline{d}_0 + \underline{F}_i^\top \underline{\lambda} \quad ; \quad i = 1, 2, \dots, n_e \quad (7.18)$$

where:  $\underline{d}_i$  ... real vector of coordinate increments at time  $t_i$

$\underline{d}_0$  ... real vector of initial coordinate increments at  
reference time  $t_0$

$\underline{\lambda}$  ... real coefficient vector

$\underline{F}_i$  ... real Vandermonde matrix

$\underline{y}_i$  ... real vector of coordinate residuals.

(Note: The dimension of the vectors in eqn. (7.18) is twice the dimension of the complex vectors in eqn. (7.16).)

The relationship between the product of two complex numbers and its equivalent expression in matrix form was given in Sub-section 4.2.2, (cf. (4.24),(4.25)). The complex element  $a_j$  of each vector  $\underline{a}$  in (7.18) is simply replaced by a real subvector  $(\text{Re}(a_j), \text{Im}(a_j))$ , whereas

each element in the Vandermonde matrix  $f_{jk} \in \mathbb{C}$  is replaced by the submatrix

$$\underline{F}_{jk} = \begin{bmatrix} \operatorname{Re}(f_{jk}) & -\operatorname{Im}(f_{jk}) \\ \operatorname{Im}(f_{jk}) & \operatorname{Re}(f_{jk}) \end{bmatrix} \quad (7.19)$$

The Vandermonde matrix  $\underline{F}_i$  can be regarded as a special case of a design matrix (Vaníček and Krakiwsky, 1982). Thus eqn. (7.19) re-written in the form of the least-squares model explicit in  $\underline{l}$  reads

$$\begin{bmatrix} y_1 \\ y_2 \\ \cdot \\ \cdot \\ y_{n_e} \end{bmatrix} = \begin{bmatrix} \underline{I} & \vdots & \underline{F}_1^T \\ \underline{I} & \vdots & \underline{F}_2^T \\ \cdot & \vdots & \cdot \\ \cdot & \vdots & \cdot \\ \underline{I} & \vdots & \underline{F}_{n_e}^T \end{bmatrix} \cdot \begin{bmatrix} \underline{d}_0 \\ \lambda \end{bmatrix} - \begin{bmatrix} \underline{d}_1 \\ \underline{d}_2 \\ \cdot \\ \cdot \\ \underline{d}_{n_e} \end{bmatrix} \quad (7.20)$$

$$\underline{v} = \underline{A} \cdot \underline{x} - \underline{l}$$

#### 7.4 Combined Model

The vectors of adjusted coordinates which are obtained from the individual network adjustments

$$\hat{\underline{d}}_i ; \quad i=1,2,\dots,n_e$$

with their covariance matrices

$$C_{\hat{\underline{d}}_i} \text{ or } \hat{C}_{\hat{\underline{d}}_i}$$

represent the data series (and its metrization) of the approximation in space and time.

The least-squares models of the individual adjustments of each epoch and the model of the least-squares approximation can be combined to one simultaneous adjustment model

$$f_s(\underline{\lambda}, \underline{l}_1, \underline{l}_2, \dots, \underline{l}_{n_e}) = \underline{0} . \quad (7.21)$$

This model provides the functional relationship between the original

geodetic observations  $\underline{l}_i$  and the unknown coefficients  $\underline{\lambda}$  of the approximation in space and time.

The normal equations of the approximation in hypermatrix form are obtained if the least-squares principle is applied to the approximation model (7.20)

$$\sum_{i=1}^{n_e} \begin{bmatrix} \underline{C}_i^{-1} & \underline{C}_i^{-1} \underline{F}_i^T \\ \underline{F}_i \underline{C}_i^{-1} & \underline{F}_i \underline{C}_i^{-1} \underline{F}_i^T \end{bmatrix} \begin{bmatrix} \hat{\underline{d}}_0 \\ \hat{\underline{\lambda}} \end{bmatrix} - \sum_{i=1}^{n_e} \begin{bmatrix} \underline{C}_i^{-1} \hat{\underline{d}}_i \\ \underline{F}_i \underline{C}_i^{-1} \hat{\underline{d}}_i \end{bmatrix} = \underline{0}, \quad (7.22)$$

where  $\underline{C}_i = \underline{C}_{\hat{\underline{d}}_i}$  or  $\hat{\underline{C}}_{\hat{\underline{d}}_i}$ .

Considering eqn. (7.3 to 7.7) yields

$$\sum_{i=1}^{n_e} \begin{bmatrix} \underline{N}_i & \underline{N}_i \underline{F}_i^T \\ \underline{F}_i \underline{N}_i & \underline{F}_i \underline{N}_i \underline{F}_i^T \end{bmatrix} \begin{bmatrix} \hat{\underline{d}}_0 \\ \hat{\underline{\lambda}} \end{bmatrix} - \sum_{i=1}^{n_e} \begin{bmatrix} \underline{N}_i \underline{N}_i^{-1} \underline{u}_i \\ \underline{F}_i \underline{N}_i \underline{N}_i^{-1} \underline{u}_i \end{bmatrix} = \underline{0}. \quad (7.23)$$

The product  $\underline{N}_i \underline{N}_i^{-1}$  in (7.23) requires careful consideration. The inverse  $\underline{N}_i^{-1}$  exists only if the network of the epoch  $i$  does not suffer from formulation or configuration defects. If  $\underline{N}_i$  is singular, the product is a singular unit matrix (Bjerhammar, 1973) which may, however, be replaced by the limit

$$\lim_{c \rightarrow 0} (\underline{N}_i + c \underline{I})(\underline{N}_i + c \underline{I})^{-1} = \underline{I}. \quad (7.24)$$

This limit clearly exists if  $(\underline{N}_i + c \underline{I})$  with  $0 < c < 1$  is regular, which is always the case for normal equation matrices of networks with formulation or configuration defects. A proof using generalized inverse techniques is given in Appendix IV.

After eliminating the parameter subvector  $\hat{\underline{d}}_0$ , there follow the normal equations (Krakiwsky, 1975)



$$\begin{aligned} [\underline{N}_{22} - \underline{N}_{21} \underline{N}_{11}^{-1} \underline{N}_{12}] \hat{\underline{\lambda}} + \underline{u}^{(2)} - \underline{N}_{21} \underline{N}_{11}^{-1} \underline{u}^{(1)} &= \underline{0} \\ \underline{N}_{11} \hat{\underline{\lambda}} + \underline{u} &= \underline{0} \end{aligned} \quad (7.25)$$

$$\begin{aligned} \text{where: } \underline{N}_{11} &= \sum_{i=1}^{n_e} \underline{N}_i, & \underline{N}_{12} &= \sum_{i=1}^{n_e} \underline{N}_i \underline{F}_i^T, & \underline{u}^{(1)} &= \sum_{i=1}^{n_e} \underline{u}_i \\ \underline{N}_{21} &= \sum_{i=1}^{n_e} \underline{F}_i \underline{N}_i, & \underline{N}_{22} &= \sum_{i=1}^{n_e} \underline{F}_i \underline{N}_i \underline{F}_i^T, & \underline{u}^{(2)} &= \sum_{i=1}^{n_e} \underline{F}_i \underline{u}_i. \end{aligned}$$

It should be noted that the matrix  $\underline{N}_{11}$  must not be singular:

$$\det(\underline{N}_{11}) = \det\left(\sum_{i=1}^{n_e} \underline{N}_i\right) \neq 0. \quad (7.26)$$

This condition becomes clear if one realizes that  $\underline{N}_{11}$  is the normal equation matrix of the time invariant model of the kinematic network. This model must not suffer from formulation or configuration defects.

Before we discuss the solution of the simultaneous least-squares model, let us consider the normal equations of the special types of kinematic networks with design and statistical model invariant in time. In these cases, the individual design matrices, the covariance matrices and subsequently the normal equation matrices are all invariant in time:

$$\begin{aligned} \underline{A}_1 &= \underline{A}_2 = \dots = \underline{A}_{n_e} = \underline{A} \\ \underline{C}_1 &= \underline{C}_2 = \dots = \underline{C}_{n_e} = \underline{C} \\ \underline{N}_1 &= \underline{N}_2 = \dots = \underline{N}_{n_e} = \underline{N}. \end{aligned} \quad (7.27)$$

Under these conditions, the submatrices in eqn. (7.25) are given by:

$$\begin{aligned} \underline{N}_{11} &= n_e \cdot \underline{N} & \underline{N}_{12} &= \underline{N} \sum_{i=1}^{n_e} \underline{F}_i^T & \underline{u}^{(1)} &= \sum_{i=1}^{n_e} \underline{u}_i \\ \underline{N}_{21} &= \sum_{i=1}^{n_e} \underline{F}_i \cdot \underline{N} & \underline{N}_{22} &= \sum_{i=1}^{n_e} \underline{F}_i \cdot \underline{N} \cdot \sum_{i=1}^{n_e} \underline{F}_i^T & \underline{u}^{(2)} &= \sum_{i=1}^{n_e} \underline{F}_i \underline{u}_i. \end{aligned} \quad (7.28)$$

With  $\underline{N}_{11}^{-1} = 1/n_e \underline{N}^{-1}$  and eqn. (7.25), the normal equations can be written as follows:

$$(n_e - 1)/n_e \sum_{i=1}^{n_e} \underline{F}_i \cdot \underline{N} \cdot \sum_{i=1}^{n_e} \underline{F}_i^T \hat{\underline{\lambda}} + \sum_{i=1}^{n_e} (\underline{F}_i \underline{u}_i) - 1/n_e \sum_{i=1}^{n_e} \underline{F}_i \sum_{i=1}^{n_e} \underline{u}_i = \underline{0}. \quad (7.29)$$

In the two-epoch case this yields

$$1/2(\underline{F}_1 + \underline{F}_2) \underline{N} (\underline{F}_1 + \underline{F}_2)^T \hat{\underline{\lambda}} + 1/2(\underline{F}_1 - \underline{F}_2)(\underline{u}_2 - \underline{u}_1) = \underline{0} \quad (7.30)$$

$$(\underline{F}_1, +\underline{F}_2) \underline{N} (\underline{F}_1, +\underline{F}_2)^T \hat{\underline{\lambda}} - (\underline{F}_1, -\underline{F}_2) \underline{A}^T \underline{C}^{-1} (\underline{l}_2 - \underline{l}_1) = \underline{0}.$$

This expression is nothing other than the set of normal equations for differences of pairs of corresponding observations  $\Delta \underline{l} = \underline{l}_2 - \underline{l}_1$ .

### 7.5 Ortho-Normalization

The normal equations (7.25) have to be transformed into ortho-normal solution space in order to obtain statistically independent coefficients. The Gram-Schmidt ortho-normalization procedure can be applied to the normal equation matrix if it is in the form  $\underline{N} = \underline{A}^T \underline{A}$  or  $\underline{N} = \underline{A}^T \underline{W} \underline{A}$ , where  $\underline{W}$  denotes a diagonal weight matrix. In the more general case where  $\underline{W}$  is not diagonal, the method of Cholesky decomposition can be applied. It will be shown in Appendix II that the Cholesky decomposition of a symmetric, positive definite matrix  $\underline{N} = \underline{A}^T \underline{A}$  into the quadratic form  $\underline{N} = \underline{R}^T \underline{R}$ , (where  $\underline{R}$  is an upper-triangular matrix) is mathematically equivalent to the Gram-Schmidt ortho-normalization of the row-vectors of  $\underline{A}$ .

The orthonormalized normal equations with  $\underline{R}$  resulting from the Cholesky decomposition

$$\underline{N} = \underline{R}^T \underline{R} \quad (7.31)$$

are

$$(\underline{R}^{-1})^T \underline{R}^T \underline{R} \underline{R}^{-1} \hat{\underline{\lambda}}_0 - (\underline{R}^{-1})^T \underline{u} = \underline{0} \quad (7.32)$$

where  $\underline{R}$  is an upper-triangular matrix. From the above it follows that

$$\underline{S}^T \underline{S} \hat{\underline{\lambda}}_0 - (\underline{R}^{-1})^T \underline{u} = \underline{0} \quad (7.33)$$

where  $\underline{S}$  is ortho-normal and

$$\hat{\underline{\lambda}}_0 = (\underline{R}^{-1})^T \underline{u} \quad (7.34)$$

where  $\underline{\lambda}_0$  is the vector of orthonormal (Fourier-) coefficients.

The covariance matrix of these coefficients is

$$\underline{C}_{\hat{\lambda}_0} = \underline{I} \quad (\sigma_0^2 \text{ known}) \quad (7.35)$$

and 
$$\underline{\hat{C}}_{\hat{\lambda}_0} = \hat{C}_0^2 \underline{I} \quad (C_0^2 \text{ unknown}) . \quad (7.36)$$

### 7.6 Statistical Testing

The concept adopted for the selection of base functions is discussed in Sub-section 6.1. This selection and the choice of the degree of polynomials are, in general, rather arbitrary. For this reason, it should be borne in mind when the results are being assessed that some uncertainty always remains in the adopted model. The question, whether or not a certain base function  $f_j$  should have been considered in the model, can be answered after the corresponding coefficient  $\hat{\lambda}_j$  has been examined statistically. The testing is preferably performed on the orthonormal coefficients because of their property of statistical independence.

#### 7.6.1 Confidence Region of the Coefficient Vector

We postulate the original geodetic observations to be normally distributed. The original, as well as the ortho-normal coefficients, are simply linear combinations of the observations. It follows (Vaníček and Krakiwsky, 1982) that the ortho-normal coefficients are stochastic quantities with a multi-variate normal distribution:

$$\hat{\lambda}_{\lambda_0} = N(\xi; \hat{\lambda}_0, \mathbb{I}) \quad (7.37)$$

if  $\sigma_0^2$  is assumed to be known.

Using the  $\chi^2$ -distributed statistic

$$y = (\hat{\lambda}_0 - \lambda_0)^T (\hat{\lambda}_0 - \lambda_0) \quad (7.38)$$

the following probability statement, for a prescribed significance level  $\alpha$  and an  $u$ -dimensional solution space, can be written

$$\text{pr}((\hat{\lambda}_0 - \lambda_0)^T (\hat{\lambda}_0 - \lambda_0) \leq \xi_{y, 1-\alpha}) = 1 - \alpha, \quad (7.39)$$

where  $y$  is determined from the  $\chi^2$ -probability density function (p.d.f).

The confidence region associated with (7.39) is a hyper-sphere in the  $u$ -dimensional orthonormal solution space with radius  $\xi$  centered at  $\underline{0}$ .

### 7.6.2 Null Hypothesis

In order to test statistically whether the signal (trend) of a certain model, as estimated by the coefficient vector  $\hat{\lambda}_0$ , is significant or not on a prescribed level of significance, a null hypothesis is to be established. If there is no signal present in the data series, the expectation of each coefficient would be zero

$$H_0 : E(\hat{\lambda}_{0_i}) = 0 ; i=1,2,\dots,u. \quad (7.40)$$

If  $H_0$  is true, any strain which can be predicted from  $\hat{\lambda}_0$  is to be considered spurious and should be discarded.

## 7.6.3 Statistical Filtering Procedure

The property of ortho-normality of coefficients enables us to design very useful statistical test procedures. No matter how many coefficients we decide to discard, the rest remain unchanged. Each coefficient can thus be tested individually and in an arbitrary order. If those coefficients which are found to be insignificant are simply discarded, the remaining coefficients still represent the least-squares solution of the reduced functional model. Each individual ortho-normal coefficient  $\hat{\lambda}_0$  can thus be considered to define a different approximation model in a one-dimensional solution space. Based on eqn. (7.39), the following test of the null hypotheses:

$$H_0 : E(\hat{\lambda}_{0_i}) = 0 \quad ; \quad i=1,2,\dots,u \quad (7.41)$$

is performed:

$$\begin{cases} \text{if } \hat{\lambda}_{0_i} \leq \xi_{y,1-\alpha} & \dots H_0 \text{ accepted} \\ \text{else} & \dots H_0 \text{ rejected} \end{cases} \quad (7.42)$$

whereby the probability density function of  $y$  is the normal p.d.f. if  $\sigma_0^2$  is known and the student p.d.f. if  $\sigma_0^2$  is unknown.

If  $H_0$  is accepted, the base function  $f_i$  is to be discarded in the model. This is achieved by simply setting:

$$\begin{cases} \text{if } H_0 : \hat{\lambda}'_{0_i} = 0 \quad , \quad \sigma_{\hat{\lambda}'_{0_i}}^2 = 0 \\ \text{else} : \hat{\lambda}'_{0_i} = \hat{\lambda}_{0_i} \quad , \quad \sigma_{\hat{\lambda}'_{0_i}}^2 = 1 \end{cases} \quad (7.43)$$

the coefficient vector  $\hat{\lambda}'_0$  and its covariance matrix:  $\text{diag}(\sigma_{\hat{\lambda}'_{0_i}}^2)$  define the final approximation function in ortho-normal space, in which each base function is significant at the level  $\alpha$ .

#### 7.6.4 Test on the Quadratic Form $\hat{\lambda}_0^T \hat{\lambda}_0$

It should be noted that in the above statistical filtering procedure each coefficient is examined on its own, i.e. 'out of context' (Vaniček and Krakiwsky, 1982). The existence of the other elements is deliberately disregarded.

The following test is based on the probability statement (7.39) and tests simultaneously the entire set of ortho-normal coefficients with respect to  $H$  (7.40):

$$\begin{cases} \text{if } \hat{\lambda}_0^T \hat{\lambda}_0 \leq \xi_{\gamma, 1-\alpha} & \dots H_0 \text{ accepted} \\ \text{else} & \dots H_0 \text{ rejected} \end{cases} \quad (7.44)$$

where  $\gamma$  is obtained from the  $\chi^2$ -distribution if  $\sigma_0^2$  is known and from the  $F$  distribution if  $\sigma_0^2$  is unknown (Wells and Krakiwsky, 1971).

The statistical test (7.44) is a useful tool for finding out if any deformation has occurred within the area and time-span in question.

#### 7.7 Back-Transformation into Original Solution Space

The original, real coefficients are found from the transformation

$$\begin{aligned} \hat{\lambda} &= \underline{N}^{-1} \underline{u} \\ &= \underline{R}^{-1} (\underline{R}^{-1})^T \underline{u} \\ &= \underline{R}^{-1} \hat{\lambda}_0' \end{aligned} \quad (7.45)$$

The back-solution of the eliminated parameters  $\hat{\sigma}_0$  is found from (7.23)

$$\underline{N}_{11} \hat{\sigma}_0 + \underline{N}_{12} \hat{\lambda} - \underline{u}^{(1)} = \underline{0} \quad (7.46)$$

$$\hat{\underline{d}}_0 = - \underline{N}_{11}^{-1} (\underline{N}_{12} - \underline{u}^{(i)}) \quad (7.47)$$

where  $\hat{\underline{d}}_0$  are the predicted coordinate increments at the reference time  $t_0$ . The adjusted coordinate increments of each epoch of observation  $i$  are found from eqn. (7.20)

$$\hat{\underline{d}}_i = \hat{\underline{d}}_0 + \underline{F}_i^T \hat{\underline{\lambda}} \quad ; i = 1, 2, \dots, n_e. \quad (7.48)$$

Finally, the residuals of the original observations of each epoch can be found from eqn. (7.2)

$$\hat{\underline{v}}_i = \underline{A}_i \hat{\underline{d}}_i - \underline{l}_i \quad ; i = 1, 2, \dots, n_p, \quad (7.49)$$

and the estimate of the variance factor from

$$\hat{\sigma}_0^2 = \frac{\sum_{i=1}^{n_e} \hat{\underline{v}}_i^T \underline{C}_i^{-1} \hat{\underline{v}}_i}{df} \quad (7.50)$$

where:  $df = \sum_{i=1}^{n_e} n_i + n_c - \sum_{i=1}^{n_e} u_i - u_0 - u_3$

$n_i$  ... number of observations of  $i$ -th epoch

$n_c$  ... number of constrained Fourier coefficients

$u_i$  ... number of network nuisance parameters  
of  $i$ -th epoch

$u_0$  ... number of eliminated coordinates at time  $t_0$

$u_3$  ... number of real Fourier coefficients.

The covariance matrix of the original coefficients of the approximation is

$$\underline{\hat{C}}_{\underline{\lambda}} = \underline{R}^{-1} \underline{C}_{\underline{\lambda}_0} (\underline{R}^{-1})^T = \underline{R}'^{-1} (\underline{R}'^{-1})^T \quad ; (\sigma_0^2 \text{ known}) \quad (7.51a)$$

or:

$$\hat{\underline{C}}_{\underline{\lambda}} = \hat{\sigma}_0^2 \underline{R}'^{-1} (\underline{R}'^{-1})^T \quad ; (\sigma_0^2 \text{ unknown}) . \quad (7.51b)$$

### 7.8 Additional Nuisance Parameters

In some cases, the network scale of repeated trilateration networks may not be determined with great certainty. This may happen, for example, if different EDM-instruments had been used in different observation campaigns. Differences between the instrument scales may, in this case, bias the results of the strain analysis. A similar kind of difficulty may occur with systematic effects in the orientation of individual networks.

These problems can be circumvented by introducing additional constant conformal terms associated with each epoch of observation in eqn. (7.16). The mathematical formulation including these unknown nuisance parameters is outlined in the external Appendix.

### 7.9 Prediction in Space and Time

#### 7.9.1 Relative Displacements and Strain

The displacement field, relative to the fixed station and to the reference time  $t_0$ , can be predicted for any point  $z$  and at any instant of time  $t$  from the approximation function in space and time (7.14)

$$\hat{h}_{(n,m,l)}(z, \bar{z}, t) = \underline{f}(z, \bar{z}, t) \cdot \hat{\underline{\lambda}}^* \quad (7.52)$$

and the velocity field from

$$\dot{\hat{h}}_{(n,m,l)}(z, \bar{z}, t) = \dot{\underline{f}}(z, \bar{z}, t) \cdot \hat{\underline{\lambda}}^* \quad (7.53)$$

where  $\hat{\underline{\lambda}}^*$  is the complex analog to the coefficient vector and  $\dot{\underline{f}}(z, \bar{z}, t)$  is



the base according to eqn. (7.15) in which  $\bar{\tau}_k(t)$  is to be replaced by its time derivative  $\dot{\bar{\tau}}_k = \frac{d\bar{\tau}_k}{dt}$

The complex strain components are predicted from:

$$\mathcal{U}(z, t) = \underline{\Phi}'_{(m)}(z) \cdot \underline{A} \cdot \underline{\bar{T}}(t) \quad (7.54)$$

$$\mathcal{V}(\bar{z}, t) = \underline{\Phi}'_{(m)}(\bar{z}) \cdot \underline{B} \cdot \underline{\bar{T}}(t) \quad (7.55)$$

and the strain-rate components by:

$$\dot{\mathcal{U}}(z, t) = \underline{\Phi}'_{(m)}(z) \cdot \underline{A} \cdot \dot{\underline{\bar{T}}}(t) \quad (7.87)$$

$$\dot{\mathcal{V}}(\bar{z}, t) = \underline{\Phi}'_{(m)}(\bar{z}) \cdot \underline{B} \cdot \dot{\underline{\bar{T}}}(t) . \quad (7.88)$$

### 7.9.2 Statistical Estimates

The variance of the relative displacements and the velocities, as well as the variance of the real strain components, is simply found by applying the covariance law to the approximation function in its real form (7.18).

## SECTION 8

## TEST COMPUTATIONS

8.1 Concept of Numerical Testing and General Experience

A series of numerical tests, using simulated as well as real data, was performed with the developed mathematical models. The main objectives of these computations were as follows:

- 1) to confirm numerically the correctness of the mathematical model developed for the simultaneous network adjustment and least-squares approximation,
- 2) to test the developed software,
- 3) to gain experience with the application of complex, algebraic polynomials to the approximation of relative displacement fields,
- 4) to investigate the numerical treatment of singular approximation models.

Prior to the development of the program CRUSTRAIN, a computer program DACAP (Displacement Approximation by Complex Algebraic Polynomials) was written particularly for the approximation of displacement fields in space. This program was chiefly designed as a diagnostic tool for the trend-analysis of distortions in geodetic networks (Vaníček et al., 1981). The continuous approximation functions in space (cf.

6.3.1) and the statistical filtering procedures (cf. 7.6.3) are incorporated in this program. No further comment shall be made on this software and the diagnosis of geodetic networks in this work. A series of tests on the approximation in space were performed with this program. The experience gained from these tests is outlined as follows:

- The fitting of complex, algebraic polynomials of different degrees to discrete displacement fields gives numerically reasonable results up to degrees 20/20 of the conformal/anti-conformal polynomials, if sufficient data is provided.
- The danger of spurious oscillations of the strain in space increases towards the periphery of the area covered by data points.
- Small irregularities in displacement, which are encountered in the discrete displacement field, are filtered out satisfactorily by the least-squares approximation using statistical filtering.

## 8.2 Test with Simulated Networks

A series of tests using artificial data from simulated kinematic networks was performed with program CRUSTRAIN (cf. Table 8.1). The results of simultaneous network adjustments and strain approximations of two-epoch cases with formulation or configuration defects (test No.2 - 4) confirms the correctness of the mathematical model.

The developed method allows one to compute the four components of

uniform strain, even if the configurations of some epochs suffer from formulation or configuration defects (cf. Table 8.1, test No.2 and 3). Singularities are encountered in the normal equations of the simultaneous adjustment and approximation model if the time invariant model (cf. 7.4) suffers from formulation or configuration defects. It may also occur that the functions we have selected are not real base functions (cf. Table 8.1, test No.4).

From the experience with multi-epoch analyses, it was learned that it is sometimes difficult to avoid singularities caused by the ill-posing of the approximation problem. The following numerical procedure was thus introduced into the Cholesky square-root algorithm, which automatically sets indeterminable coefficients of the approximation model (having a defect of one kind or another) to zero. A numerical check is carried out on the reduced diagonal elements  $n_{ii}$  of the normal equation matrix  $\underline{N}$  before each reduction cycle. If  $n_{ii}$  is inferior to  $10^{-12}$ , a small weight  $p = 10^{-9}$  is added to the element. With this numerical manipulation, indeterminable coefficients are constrained to zero. As they will have a large variance, they will subsequently be removed by the statistical filtering procedure (cf. 7.6.3). This is the case in test No.4 (cf. table 8.1), where the indeterminable differential rotation is set to zero.

Note: The symbols used in Table 8.1 have the following meaning:

- $n_i, u_i$  ... number of observations and unknowns of each network
- $u_e$  ... number of eliminated station coordinates
- $u_c$  ... number of real approximation coefficients.

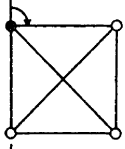
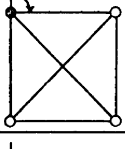
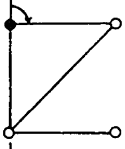
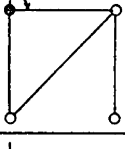
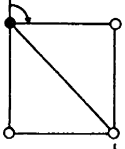
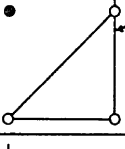
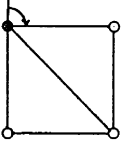
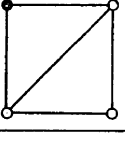

| Test configuration at epoch: |   | individual network adjustment |       |       |                              | time invariant model |            |                 | adjustment and approximation model |       |       |    |   |
|------------------------------|---|-------------------------------|-------|-------|------------------------------|----------------------|------------|-----------------|------------------------------------|-------|-------|----|---|
| No.                          |   | i                             | $n_i$ | $u_i$ | $def(N_i)$                   | $\sum n_i$           | $\sum u_i$ | $def(\sum N_i)$ | n                                  | $u_a$ | $u_c$ | df | $def(N)$                                  |
| 1                            |    | 1                             | 7     | 6     | 0                            | 14                   | 6          | 0               | 14                                 | 6     | 4     | 4  | 0   |
|                              |    | 2                             | 7     | 6     | 0                            |                      |            |                 |                                    |       |       |    |   |
| 2                            |    | 1                             | 5     | 6     | 1 configuration defect       | 10                   | 6          | 0               | 10                                 | 6     | 4     | 0  | 0   |
|                              |   | 2                             | 5     | 6     | 1 configuration defect       |                      |            |                 |                                    |       |       |    |   |
| 3                            |  | 1                             | 6     | 6     | 0                            | 10                   | 6          | 0               | 10                                 | 6     | 4     | 0  | 0   |
|                              |  | 2                             | 4     | 6     | 2 datum defect (translation) |                      |            |                 |                                    |       |       |    |   |
| 4                            |  | 1                             | 6     | 6     | 0                            | 11                   | 6          | 0               | 11                                 | 6     | 4     | 1  | 1 determinacy defect ( $\Delta$ rotation) |
|                              |  | 2                             | 5     | 6     | 1 datum defect (orientation) |                      |            |                 |                                    |       |       |    |   |

Table 8.1

Tests with simulated kinematic networks

● fixed station; — observed distance;  observed azimuth

### 8.3 Practical Test with a Quadrilateral in the Swiss Jura

#### 8.3.1 Introduction to the Jura Tectonics

Despite the long tradition of investigations of the Swiss Jura tectonics, there are still controversial hypotheses as to the origin of the Jura mountain folding. The fundamental question is, whether the basement below the Jura was actively moving with the sedimentary cover, or if the basement was only playing a passive role in the folding caused by remote tectonic forces.

There is a whole net of fault lines known to exist in the Jura region. The hypothesis of folding by wrench faulting (Pavoni, 1961) convincingly explains the development of the fault structures by relating them to relative strike-slip movements in the basement. It also explains the occurrence of earthquakes with focal depths of 5 to 6 kilometres in this region (Pavoni and Peterschmitt, 1974).

Among the most noticeable faults on the tectonic map of Switzerland (cf. Figure 8.1) are the faults crossing the Jura mountain chain. A detailed geological study and survey was undertaken by the University of Neuchâtel (Aubert, 1959) in the region of the fault Vallorbe-Pontarlier.



Figure 8.1

Section of tectonic map of Switzerland

Map scale 1 : 500 000. The circle indicates the monitoring network 'LE PONT' which straddles the fault Vallorbe-Pontarlier.

The fault line can easily be followed on the topographical map from the southern base of the Jura, crossing various synclines and anticlines in south-north direction, until it reaches the city of Pontarlier in France. It is evident from the geological investigations that a left lateral relative fault displacement of about 3.5 km has taken place within the geological time span from the epoch of transgression of the upper miocene, about 10 million years ago, to the present. If, as an approximation, it is assumed that the relative movement has occurred linearly in time from the miocene to the present, a relative velocity of 3.5 cm per century can be estimated.

Repeated surveying of precise kinematic networks in the fault zone was initiated ten years ago as a contribution to the 'Swiss Geodynamic Project' (Fischer, 1974). From the outcome of these investigations, it should be possible to determine if the relative movements evident within a geological time span are continuing in the present. Monitoring contemporary kinematics of the crust in space and time, together with seismo-tectonic research, will hopefully lead to a better understanding of the Jura tectonics in the future.

### 8.3.2 Precise Geodetic Observations

In 1973 two small quadrilateral networks straddling the fault Vallorbe-Pontarlier at two locations were designed and monumented (Jeanrichard, 1974). Geological considerations, as well as the topography and the criteria of an optimal net design, were responsible



for the choice of the location of the stations. The first network is located at 'Pré de l'Haut Dessous', on a plateau south-east of the 'Col du Mollendruz'. The second quadrilateral is situated near 'Le Mont du Lac', one kilometre from the 'Lac de Joux'. The length of the lines of sight varies between 210 and 585 m. All stations were monumented with small bronze markers cemented into the bedrock. In addition, three eccentric markers within a distance of a few metres were established with each station. They are used to monitor relative displacements of individual markers and to check if the instruments are mounted exactly centric over the station. They also serve for reconstruction in case a marker gets lost.

The first observation campaign took place in June 1973. All distances were measured using a precise electro-optical EDM instrument (KERN Mekometer ME-3000). The Mekometer is one of the most precise geodetic short range EDM instruments presently on the market (Elmiger and Sigrist, 1976). The manufacturer claims an accuracy of

$$\sigma_D^2 = (0.2\text{mm})^2 + (10^{-6} \cdot D)^2 \quad (8.1)$$

The directions were measured in four sets with a KERN DKM2-A theodolite (Aeschlimann, 1972). The precise centering of the instruments and targets was obtained using an optical precision plummet. During the observations, the centering was periodically checked. The observations were subsequently corrected for small excentricities.

The networks have since been re-measured twice, in 1974 and 1978. As the same Mekometer was not available, a different instrument of the

same type had to be employed each time. The next repetition of the survey is planned for summer 1983.

### 8.3.3 Crustal Strain Analysis of the Network 'LE PONT'

#### a) Separate Network Adjustments:

The quadrilateral at 'Pré de l'Haut Dessous' (it will be called network 'LE PONT' here) was chosen for practical testing. The observations of all epochs were introduced into separate network adjustments. The same set of arbitrary minimum constraints (Station No. 6, fixed; cf. Figure 8.2) was introduced. The orientation of each network was simulated by one artificial azimuth observation. The following statistical model of the observations was assumed:

$$\text{- directions:} \quad \sigma_{\alpha}^2 = (0.17 \text{ mgon})^2 \quad (8.2)$$

$$\text{- distances:} \quad \sigma_{\rho}^2 = (0.2\text{mm})^2 + (10^{-6}D)^2 \quad (8.3)$$

(Note: 1 gon is equivalent to  $0.785 \cdot 10^{-2}$  rad)

All observations were screened for blunders and outliers, and the residuals of the adjustment were statistically tested using a ' $\chi^2$ -goodness of fit test'. Based on these tests, the assumption of normally distributed observations was accepted. The estimates of the variance factor  $\hat{\sigma}_0^2$  resulting from the least-squares adjustments are shown in Table 8.2.

| year | $\hat{\sigma}_0^2$ (known) | $\hat{\hat{\sigma}}_0^2$ | deg. of freedom | $\chi^2$ -test |
|------|----------------------------|--------------------------|-----------------|----------------|
| 1973 | 1                          | 1.07                     | 15              | passes         |
| 1974 | 1                          | 1.15                     | 15              | passes         |
| 1978 | 1                          | 0.67                     | 15              | passes         |

Table 8.2

Statistical results of the network adjustments

b) Strain Analysis:

Preliminary similarity transformations of the three sets of adjusted coordinates revealed scale differences of up to 3.5 ppm among the three network results. These scale changes are probably due to biases in the measuring frequencies and residual systematic effects in the atmospheric compensation of the Mekometers. This is not surprising, considering the unfavorable fact that three different Mekometers had to be employed in the observation campaigns. The detected scale differences are most likely not reflecting any real dilatation of the crust. Thus, from the four determinable strain components, only the two shear components can be associated with a possible crustal deformation. (Shear does not depend on the change in network scale except for second order effects.) In the present case of a simple quadrilateral surveyed three times, only the straight-forward deformation models of a homogeneous shear accumulation, linear or piecewise linear in time are appropriate. More complex models that

admit variations of the shear rate in space or time have to be disregarded due to the lack of data.

The results of three two-epoch analyses (73-74, 73-78, 74-78) and six simultaneous multi-epoch analysis are listed in Tables 8.3 and 8.4. The variance factor  $\sigma_0^2$  was assumed to be known in the computations with odd numbers. The variances were subsequently not multiplied by the estimated variance factor  $\hat{\sigma}_0^2$ . A second series of computations (with even numbers) was performed, in which the variance factor was estimated from the separate network adjustments. The estimated shear components from the two adjustments with different statistical models are almost identical, whereas their confidence intervals vary slightly.

The results are graphically displayed by rosettes of tensor shear-rate and the 95 percent confidence regions (outer dotted lines) of total shear (cf. Figures 8.2 to 8.6). Total tensor shear rates of 0.88, 0.28 and 0.15  $\mu\text{strain/yr}$  were obtained from the two-epoch analyses, whereas 0.24  $\mu\text{strain/yr}$  of total shear were found from the simultaneous three-epoch analysis. The azimuth of the axis of positive (left lateral) maximum shear varies between -5.7 and -22.4 gon. The significance of these results will be discussed in the next section.

The approximations No.9 and 10 are based on a different deformation model in space. The direction of maximum shear is constrained in the direction of the expected relative fault movement (azimuth: -17.2 gon). This was achieved by simply rotating the coordinate system by -17.2 gon and constraining the first shear component to zero. The

results of these computations do not differ considerably from the results obtained from the approximations No.7 and 8 as far as the estimated shear-rates are concerned. However, the statistical interpretation will differ, as the parameter vector space, in this case, is reduced to one dimension.

The results of two other pairs of approximations with reduced sets of observations and one pre-analysis assuming the execution of the next survey campaign in April 1982 are presented in Tables 8.3 and 8.4. The analyses of only the distance observations (No.11 and No.12) yield results similar to the multi-epoch analyses with all observations, with the exception of a slightly increased variance of the estimated quantities. The strain from only the observed directions (No.13 and No.14) is determined very weakly. The results of this analysis are not incompatible with the shear estimated from the complete set of observations.

It should be noted that the interpretation of estimated homogeneous shear in a rectangle straddling the fault, with two sides being approximately parallel to the fault, is ambiguous as far as the type of deformation is concerned. It is not possible to distinguish between the effect of a relative rigid bloc translation parallel to the fault due to fault creep, and the effect of shear accumulation along the fault which is locked. A more detailed interpretation is only possible if the network contains more than four stations and covers a larger area.

Approximation No. 17 is an additional multi-epoch analysis in which a rigid block translation model (cf. 6.3.2) is adopted. The direction of the relative fault movement is constrained in the direction of the fault (-17.2 gon). The definition of the crustal blocks and the resulting relative translation velocities of  $0.13 \pm 0.08$  mm/yr (right-lateral) is shown graphically in Figure 8.7.

The shape of the confidence region of shear demonstrates that the design of the network is not optimal as far as the determination of shear in the direction of the expected fault is concerned. This is not surprising, if we consider that shear in this direction is mainly determined from the change in the ratio of the two diagonal distances 5-7 and 6-8.

#### 8.3.4 Statistical Testing

Statements about detected crustal strain are valuable only if their statistical significance can be proven. A serious statistical assessment of the derived strain quantities was therefore considered to be an important objective of this test.

a) Null hypothesis:

$H_0$  (cf. eqn.(7.40)) : No shearing deformation occurred within the zone and time span of investigation.

b) Statistical Filtering:

All Fourier-coefficients estimated from the different approximation models were inferior to the values of abscissa  $\xi$  of the pertinent probability distribution function on the level of significance  $\alpha = 0.05$  (cf. table 8.3). According to this test, the hypothesis  $H_0$  would have to be accepted and all coefficients set to zero.

c) Test on the quadratic form  $\hat{\lambda}_0^T \hat{\lambda}_0$ :

The test on the quadratic form of the Fourier-coefficient vector (cf. eqn.(7.44)) simultaneously tests all coefficients in context. Again, the quadratic forms estimated from all test models were inferior to the abscissa  $\xi$  of the  $\chi^2$  or the F-distribution on the level  $\alpha$ .

d) Result:

The detected shear is not significant on the  $\alpha = 0.05$  (95 percent probability) level. It should, however, be noted that if the direction of maximum shear is constrained to the expected fault axis, the resulting shear is found to be significant on a 93 percent probability level.

The limits of the 95 percent confidence regions of maximum shear are plotted by the outer dotted lines in Figures 8.2 to 8.6. The estimated maximum shear is significant on the  $\alpha$  level of significance if the ends of the maximum shear axes lie outside the confidence limits.

### 8.3.5 Interpretation

The rate of shearing strain can be estimated from geological evidence if a linear movement in time is assumed. Geological investigations yield a relative horizontal left lateral movement (azimuth:  $-17$  gon) of 35mm per century (cf. 8.3.1). If, as a simple assumption, a relative rigid bloc translation in the expected fault direction is assumed, a shear-rate of about  $0.6 \mu\text{strain/yr}$  for the rectangle straddling the fault is obtained.

The geometrical interpretation of the estimated shear from their graphical representation by shear-rosettes is not difficult. However, one should consider that a rotation of the shear-rosette by  $90^\circ$  also changes the shear in a given direction from left lateral to right lateral, or the other way round. To avoid mis-interpretations, the definition of the sign of the shear has to be considered very carefully. In this analysis positive shear values correspond to left lateral shear and are represented by solid lines, whereas negative, right lateral shear is depicted by broken lines. This means that perpendicular to an active left lateral fault, left lateral shear can be expected to accumulate. In other words, the strike of a right lateral fault will be in the direction of maximum positive shear (solid line) and that of a left lateral in the direction of maximum negative shear (broken line).

In an attempt to interpret the results, let us for the moment assume the results to be significant. Looking at Figures 8.2 to 8.5, one is



at first impressed by how well the shear axes and the expected fault strike agree. However, the estimated shear is exactly expressing the opposite of what one would expect. The estimated shear normal to the expected fault direction is right lateral, whereas the fault definitely moved left laterally within a geological time span. How could the crust be deformed in this way, if the relative movement in the fault zone is still continuing the same way it did some million years ago?

There is a case in which such a seemingly opposite deformation would occur. If the fault line was not exactly below the quadrilateral and accumulated shearing strain was released (e.g. by fault creep), the estimated direction of maximum shear from the network analysis would be exactly as in our investigation. This interpretation is based on Reid's Elastic Rebound Model (Benioff, 1964; cf. Figure 1.3). Looking at the tectonic map (cf. Figure 8.1) more carefully, one finds a whole group of parallel fault traces in this zone. Thus an active strike-slip fault movement outside the network might not be all that unrealistic.

### 8.3.6 Conclusions and Recommendations

It is very likely that the crust at 'Pré de l'Haut Dessous' in the zone of the fault Vallorbe-Pontarlier has been deformed by a left lateral tensor shear of  $0.24 \pm 0.13$   $\mu$ strain/yr (azimuth: -15 gon) within the years 1973 to 1978. Using the geodetic data presently available, it is not possible to prove this statement on the usually assumed 95 percent

level of probability. However, a different null hypothesis, that no shearing deformation (with the axis of maximum shear in the direction of the expected relative fault movement) had occurred, would have to be rejected on the 93 percent level of significance.

It was found from the pre-analysis (Experiment No.15) that if the next repetition of the geodetic observations was executed according to the same observation program already in April 1982, the standard deviation of the estimated shear strain rate could be reduced from the present 0.13 to 0.07  $\mu$ strain/yr. It is recommended to re-survey the kinematic networks at least every three years. In this way, the time behavior of the deformation could be investigated. More detailed information about the strain accumulation and release in space would be available if the network could be extended at both sides of the fault.

| No. | Time span | $\Delta t$<br>yr | k/u | tensor shear-rate<br>$\mu\text{strain/yr}$ |   |           |   | total tensor shear-rate<br>$\mu\text{strain/yr}$ |   |                      |  |
|-----|-----------|------------------|-----|--|---|-----------|---|--|---|----------------------|--|
|     |           |                  |     | $\hat{\tau}$                               | $\frac{\sigma_{\tau}^2}{\sigma_{\tau}^2}$ | $\hat{v}$ | $\frac{\sigma_{\tau}^2}{\sigma_{\tau}^2}$ | $\hat{\gamma}_T$                                 | $\frac{\sigma_{\tau}^2}{\sigma_{\tau}^2}$ | $\hat{a}_r$<br>[gon] | $\frac{\sigma_{\tau}^2}{\sigma_{\tau}^2}$<br>[gon] |
| 1   | 73-74     | 0.95             | k   | 0.16                                       | 0.67                                      | -0.86     | 0.72                                      | 0.88   | 0.73                                      | -5.7                 | 23.8   |
| 2   |           |                  | u   | 0.16                                       | 0.74                                      | -0.86     | 0.80                                      | 0.88   | 0.81                                      | -5.7                 | 26.4   |
| 3   | 73-78     | 5.02             | k   | 0.11                                       | 0.13                                      | -0.26     | 0.14                                      | 0.28   | 0.14                                      | -12.8                | 13.9   |
| 4   |           |                  | u   | 0.11                                       | 0.12                                      | -0.26     | 0.13                                      | 0.28   | 0.14                                      | -12.8                | 13.5   |
| 5   | 74-78     | 4.06             | k   | 0.10                                       | 0.16                                      | -0.12     | 0.17                                      | 0.15   | 0.17                                      | -22.4                | 31.4   |
| 6   |           |                  | u   | 0.10                                       | 0.16                                      | -0.12     | 0.17                                      | 0.15   | 0.17                                      | -22.4                | 30.9   |
| 7   | 73/74/78  | 5.02             | k   | 0.11                                       | 0.12                                      | -0.22     | 0.13                                      | 0.24   | 0.13                                      | -14.6                | 15.2   |
| 8   |           |                  | u   | 0.11                                       | 0.11                                      | -0.21     | 0.12                                      | 0.24   | 0.13                                      | -14.8                | 14.5   |
| 9   | 73/74/78  | 5.02             | k   | 0  | 0   | -0.24     | 0.13                                      | 0.24   | 0.13                                      | -17.2                | 0  |
| 10  |           |                  | u   | 0  | 0   | -0.24     | 0.12                                      | 0.24   | 0.12                                      | -17.2                | 0  |
| 11  | 73/74/78  | 5.02             | k   | 0.13                                       | 0.13                                      | -0.18     | 0.15                                      | 0.23   | 0.16                                      | -19.3                | 16.8   |
| 12  |           |                  | u   | 0.11                                       | 0.12                                      | -0.14     | 0.14                                      | 0.18   | 0.14                                      | -21.3                | 19.8   |
| 13  | 73/74/78  | 5.02             | k   | -0.30                                      | 0.40                                      | -0.51     | 0.32                                      | 0.60   | 0.42                                      | -17.1                | 16.2   |
| 14  |           |                  | u   | -0.32                                      | 0.39                                      | -0.51     | 0.31                                      | 0.60   | 0.41                                      | -17.6                | 15.3   |
| 15  | 73....82  | 8.86             | k   | -  | 0.06                                      | -         | 0.07                                      | -  | -   | -                    | -  |
| 17  | 73/74/78  | 5.02             | k   | (rel. transl. vel.: $0.13 \pm 0.08$ mm/yr) |   |           |   | -17.2  |   |                      | 0  |

$a_r$  ... azimuth of maximum right lateral shear  
 k ...  $\sigma_{\tau}^2$  known  
 u ...  $\sigma_{\tau}^2$  unknown

Table 8.3

LE PONT: Predicted uniform tensor shear rates

| No. | Var.factor<br>$\hat{C}_0^2$ | df | Fourier coeff.        |                       |   | Statistical Testing: $\alpha=0.05$ |     |         |     |
|-----|-----------------------------|----|-----------------------|-----------------------|---|------------------------------------|-----|---------|-----|
|     |                             |    | $\hat{\lambda}_{0_1}$ | $\hat{\lambda}_{0_2}$ | $\frac{\hat{\lambda}_{0_1}^2 + \hat{\lambda}_{0_2}^2}{\hat{C}_0^2}$ | $\xi_1$                            | p/f | $\xi_2$ | p/f |
| 1   | 1.229                       | 32 | 1.20                  | 0.09                  | 1.45  | 1.96                               | p   | 5.99    | p   |
| 2   | 1.106                       | 32 | 1.14                  | 0.08                  | 1.18  | 2.06                               | p   | 6.60    | p   |
| 3   | 0.953                       | 32 | 1.90                  | 0.64                  | 4.02  | 1.96                               | p   | 5.99    | p   |
| 4   | 1.096                       | 32 | 2.03                  | 0.69                  | 4.19  | 2.05                               | p   | 6.60    | p   |
| 5   | 0.973                       | 32 | 0.70                  | 0.56                  | 0.80  | 1.96                               | p   | 5.99    | p   |
| 6   | 1.069                       | 32 | 0.73                  | 0.58                  | 0.81  | 2.03                               | p   | 6.60    | p   |
| 7   | 1.052                       | 51 | 1.69                  | 0.70                  | 3.35  | 1.96                               | p   | 5.99    | p   |
| 8   | 1.087                       | 51 | 1.84                  | 0.77                  | 3.98  | 2.04                               | p   | 6.36    | p   |
| 9   | 1.033                       | 52 | 1.82                  | -                     | 3.31  | 1.96                               | p   | 3.84    | p   |
| 10  | 1.198                       | 52 | 1.99                  | -                     | 3.31  | 2.02                               | p   | 4.02    | p   |
| 11  | 1.198                       | 27 | 1.26                  | 0.72                  | 2.11  | 1.96                               | p   | 5.99    | p   |
| 12  | 1.176                       | 27 | 1.10                  | 0.76                  | 1.52  | 2.13                               | p   | 6.70    | p   |
| 13  | 0.827                       | 18 | 1.61                  | 0.07                  | 2.60  | 1.96                               | p   | 5.99    | p   |
| 14  | 1.420                       | 18 | 1.99                  | 0.05                  | 2.79  | 2.34                               | p   | 7.10    | p   |
| 15  | - pre-analysis -            |    |                       |                       |   |                                    |     |         |     |
| 17  | 1.043                       | 52 | 1.66                  | -                     | 2.76  | 1.96                               | p   | 5.99    | p   |

$\xi_1$  ... abscissa of pertinent p.d.f. for test on  $\hat{\lambda}_{0_i}$   
 $\xi_2$  ... abscissa of pertinent p.d.f. for test on quadratic form  
 p ... test passes  
 f ... test fails

Table 8.4

LE PONT: Statistical Testing

Legend to the Graphical Representation of Strain:

-----

(in Figures: 8.2 to 8.7)

A comprehensive explanation of the displayed strain figures (shear-rosettes) is given in Section 5.

- Map Scale: 1: 3500
- Scale of Strain Figures:
  - Figures: 8.2, 8.4, 8.5, 8.6: 1.4 cm  $\hat{=}$  1  $\mu$ strain/yr
  - Figure : 8.3: 7 cm  $\hat{=}$  1  $\mu$ strain/yr
- Rosettes of Tensor Shear-Rate:
  - The radial distance to the solid/broken curve indicates the magnitude of left/right lateral tensor shear in the given direction.
- Standard Deviation of Shear-Rates:
  - The radial distance to the inner dotted line indicates one standard deviation of the shear-rate in the given direction.
- 95 Percent Confidence Region of Maximum Shear:
  - The outer dotted line limits the 95 percent confidence regions for the ends of the maximum shear axes.
- Principal Strains: Solid lines indicate extension; broken lines, contraction.

Table 8.5

Legend to the Figures 8.2 to 8.7

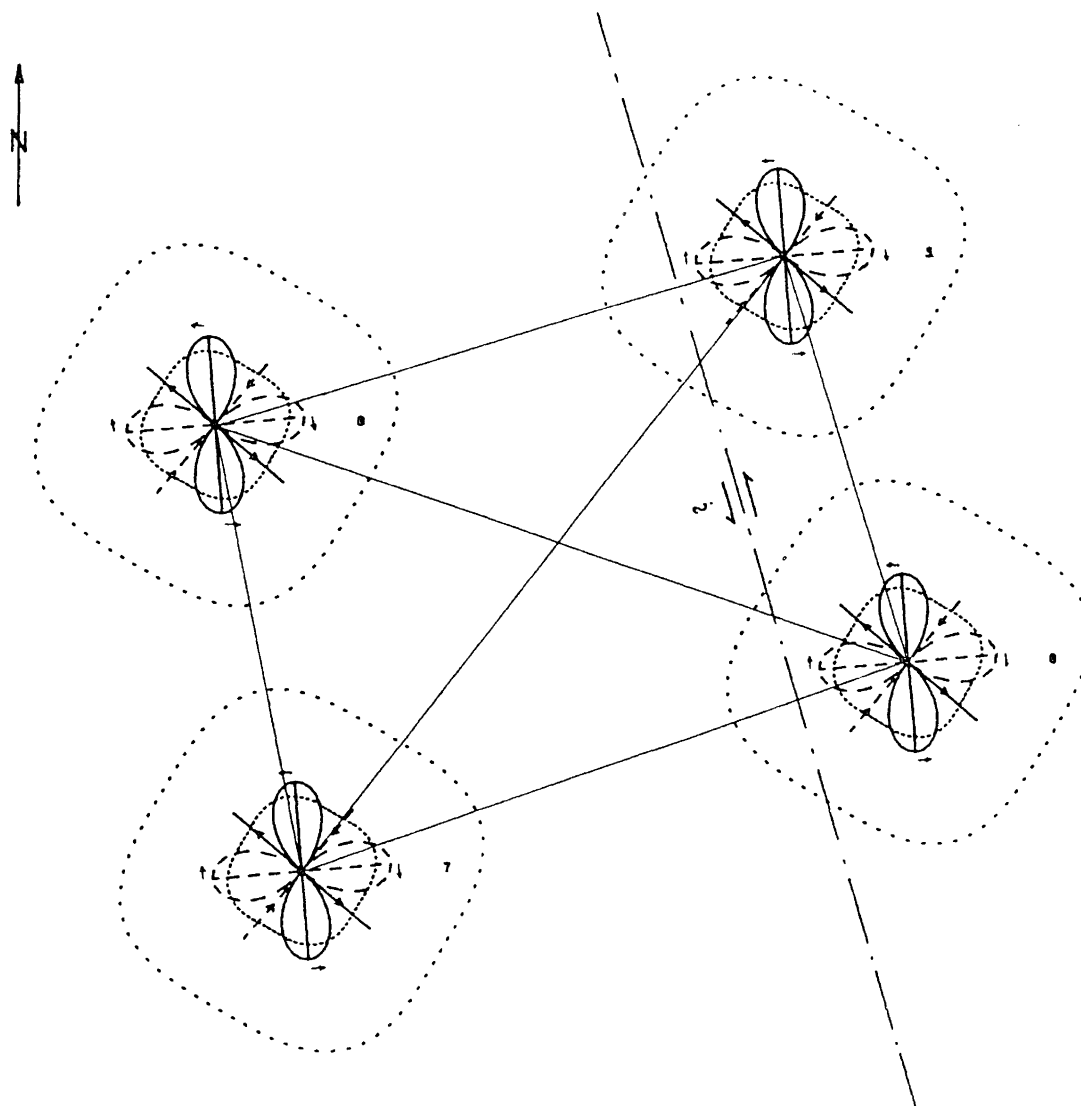


Figure 8.2

LE PONT: uniform tensor shear-rate 1973-74 (Two-epoch approx. No. 1)

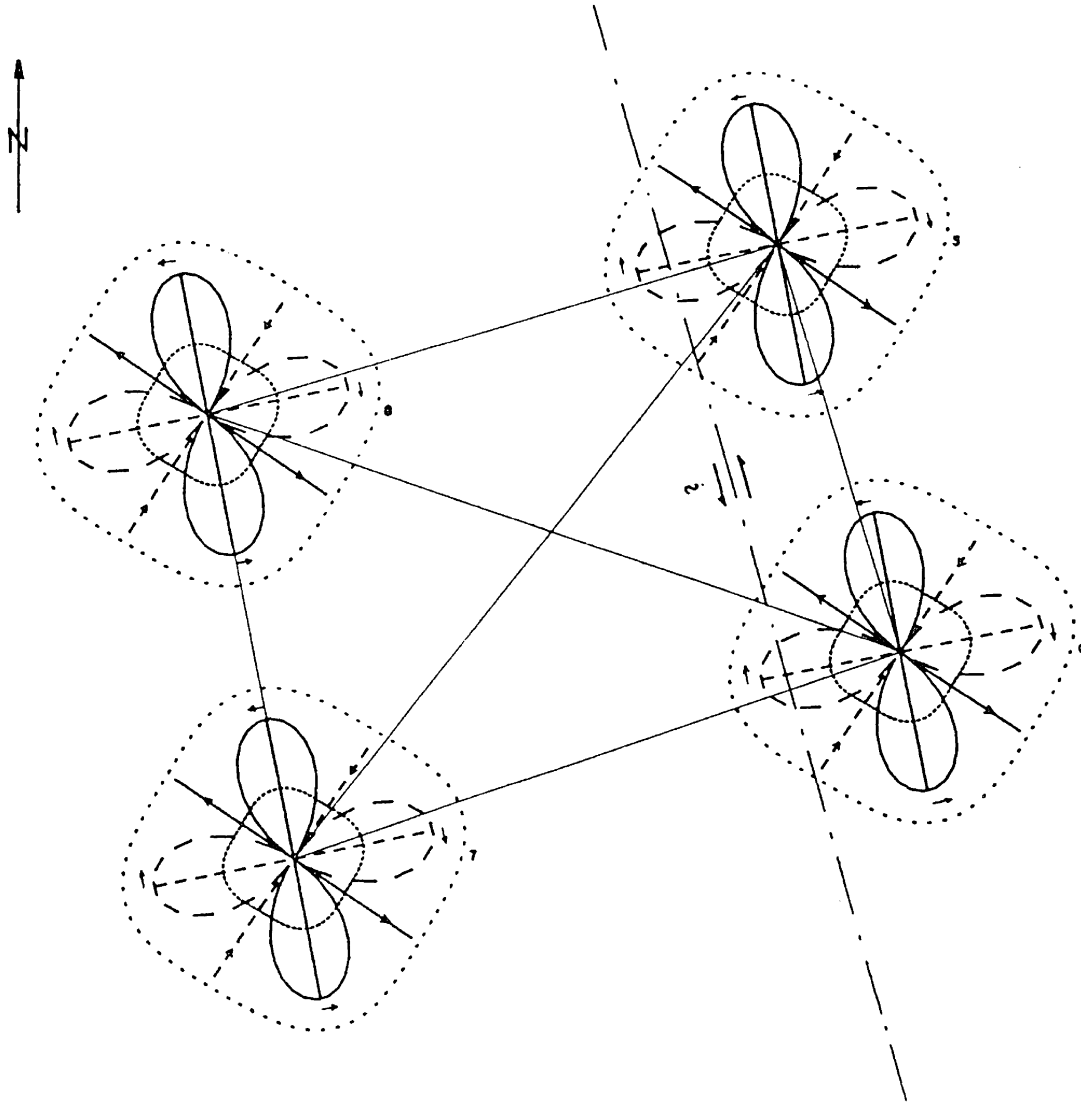


Figure 8.3

LE PONT: uniform tensor shear-rate 1973-78 (Two-epoch approx. No. 3)

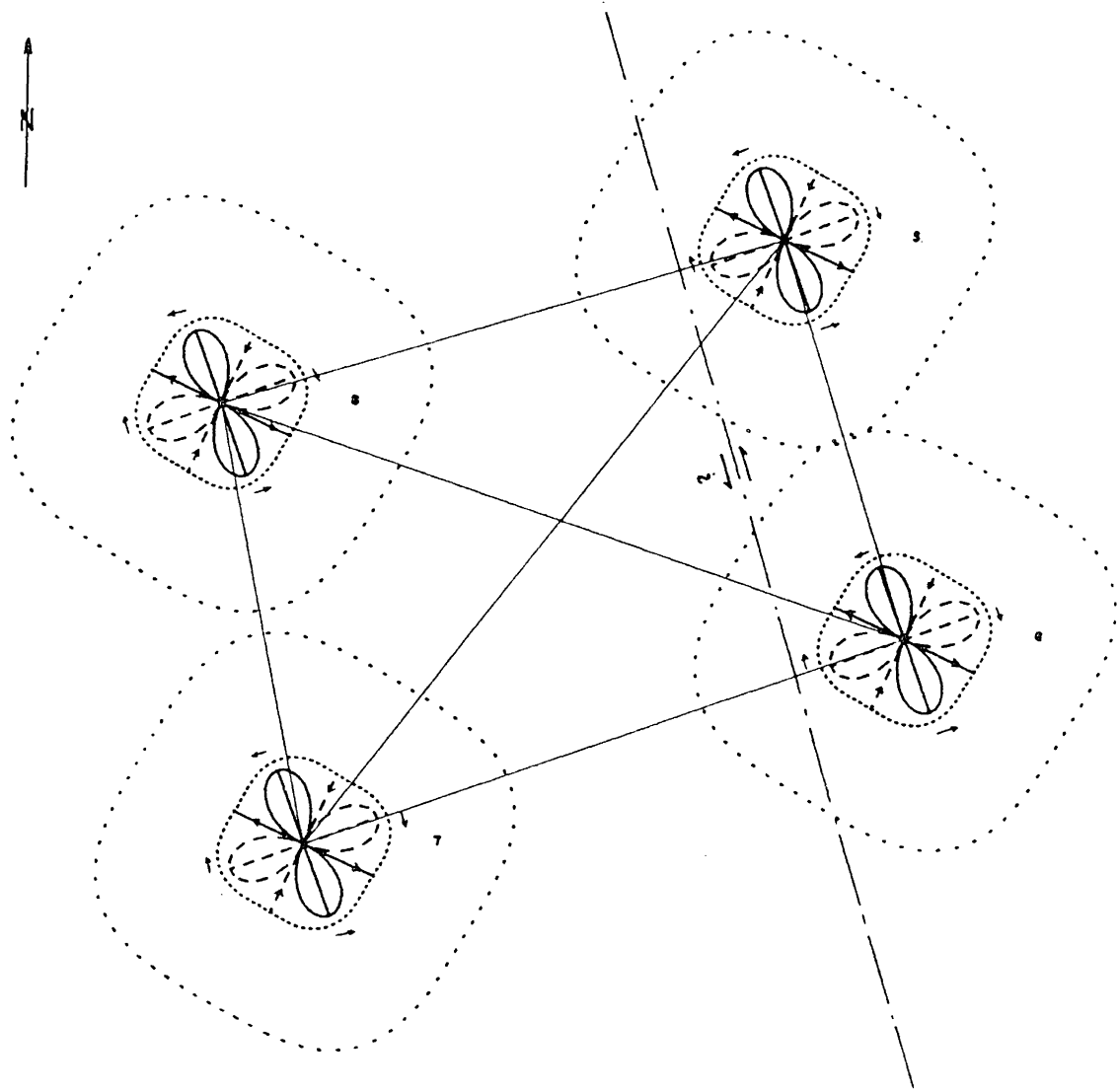


Figure 8.4

LE PONT: uniform tensor shear-rate 1974-78 (Two-epoch approx. No. 5)



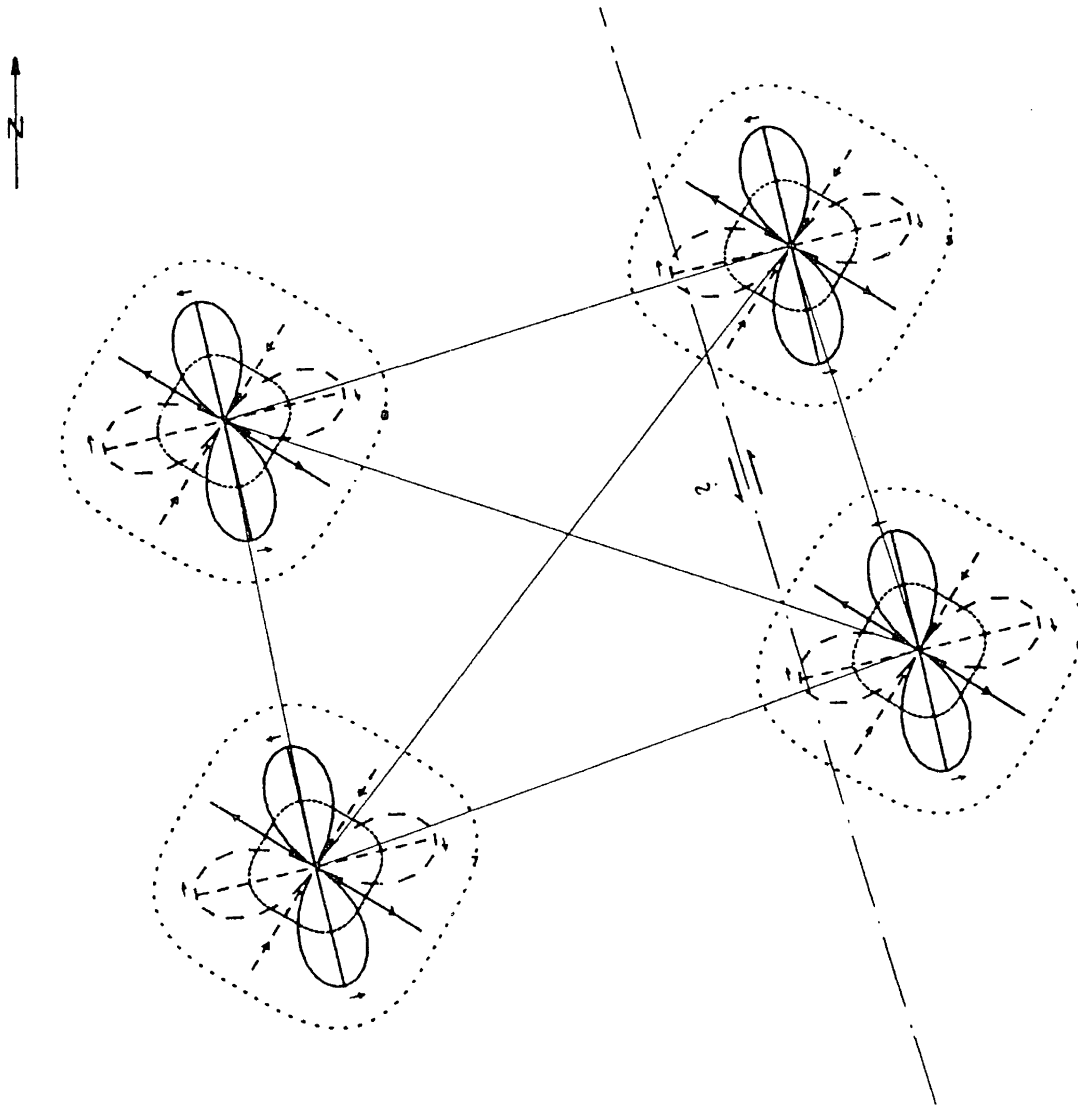


Figure 8.5

LE PONT: uniform tensor shear-rate 1973-78  
(multi-epoch approx. No. 7)

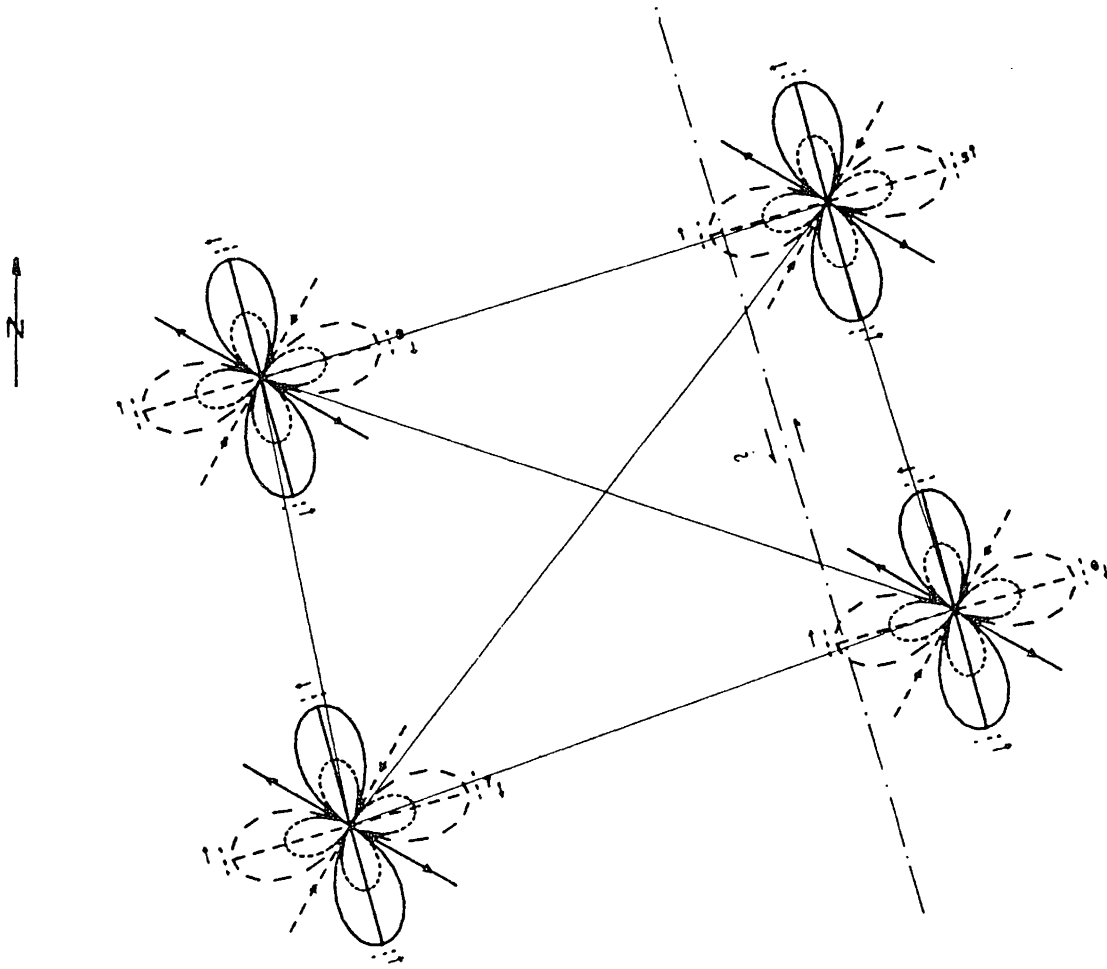


Figure 8.6

LE PONT: uniform tensor shear-rate 1973-78

(multi-epoch approx. No. 9, 1973/74/78)

The orientation of the axis of maximum shear is constrained in the direction of the fault.

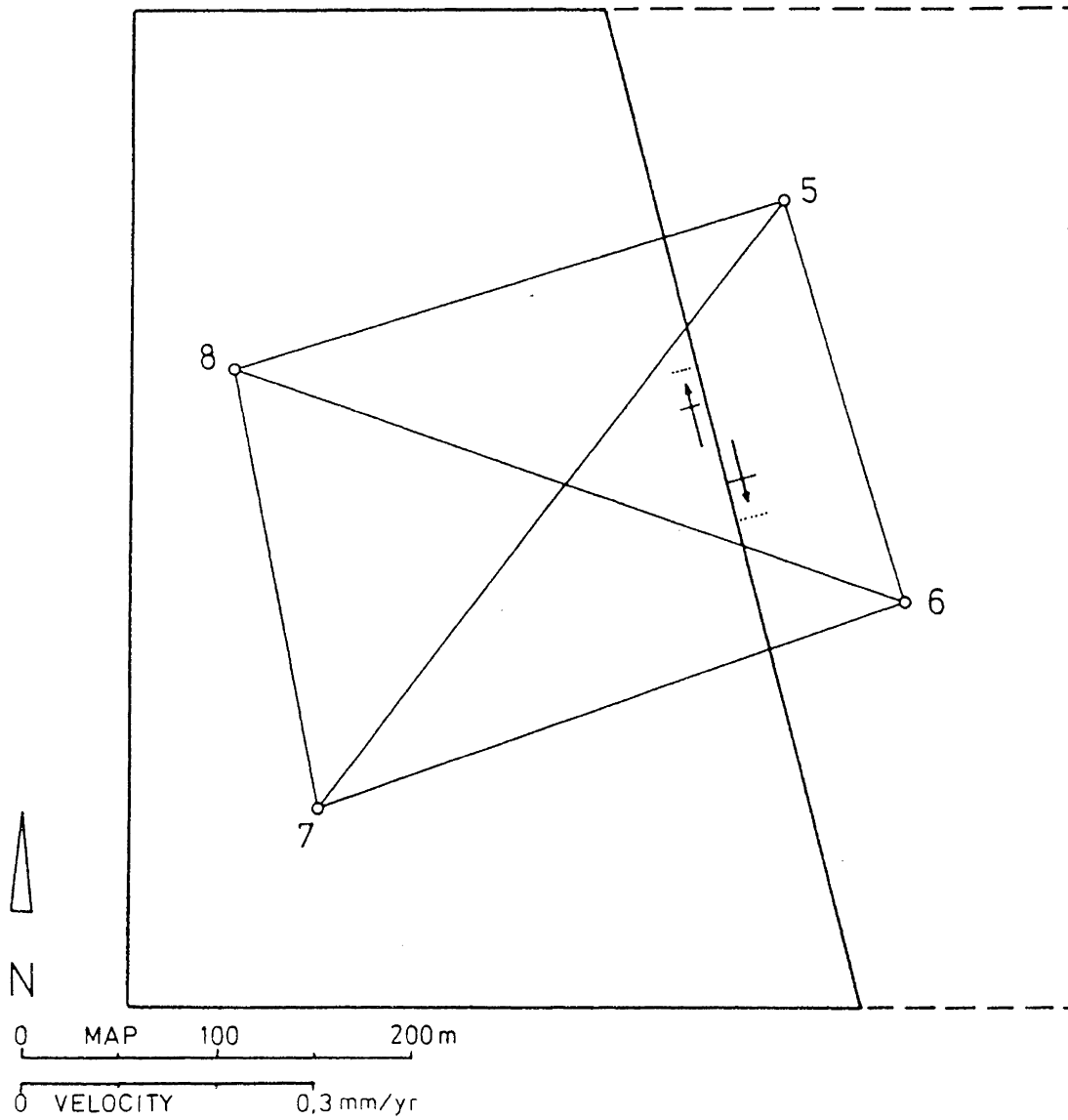


Figure 8.7

LE PONT: velocity of rigid block translation 1973-78

(multi-epoch approx. No. 17, 1973/74/78)

The translation is constrained in the direction of the fault.

## SECTION 9

## APPLICATION TO THE HOLLISTER NETWORK

9.1 Tectonics and Seismicity of the Hollister Area

## 9.1.1 Junction of Two Active Strike-Slip Faults

The Californian transcurrent plate boundary between the American and the Pacific plates has been an object of intensive geodynamic research (Kovach and Nur, 1973). The junction of two active strike-slip faults between Gabilan Range and Diablo Range (cf. Figure 9.1) is marked by relatively high seismicity and is of particular significance to prediction oriented earthquake research.

The area of the present investigation extends from  $36^{\circ}45'$  N lat. to  $37^{\circ}00'$  N lat. and from  $121^{\circ}20'$  W long. to  $121^{\circ}35'$  W long.. The San Andreas and Calaveras fault zones divide the region into three blocks (cf. Figure 9.1):

- (1) the Gabilan block, located southwest of the San Andreas fault zone,
- (2) the Diablo block, located northeast of the Calaveras fault zone and
- (3) the Sargent wedge, located between the San Andreas and Calaveras fault zones.

Pavoni (1973) investigated the geological structure of the zone using geological and gravity data along a southwest-northeast profile which

crosses the surface trace of the San Andreas fault. The San Andreas fault separates granitic rocks of the Gabilan block on the southwest side from the young sedimentary filling of the Hollister trough on the northeast side of the fault zone. The sedimentary filling of the trough reaches a depth of several kilometres on both sides of the Calaveras fault.

The location of faults and seismicity in this area are shown in Figure 9.1 (Brown and Lee, 1971). Detail Calaveras and San Andreas fault traces at the junction near Hollister are presented in Figure 9.2 according to Pavoni (1982). Appreciable right-lateral fault creep (12 mm/yr) is known to occur southeast of San Juan Bautista on the San Andreas fault and on the Calaveras fault north of Hollister (15 mm/yr). No evidence of significant slip has recently been found on the Sargent fault, which is believed to be a locked, abandoned segment of the San Andreas fault (Savage et al., 1979).

#### 9.1.2 Local Seismicity

Four moderate ( $M_L > 4$ ) earthquakes, probably accompanied by appreciable co-seismic relative movements, have occurred in the zone within the decade 1970-1980. The location, magnitude and time of the largest four seismic events were provided by the U.S.G.S. (cf. Table 9.1 and Figure 9.3).

## LIST OF SEISMIC EVENTS IN THE HOLLISTER AREA, CALIFORNIA 1970-80

| No. | Name         | Location                     | Magn.<br>$M_L$ | Date     | Time<br>(yr) |
|-----|--------------|------------------------------|----------------|----------|--------------|
| 1   | S.J.Bautista | 5 km SE of San Juan Bautista | 4.9            | 3.10.72  | 1972.759     |
| 2   | Gilroy       | 3 km SE of Gilroy            | 4.4            | 10.1.74  | 1974.027     |
| 3   | Hollister    | 10 km NW of Hollister        | 5.1            | 28.11.74 | 1974.910     |
| 4   | Coyote Lake  | 30 km NW of Hollister        | 5.9            | 6.8.79   | 1979.597     |

Table 9.1

The largest seismic events in the Hollister area, 1970-80

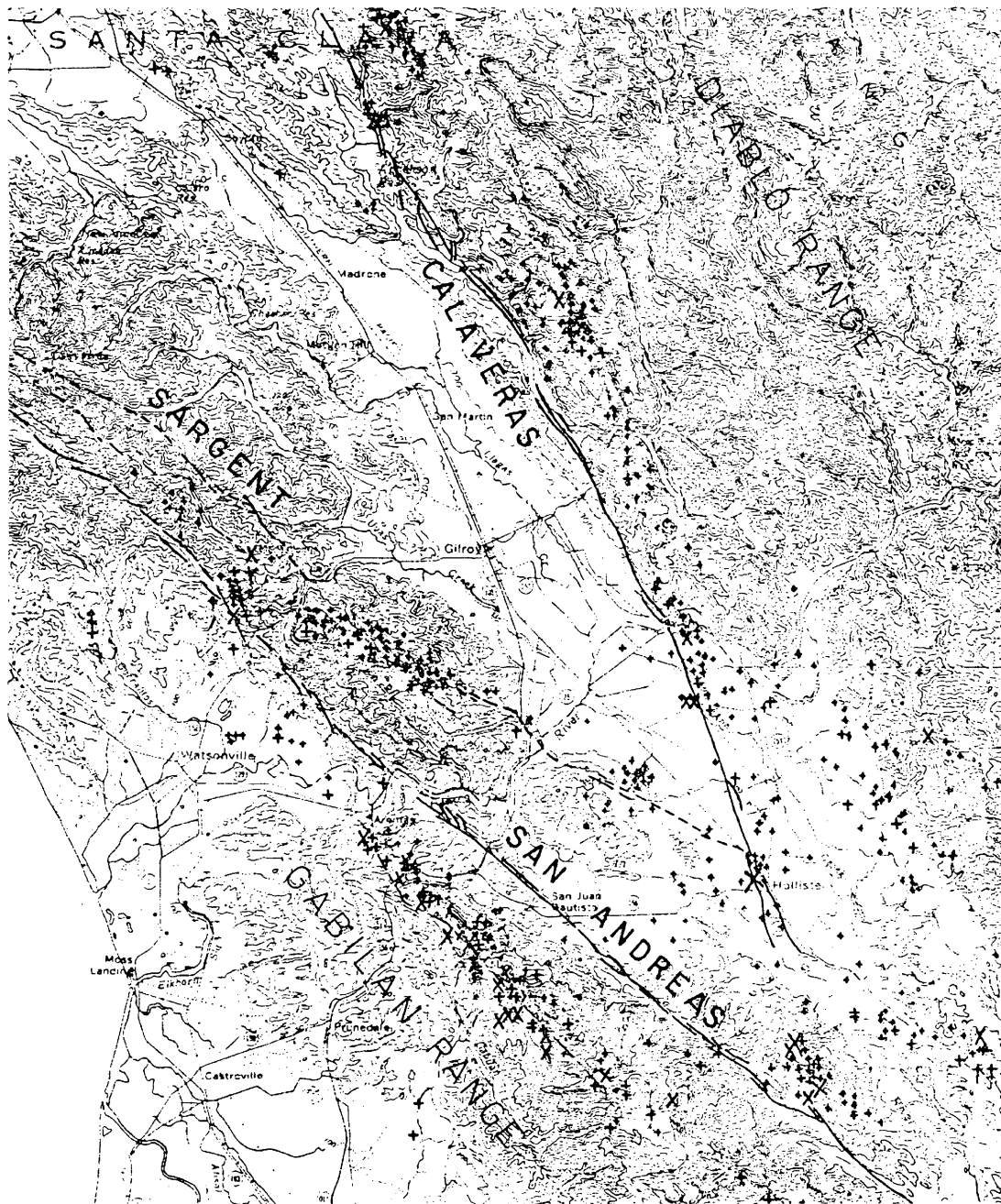


Figure 9.1

Fault locations and actual seismicity (1969-70) in the Hollister area

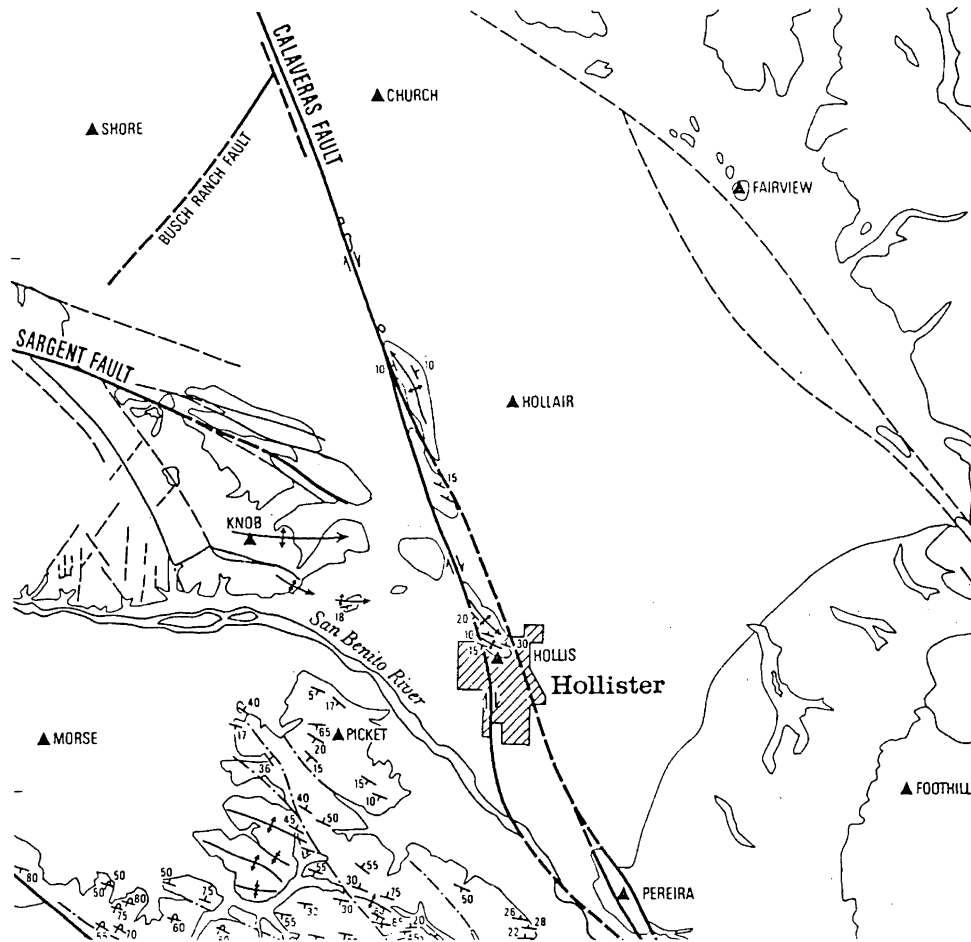


Figure 9.2

Detailed map of the junction of two faults near Hollister



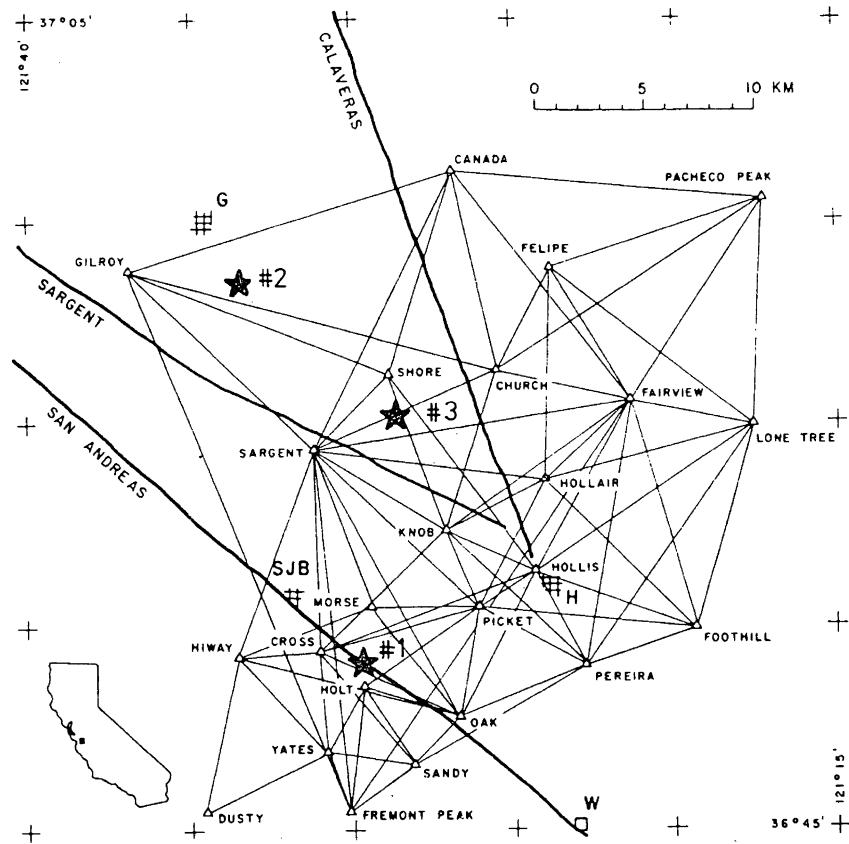


Figure 9.3

Kinematic network Hollister 1970-80

## 9.2 Geodetic Data

The kinematic network HOLLISTER is a monitoring configuration near Hollister, California, which has been partly or completely surveyed each year from 1970 to 1980 by the U.S. Geological Survey (U.S.G.S.). The 24-station trilateration network straddles the San Andreas and the Calaveras faults as well as the Sargent fault zone (cf. Figure 9.3).

### 9.2.1 Precise EDM Observations

The discussion in this sub-section is based on a detailed description of the observation procedure by Savage and Prescott (1973). The length of the 85 lines in the network are precisely measured with an electro-optical Laser-EDM instrument (Geodolite) which has a resolution of about 1 mm. The accuracy of the observations is limited by the variability of the refractivity of the air along the light path. Refractivity corrections, which are based on temperature and humidity measurements of the atmosphere from an airplane flying along the line of sight and atmospheric pressure measurements at both end points, are taken into account. The atmospheric measurements are taken from two separate thermistor and hygistor probes mounted on either side of the aircraft. The atmospheric refraction correction to the observed EDM-distance is found by integrating the measured variation of the index of refraction along the light path.

High-frequency and intermediate-frequency fluctuations in refractivity are eliminated by signal averaging and repeated measurement while the

aircraft is in flight. In order to insure the stability of the modulation frequency of the Geodolite, the frequency is measured with a quartz oscillator before and after each line measurement.

The accuracy of so measured distances has been estimated from pairs of distances  $s_1, s_2$  from a repeated survey of a horizontal geodetic network in a tectonically quiet area. The differences  $\Delta s = s_2 - s_1$  of 30 pairs of distances measured within a 3 month interval were found to be consistent with a normally distributed sample of zero mean and variance

$\sigma_{\Delta s}^2$  as given by

$$\sigma_{\Delta s}^2 = 2 a^2 + 2 b^2 s^2 \quad (9.1)$$

where  $a = 3 \text{ mm}$  and  $b = 2 \cdot 10^{-7}$ . The authors assumed uncorrelated pairs of observations  $s_1$  and  $s_2$ . Applying the law of variance propagation, they concluded that the variance of a single observation should be

$$\sigma_s^2 = a^2 + b^2 s^2. \quad (9.2)$$

It should be emphasized that this estimate was derived from pairs of observations of the same observable. Line dependent systematic effects can cause cross-correlation of such series of observations. In (9.2) these correlations are neglected, causing the estimate to be too optimistic (Vaniček and Krakiwsky, 1982). It is often experienced by geodesists that the a posteriori estimates of the variance of the observations from a network adjustment are larger than the estimates from differences of pairs of the same observations.

If the observations  $s'_1$  and  $s'_2$  are assumed to be correlated with

$$\rho_{s'_1 s'_2} = \frac{\sigma_{s'_1 s'_2}}{\sigma_{s'_1}^2}, \quad (9.3)$$

where  $\tilde{\sigma}_{S_1'}^2 = \tilde{\sigma}_{S_2'}^2 = \tilde{\sigma}_{S'}^2$

then the variance of the difference  $\Delta s'$  follows from the covariance law

$$\begin{aligned}\tilde{\sigma}_{\Delta S}^2 &= 2\tilde{\sigma}_{S'}^2 - 2\tilde{\sigma}_{S_1'S_2'} \\ &= 2\tilde{\sigma}_{S'}^2(1 - \rho_{S_1'S_2'}) .\end{aligned}\quad (9.4)$$

Or inversely, the variance of a single observation is given by

$$\tilde{\sigma}_{S'}^2 = \frac{\tilde{\sigma}_{\Delta S}^2}{2(1 - \rho_{S_1'S_2'})} > \tilde{\sigma}_S^2 \quad (9.5)$$

For the separate network adjustments by the variation of coordinates,  $\tilde{\sigma}_S$  would be a more realistic assumption if  $\rho_{S_1'S_2'}$  was known.  $\tilde{\sigma}_S^2$  applies in the case of strain approximation from differences of observations  $\Delta s$ .

### 9.2.2 Station Elevations and Approximate Coordinates

Geodetic (ellipsoidal) station coordinates (related to the Clarke 1866 ellipsoid of the North American Datum) are available for all stations because most stations of the Hollister network are also part of a geodetic, horizontal control network surveyed by the U.S. Coast and Geodetic Survey (now U.S.N.G.S.) in 1962. These coordinates were provided by the U.S.G.S. and serve as time invariant approximate coordinates after their transformation into the coordinate system of the UTM map projection (cf. external Appendix).

The elevations of the network stations are rather poorly determined. They have been compiled from various sources. As most of them are related to the geodetic vertical control network of the U.S.N.G.S., they may be considered as approximate orthometric heights related to

the North American Vertical Datum (Sea Level Datum 1929). Geoidal heights could not be provided by the U.S.G.S.. Some of the heights were determined by vertical angles; only a few by altimetry. The standard deviation of the heights is estimated by the U.S.G.S. to be, in general, about 0.3 m (Savage,1982). However, exceptionally large, individual height errors have to be expected.

### 9.2.3 Reduced Observations

According to the standard geodetic approach, the observations which were collected in physical space have to be transformed into a three-dimensional and, subsequently, into a two-dimensional geometrical space (ellipsoid or mapping plane). This can only be done if detailed information on the gravity field is available (e.g. geoidal heights are known).

The strain field parameters as they are sought in this analysis depend on the differences of repeated observations, provided that the observations belong to the same observation space. Under the assumption that temporal variations of the gravity field are negligibly small, effects of the incompletely modeled relationship between physical and geometrical spaces cancel out when strain is computed. Thus, standard procedures (Bomford,1971) can be used to reduce the observations onto the ellipsoid.

According to the reduction procedure applied by the U.S.G.S., mark to mark distances in three-dimensional space are first computed from the

distance observations corrected for refractivity variations. By assuming the given station elevations (cf. 9.2.2) to be equal to geodetic heights, the mark to mark distances are subsequently reduced to the Clarke 1866 ellipsoid (Savage, 1982). (Note: This reduction is not rigorous, as approximate orthometric heights are used rather than geodetic heights.) Both values, the mark to mark distances as well as the so reduced 'ellipsoidal' distances, were provided by the U.S.G.S. (cf. External Appendix ).

#### 9.2.4 Distribution of the Observations in Time

The temporal distribution of the distance observations collected between 1970.0 and 1981.0 is graphically displayed by a histogram in Figure 9.4.

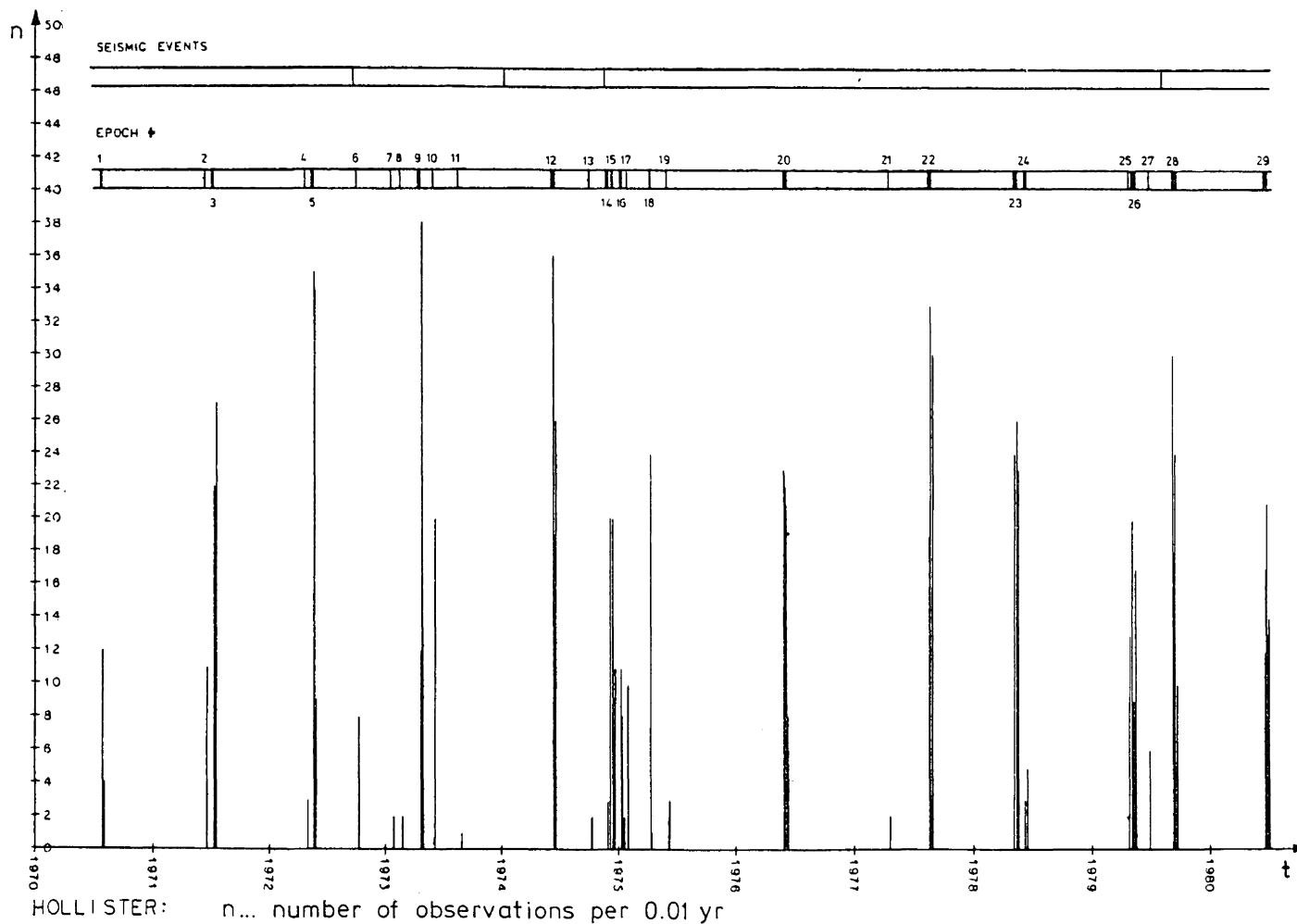


Figure 9.4

Histogram displaying the distribution of observations in time

### 9.3 Preceding Analyses

Many relative horizontal crustal movement investigations that use geodetic data of the Hollister area can be found in the literature. The brief outline in this subsection is mainly based on a summary of this research provided by Savage et al. (1979).

The U.S. Coast and Geodetic Survey completed a triangulation arc across the San Andreas and Calaveras faults in the vicinity of Hollister in 1930. The same configuration was re-observed in 1951 and 1962. Electro-optical (Geodimeter) distance measurements of the same lines were later collected by various institutions. A number of these stations are also part of the kinematic Hollister network (1970-80). Various researchers have attempted to derive fault slip or strain from the data for the periods 1930 to 1951 and 1951 to 1962. (Whitten, 1960; Scholz and Fitch, 1969; Savage and Burford, 1970, 1971; Nason, 1971). Interpretations have been made in terms of rigid block motion (with blocks bounded by the San Andreas and Calaveras faults) by uniform strain across the entire area, or by rigid block motion combined with strain accumulation within the blocks.

Researchers of the U.S.G.S. analyzed and interpreted the 1970-80 Hollister data. The method applied was that of Frank (cf. Sub-section 1.4; Prescott, 1976) Average rates of line length changes  $dl/dt$  were estimated from the re-observed distances of each line. From these rates, the spatially uniform strain-rate field constant in time can be estimated by a least-squares adjustment using the temporally



constrained kinematic model (2.33) and a set of minimal-constraints defining the indeterminable rotation of the displacement field.

An attempt was made by Savage et al. (1976) to detect pre-seismic and co-seismic deformations associated with the moderate ( $M_L=5.1$ ) Hollister earthquake of November 28, 1974. However, the authors could detect none from the analysis of geodetic data from 1969 to 1975.

EDM observations from 1971 to 1978 were used by Savage et al. (1979) for a thorough deformation analysis. A rigid block motion model for the three blocks bounded by the San Andreas and Calaveras faults was assumed. Relative block velocities (cf. Table 9.6) were found with their directions being in agreement with the strike (direction) of the faults. In addition, uniform strain-rates (cf. Table 9.5) constant in time over the whole area as well as individual strain-rates within each block were estimated.

Scientists of the University of Washington have been operating a precise multiwavelength distance-measuring (MWDM) instrument at station Hollister, near the Calaveras fault trace, since September 1975 (Huggett et al., 1977; Slater and Burford, 1979). Nine base lines of up to 11 km length radiating from Hollister have been measured almost daily. The three wavelength instrument (developed by the Applied Physics Laboratory of the University of Washington) operates on the dispersive measuring principle. The standard deviation of an observed distance is claimed to be (Huggett and Slater, 1975)

$$\sigma_D < 1 \cdot 10^{-7} \cdot D . \quad (9.6)$$

The interpretation of the MWDM data was made in terms of Calaveras fault slip-rates based on a simple rigid block translation model. An average right-lateral slip-rate parallel to the fault of 16.8 mm/yr was estimated from the observations between fall 1975 and spring 1979 (Slater, 1981). A small, apparently convergent trend of the crustal blocks towards the Calaveras fault is reported for the same interval of time. A comparison of the MWDM data with fault creepmeter records obtained near Hollister was made by Slater and Burford (1979). The time variation of the length of the fault crossing lines reflects creeping on the Calaveras fault associated with heavy rainfall and co-seismic slip associated with the Coyote Lake earthquake (Slater, 1981).

#### 9.4 Separate Network Adjustments

A histogram displaying the number of observations for 1/100 yr ( $\approx 3.6d$ ) time intervals (cf. Figure 9.4) reveals that most re-observations were made during short field campaigns of a few days. The whole set of observations is therefore divided into 29 epochs, each spanning a time interval  $\Delta T$ , whereby

$$\Delta T < 15 \text{ d} \quad ; \quad i=1,2,\dots,n_e. \quad (9.7)$$

If the limit of the temporal length variation of all network lines is (Savage et al., 1979)

$$|\dot{l}_j| = |dl_j/dt| < 0.03 \text{ m/yr} \quad ; \quad j=1,2,\dots,n \quad (9.8)$$

the bias from the discretization in time would be

$$|\Delta l_{ij}| < |dl_j/dt| \cdot \Delta T_j / 2 \quad ; \quad i=1,2,\dots,n_e; \quad j=1,2,\dots,n \quad (9.9)$$

$$|\Delta l_{ij}| < 0.0006 \text{ m}$$

which is much smaller than the variance of the observations and will be neglected. (Note: Episodic changes associated with earthquakes and creep events are not considered here.)

The number of observations in one epoch varies between 1 and 88. Some epochs contain the re-observation of the whole network, whereas others contain only a single observation. An example of a typical incomplete configuration which was observed between 1979.335 and 1979.376 (epoch No. 26) is shown in Figure 9.5. The positions of the stations HOLLAIR, KNOB, LONE T and SHORE are not determinable geometrically by the distance observations. The network of this epoch thus suffers from a configuration defect (with respect to positions).

It is interesting to realize that small height errors can cause non-negligible position errors in the horizontal network adjustment. However, the same errors cause only second order effects if strain is computed from the observation differences. The simultaneous network adjustment and approximation models proposed in this study geometrically constrain the observations of each epoch and, therefore, need reliable station heights.

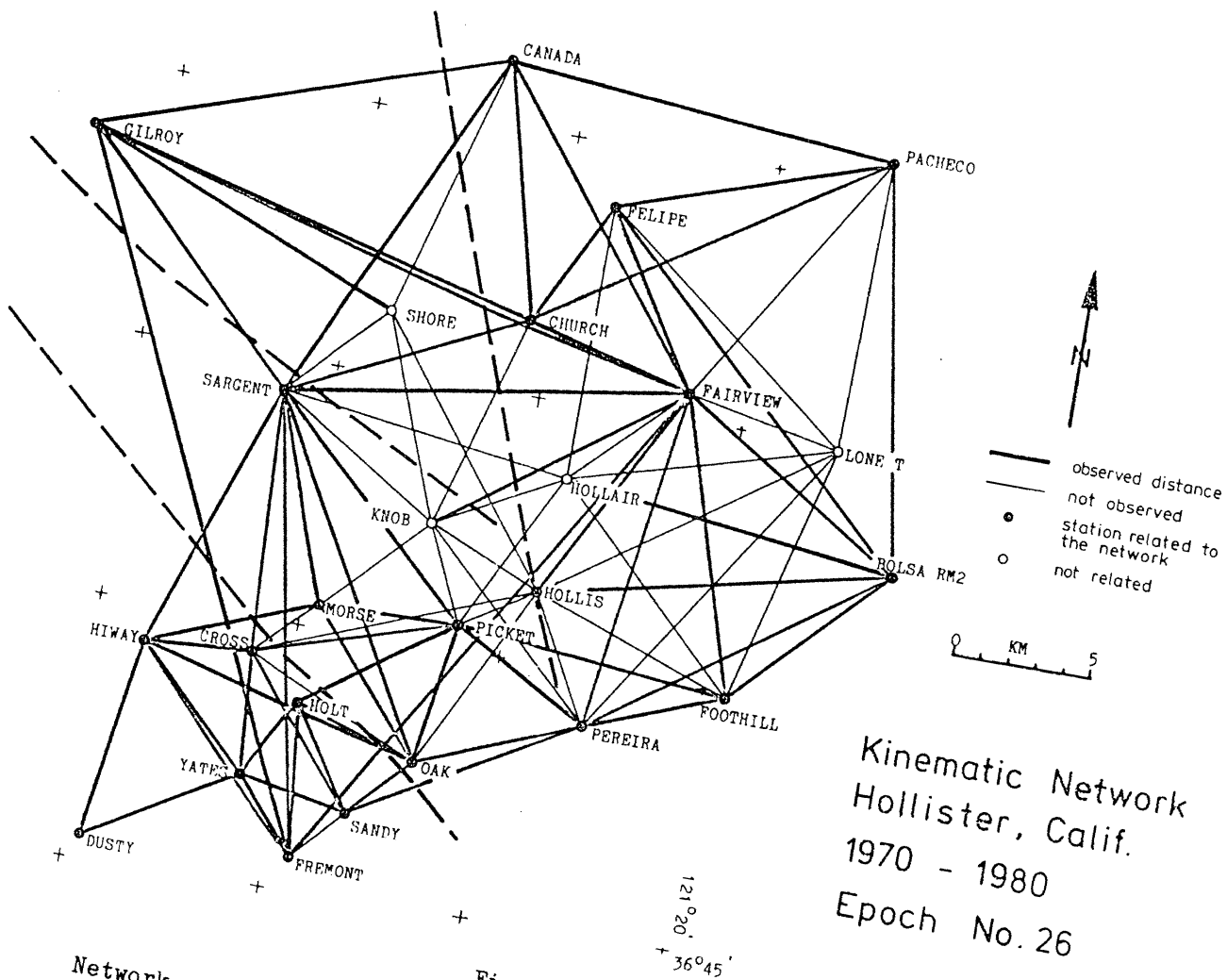


Figure 9.5  
 Network configuration of observation epoch No. 26 (1979.335-376)

The 'ellipsoidal' distances (cf. 9.2.3) obtained from the reduction using the weakly determined station heights (cf. 9.2.2) were found to be severely distorted and could, therefore, not be used in the present analysis. This was obvious from a statistical assessment of two-dimensional position adjustment results (of those networks which do not suffer from position configuration defects).

Fortunately, the distance networks contain redundant information on the relative station heights. By applying a three-dimensional network adjustment, height corrections can be estimated with the necessary accuracy and reliability needed for the reduction of the slope distances onto the ellipsoid. The given station heights are used as approximate values for the height unknowns, and mark to mark distances (cf. 9.2.3) are introduced as observations.

Even if there is no evidence of considerable vertical movements, relative height changes associated with the horizontal movements must be expected to have occurred in the Hollister area. Unfortunately, no new height determinations of the network stations had been made during the time interval in question. As transcurrent fault movement is the predominant phenomenon, drastic vertical movements (i.e. larger than 1 cm per year) are not to be expected. By adopting the U.S.G.S. argument, we are assuming that the station heights are time invariant, within the time interval in question.

Three fixed heights are generally a sufficient choice of minimal height constraints. Additionally, the height of station DUSTY was kept fixed

as it is not determinable from the network. The total set of constraints selected for the three-dimensional network adjustment is listed in Table 9.2. The three-dimensional network configuration enables us to estimate 21 corrections of station heights (nuisance parameters) simultaneously with the strain approximation.

| Station: |         |          | fixed:      |   |        |         |
|----------|---------|----------|-------------|---|--------|---------|
|          |         |          | coordinates |   | height | azimuth |
| from     | to      | at time  | x           | y | h      | a       |
| HOLLAIR  |         |          | *           | * | *      |         |
| CHURCH   |         |          |             |   | *      |         |
| MORSE    |         |          |             |   | *      |         |
| DUSTY    |         |          |             |   | *      |         |
| HOLLAIR  | SARGENT | 1972.386 |             |   |        | *       |

Table 9.2

Constraints for the three-dimensional network adjustments

As the networks of the epochs No. 3, 5, 12, 20, 28 and 29 did not suffer from configuration defects, it was possible to adjust these networks separately by the variation of positions and heights. Because of the large number of unknown parameters in these adjustments, the degrees of freedom were found to be relatively small. From the 479 observations of all the 6 adjustments, we obtained a total estimate of the variance factor  $\hat{\sigma}_0^2 = 1.23$  with the total degrees of freedom  $df = 98$ . A  $\chi^2$ -test performed on the variance factor passes on the level of significance  $\alpha = 0.05$  (95 percent probability). The estimate  $\hat{\sigma}_0^2$  is

slightly larger than its expectation, which could be due to the fact that the variance  $\hat{\sigma}_s^2$  (cf. eqn. 9.2), is used instead of the unknown  $\sigma_s^2$  (cf. eqn. 9.5).

The use of the estimates  $\hat{\sigma}_{o_j}^2$ ,  $j=1,2,\dots,n_e$ , from the individual network adjustments, to scale the covariance matrices of the observations for the subsequent least-squares approximation should not be considered because of their lack of reliability. Instead, the a priori variance factor  $\hat{\sigma}_o^2 = 1$  of the observations was assumed (to be taken as known) in all further adjustments.

## 9.5 Simultaneous Adjustments and Approximations

### 9.5.1 Assumptions

The rigid block rotation (or the spatially uniform term of average differential rotation  $\omega$ ) is not determinable from the observations of the kinematic network. If nuisance scale parameters are introduced for each epoch of observation, then the spatially uniform term of dilation is also indeterminable. The following, arbitrarily selected constraints are introduced to avoid ill-posed approximation models:

a) For all models:

$$\text{Station HOLLAIR } (x_H, y_H): \omega(x_H, y_H, t) = 0; \quad t \in \mathbb{R}$$

b) For models with unknown scale nuisance parameters:

Station HOLLAIR  $(x_H, y_H)$ :  $G(x_H, y_H, t) = 0$ ;  $t \in R$ .

### 9.5.2 Concept of Model Evaluation

The objective of the experiments reported in this Sub-section is to select those approximation models which best describe the predominant trend in the relative displacement field. An objective measure of the goodness of fit of a particular model is found from the residuals (cf. eqn. (7.49)) of the original observations as they are estimated from the simultaneous adjustment and approximation. Provided that the same statistical filtering is applied to the Fourier coefficients in all approximations, the square root of the variance factor  $\hat{G}_0$  (cf. eqn. (7.50)) estimated from the approximation is the appropriate measure for such a comparison. (Note: The estimate  $\hat{G}_0$  is used rather than  $\hat{G}_0^2$  because the former is used to scale the standard deviations.)

Given the vector of Fourier coefficients estimated from a particular model, the selection  $\hat{\lambda}'_0$  which yields the minimal estimate  $\hat{G}_0$  among all possible selections from  $\hat{\lambda}_0$  is found if those ortho-normal coefficients are set to zero, whose magnitude is smaller than their estimated (a posteriori) standard deviation  $\hat{G}_{\lambda_{0i}} = \hat{G}_0$ ;  $i=1,2,\dots,u$ . This statistical filtering criterion, which approximately corresponds to an 'out of context' test based on 68 percent a posteriori confidence regions of the coefficients, is therefore chosen for the model evaluation.

A list of selected approximation models and their estimates  $\hat{G}_0$  are given



in Table 9.4. Approximation No. 1 is a simultaneous time invariant network adjustment of all epochs. The estimate  $\hat{\sigma}_o = 5.308$  serves as a reference value for all other approximations.

The effect of possible spurious oscillations (which occur if too high a degree of the polynomials is used) was also considered in the selection of the final approximation model No.91, which is discussed in 9.5.9. The statistical testing of this final model was done on a  $\alpha = 0.05$  (95 percent probability) level of significance.

|   |   |
|---|---|
| Degrees of the Approximation Polynomials: |   |
| B :                                       | number of complex rigid bloc translation coefficients |
| C :                                       | power of the complex conformal polynomial             |
| A :                                       | power of the complex anti-conformal polynomial        |
| T :                                       | power of the time polynomial                          |
| E :                                       | number of episodic terms in the time polynomial       |
| Number of Variables:                      |   |
| Ob :                                      | number of original geodetic observations              |
| El :                                      | number of eliminated parameters                       |
| Re :                                      | total number of real coefficients                     |
| Co :                                      | number of constrained coefficients (set to zero)      |
| DF :                                      | degrees of freedom of the approximation               |
| Types of Models:                          |   |
|   | No.   |
| a) continuous in space:                   | 1 - 14  |
| b) pure rigid block translation:          | 21 - 22   |
| c) combined model (a and b):              | 31 - 91   |
| d) piecewise linear in time:              | 81  |
| e) episodic in time:                      | 71 - 75   |
| f) final selection:                       | 91  |

Table 9.3

Abbreviations used in the table of approximations (Table 9.4)

KINEMATIC NETWORK HOLLISTER (1970-80): TABLE OF APPROXIMATIONS

| Mod.<br>No. | Degr. of Polyn. |   |   |   |   | Num. of Variables |    |     |    |     | Estim.<br>$\hat{G}_0$ | Remarks            |
|-------------|-----------------|---|---|---|---|-------------------|----|-----|----|-----|-----------------------|--------------------|
|             | B               | C | A | T | E | Ob                | El | Re  | Co | DF  |                       |                    |
| 1           | 0               | 0 | 0 | 0 | 0 | 979               | 69 | 0   | 0  | 910 | 5.308                 | time-invariant     |
| 2           | 0               | 1 | 1 | 1 | 0 | 979               | 69 | 3   | 0  | 907 | 4.118                 | linear in time     |
| 3           | 0               | 2 | 2 | 1 | 0 | 979               | 69 | 7   | 1  | 904 | 3.965                 | "                  |
| 4           | 0               | 3 | 3 | 1 | 0 | 979               | 69 | 11  | 2  | 901 | 3.828                 | "                  |
| 5           | 0               | 4 | 4 | 1 | 0 | 979               | 69 | 15  | 3  | 898 | 3.819                 | "                  |
| 6           | 0               | 6 | 6 | 1 | 0 | 979               | 69 | 23  | 5  | 892 | 3.645                 | "                  |
| 11          | 0               | 1 | 1 | 6 | 0 | 979               | 69 | 18  | 5  | 897 | 4.086                 | continuous in      |
| 12          | 0               | 2 | 2 | 6 | 0 | 979               | 69 | 42  | 17 | 885 | 3.874                 | space and time     |
| 13          | 0               | 4 | 4 | 6 | 0 | 979               | 69 | 90  | 43 | 863 | 3.700                 | "                  |
| 14          | 0               | 6 | 6 | 6 | 0 | 979               | 69 | 138 | 69 | 841 | 3.465                 | "                  |
| 21          | 4               | 0 | 0 | 1 | 0 | 979               | 69 | 4   | 0  | 906 | 2.526                 | pure block transl. |
| 22          | 4               | 0 | 0 | 6 | 0 | 979               | 69 | 24  | 12 | 898 | 2.479                 | "                  |
| 31          | 4               | 1 | 1 | 1 | 0 | 979               | 69 | 7   | 1  | 904 | 2.461                 | combined model     |
| 32          | 4               | 2 | 2 | 1 | 0 | 979               | 69 | 11  | 1  | 900 | 2.436                 | (linear in time)   |
| 33          | 4               | 4 | 4 | 1 | 0 | 979               | 69 | 15  | 4  | 895 | 2.396                 | "                  |
| 34          | 4               | 6 | 6 | 1 | 0 | 979               | 69 | 27  | 4  | 887 | 2.302                 | "                  |
| 41          | 4               | 1 | 1 | 6 | 0 | 979               | 69 | 42  | 23 | 891 | 2.399                 | combined model     |
| 42          | 4               | 2 | 2 | 6 | 0 | 979               | 69 | 66  | 37 | 881 | 2.339                 | (continuous in t)  |
| 43          | 4               | 3 | 3 | 6 | 0 | 979               | 69 | 90  | 51 | 871 | 2.290                 | "                  |
| 44          | 4               | 4 | 4 | 6 | 0 | 979               | 69 | 114 | 59 | 885 | 2.265                 | "                  |
| 45          | 4               | 5 | 5 | 6 | 0 | 979               | 69 | 138 | 70 | 842 | 2.143                 | "                  |
| 46          | 4               | 6 | 6 | 6 | 0 | 979               | 69 | 162 | 77 | 825 | 2.115                 | "                  |
| 51          | 4               | 1 | 1 | 1 | 0 | 979               | 97 | 6   | 0  | 876 | 2.413                 | with scale unkn.   |
| 52          | 4               | 1 | 1 | 6 | 0 | 979               | 97 | 36  | 18 | 864 | 2.355                 | "                  |
| 72          | 4               | 6 | 6 | 1 | 4 | 979               | 69 | 135 | 53 | 828 | 2.094                 | combined model     |
| 73          | 4               | 5 | 5 | 4 | 3 | 979               | 69 | 161 | 84 | 833 | 2.091                 | (episodic in t)    |
| 74          | 4               | 5 | 5 | 4 | 4 | 979               | 97 | 176 | 90 | 796 | 2.069                 | "                  |
| 75          | 4               | 5 | 5 | 5 | 3 | 979               | 97 | 176 | 91 | 797 | 2.070                 | "                  |
| 81          | 4               | 3 | 3 | 1 | 9 | 979               | 69 | 150 | 74 | 834 | 2.252                 | piecew. lin. in t  |
| 82          | 4               | 3 | 3 | 1 | 9 | 979               | 97 | 140 | 68 | 810 | 2.219                 | (with scale unkn.) |
| 91          | 4               | 3 | 3 | 5 | 3 | 979               | 97 | 112 | 56 | 826 | 2.217                 | final model        |

Table 9.4

Table of approximations

### 9.5.3 Strain from Models Continuous in Space

Savage et al.(1979) discovered that the predominant deformation of the network can be modeled well by rigid block motion of the above mentioned three blocks. The horizontal relative displacement field (or horizontal velocity field) which corresponds to this motion is discontinuous in space. The discontinuities located along the block margins (faults) simply express the fault slip.

The approximation using functions continuous in space (to model the strain) will only yield a good fit if either the fault slip is small compared to the strain, or if high degree polynomials are employed. This is exactly what is seen from the results of the approximations No.2 to 14 (cf. Table 9.4). The estimate  $\hat{G}_0$  decreases very slowly when the space degrees of the polynomials are increased. The number of stations in the network and their distribution in space does not allow the use of polynomials much higher than degree 5 in space.

Low degree polynomials are, however, useful for estimating the over-all (average) strain. A spatially uniform strain field varying linearly in time is employed in model No.2 (cf. Table 9.5). The spatially uniform and time invariant strain-rate field is displayed by axes of maximum shear in Figure 9.5.

| Analysis              | dilation-rate<br>(u-strain/yr) | total tensor<br>shear-rate<br>(u-strain/yr) | azimuth of right-<br>lateral axis<br>(gon) |
|-----------------------|--------------------------------|---|--|
| No. 2<br>(1970-80)    | - 0.018 ± 0.001                | 0.64 ± 0.03                                 | -37.8 ± 1.3                                |
| U.S.G.S.<br>(1971-78) | - 0.05 ± 0.01                  | 0.62 ± 0.01                                 | -36.7 ± 1.1                                |

Table 9.5

Comparison of uniform strain-rates

Our estimates are in good agreement with the results obtained from the observation method (Frank's method) by the U.S.G.S. (Savage et al., 1979), except for dilation rates.

It is surprising that the simple models of linear (over-all) strain accumulation in time (Mod. No.2 to No.6) fit the data even so well. This indicates that at least the predominant fault slip-rates at both faults do not vary much within the time span of observation. Even the polynomial of degree 6 in time (Mod. No.11 to 14) does not considerably improve the fit.

The series of experiments with polynomials of higher degrees in space (No.3 to 6), or in space and time (No.11 to 14), demonstrate the limitation of the functions continuous in space for modeling spatially discontinuous displacement fields.

#### 9.5.4 Relative Rigid Block Translation

Rigid block translation seems by far to be the most predominant part in the spatially discontinuous displacement field in question. There may also be discontinuities present in rotation, shear and other strain components. In order to keep the model as simple as possible, the assumption is made that all non-translational discontinuities can be adequately approximated by the spatially continuous functions. The use of alternative spatially discontinuous models which also take into account discontinuities in strain along known faults will be discussed in Section 10.

The discontinuous approximation function in space (6.19) is employed for the modeling of the rigid block translation. After several unsuccessful experiments with various crustal block definitions, the rigid block boundaries proposed by Savage et al. (1979) are adopted. The area of the network is basically divided into the following blocks:

- Block No. 0 : Diablo block , northeast of the Calaveras fault,
- Block No. 1 : Sargent wedge, or central block, between San Andreas and Calaveras fault and
- Block No. 2 : Gabilan block , southwest of the San Andreas fault.

Apparently laying on the eastern block (No.0), the stations HOLLIS and PEREIRA 2 are located very close to the Calaveras fault (cf. Figure 9.2). The individual relative motion of these stations seems to be somewhere between that for the adjacent blocks. Two additional blocks (No.3 and No.4) containing only the immediate surroundings of these two

stations have thus been defined (cf. Figure 9.7).

First a series of approximations with only unrestricted relative block translations were computed. The direction of the relative translation velocity vectors agreed well with the fault strike of both faults, except for the time interval 1974-1977, for which convergent fault slip was obtained for the Calaveras Fault. The relative rigid block translation model (6.19) does not take into account any deformation inside the blocks. Such non-modeled deformations could alias as apparent relative translations perpendicular to the fault strike. The non-constrained block translation model was abandoned for this analysis as it seemed difficult to interpret convergent fault-slip along typical transcurrent faults. (More will be said about the problem of convergent fault movement in Section 10.)

Approximation No.21 models the average rigid block translations with constant slip-rates within the time interval in question (cf. Figure 9.7). The estimated slip-rates are given in Table 9.6.

| Analysis              | Fault slip-rates (mm/yr) |                 |
|-----------------------|--------------------------|-----------------|
|                       | San Andreas Fault        | Calaveras Fault |
| No. 21<br>(1970-80)   | 12.6 ± 0.4               | 17.9 ± 0.4      |
| U.S.G.S.<br>(1971-78) | 13.4 ± 2.2               | 16.7 ± 2.5      |

Table 9.6

Comparison of fault slip-rates

The agreement of the slip-rates obtained by the two different methods of computation is very good. No explanation was found for the large differences of the standard deviations.

With this block translation model, the estimate  $\hat{G}_0$  decreased by 52 percent compared to the time invariant model (No.1). It is striking how this simple kinematical model (No.21), with only 4 unknown real coefficients, fits the data. The comparison of this fit with the fit of the approximations using the spatially continuous models (No.2 to 6) suggests that the adopted block translation model is realistic.

Approximation No.22 applies the same rigid block model in space, taking into account the time variations; algebraic time functions of increasing degrees are used. Under the assumption of the rigid blocks, the time variation of the slip rates seems to be relatively small. Even for time polynomials of 6 th degree,  $\hat{G}_0$  decreases by less than 2 percent compared to the same model (No.21) linear in time.

There is one drawback to this simple block translation model which should be noted. If the slip-rate varies along the fault, this model can only estimate the average rate. This insufficiency could bias the results, especially in the case of the Calaveras Fault, which seems to be locked southeast of Hollister (Savage et al.,1979).

### 9.5.5 Strain and Fault Slip from Combined Models

It is very likely that the simple motion of the rigid blocks is accompanied by deformations inside the blocks. Elastic energy may be stored or released during these deformations. Insight into the development of the deformations in space and time, and their correlation with the occurrence of seismic events, should lead to a better understanding of the plate kinematics and driving forces.

A new combined model was designed by superimposing the rigid block translation model (6.19) onto the spatially continuous approximation model (6.18). This new approximation describes both the continuous as well as the discontinuous part of the deformation of the network in space. The statistical test procedure applied to the ortho-normalized coefficients of this model simultaneously selects the most significant trends of both the fault slip and the strain accumulation.

All approximations from No.31 to 34 are based on this combined model in space. A linear time model, allowing linear fault slip and linear strain accumulation in time, was assumed for the approximations No.31 to No.34. The results of approximation No.31, which combines block translation with uniform strain accumulation, are graphically displayed in Figure 9.8. The slip-rates determined through this approximation differ only very slightly from the results of the pure block motion model (San Andreas Fault:  $\Delta v = -1.25\text{mm/yr}$ , Calaveras Fault:  $\Delta v = -1.39\text{mm/yr}$ ). A significant right lateral shearing strain-rate of  $0.13 \pm 0.019$  ustrain/yr in the direction of the San Andreas Fault ( $Az=56.5 \pm$



4.Ogon) was estimated from this model.

The approximations No. 41 to 46 use the same combined model, taking into account variations with time. The considerable decrease of with increasing degree of the time function indicates that the deformation may not be developing linearly in time.

Approximation No.41 combines the time varying, spatially uniform strain accumulation with time varying rigid block translation. The very small, uniform shear-rate remains almost constant in the time interval 1972 - 1980. The estimated right lateral tensor shear-rate varies only between 0.13 and 0.16  $\mu$ strain/yr, with its azimuth varying between -38 and -69 gon. The estimated slip-rate at the San Andreas Fault apparently decreases and reaches a minimum of  $7.3 \pm 1.3$  mm/yr in 1978. Both estimated slip-rates increase considerably after 1979.

The approximations No.41 to 46 are experiments with combined models in space that vary non-linearly in time. In contrast to the small temporal variations of the spatially uniform strain-field found from the approximation No.41, considerable temporal variations are estimated as soon as the homogeneous model in space is replaced by a non-homogeneous model (Mod. No.42 to 46). The right lateral shear-rate of -0.3  $\mu$ strain (strain accumulation) found along the San Andreas fault in 1975 (Mod. No.43) decreases and changes into a left lateral rate of +0.3  $\mu$ strain in 1979. This may indicate that shearing strain was accumulated and released within the time span of the investigation. This development of the deformation is very likely

related to the occurrence of the four above-mentioned earthquakes. As co-seismic deformations are of episodic nature, the continuous and smooth time functions applied up to this point are not a good choice. Episodic, co-seismic motions may be smoothed out by the smooth functions used.

#### 9.5.6 Piecewise Linear Time Functions

In order to further investigate the temporal behaviour of the deformation, a piecewise linear and continuous time function (6.21) is chosen. The sequence of time intervals which defines the approximation function in time is given in Table 9.7.

| Episode<br>No. | Interval  |         |
|----------------|-----------|---------|
|                | Beginning | End     |
| 1              | 1970.0    | 1972.39 |
| 2              | 1972.38   | 1973.33 |
| 3              | 1973.32   | 1974.46 |
| 4              | 1974.45   | 1975.28 |
| 5              | 1975.27   | 1976.43 |
| 6              | 1976.42   | 1977.64 |
| 7              | 1977.63   | 1978.36 |
| 8              | 1978.35   | 1979.36 |
| 9              | 1979.35   | 1979.70 |
| 10             | 1979.69   | 1980.50 |

Table 9.7

Intervals of piecewise linear time function

Each interval contains at least two 'near-complete' epochs of

re-observation (cf. Figure 9.4). The same generalized polynomial as in approximation No.43 (with 4 rigid block translation parameters, 3 conformal and 3 anti-conformal algebraic terms) was chosen for the approximation in space.

The accumulated slip at both active faults, the Calaveras and the San Andreas, are displayed in Figures 9.9 and 9.10. In contrast to the analysis of the USGS, our results show significantly larger slip rates for some of the intervals in which three of the moderate earthquakes occurred (Savage et al., fig. 9 and 10, p.7606-7607, 1979). No unusual slip-rate could be associated with the 1974 Gilroy earthquake ( $M_L=4.4$ ).

The shear-rate field for some of those time intervals with large slip rates shows considerable left lateral shear, which could be interpreted as release of accumulated shearing strain during these slip episodes.

No seismic event with a magnitude  $M_L$  larger than 3.5 in the San Andreas Fault area could be associated with the anomalously large slip rate in the interval 1976.42,1977.64 exhibited by the San Andreas fault slip curve (cf. Figure 9.10).

### 9.5.7 Episodic Time Functions

From the experiments with the piecewise linear time function, we can see that three episodic motions are identifiable within the following time intervals:

- No.2 (1972.38-1973.33), possibly associated with the S.J. Bautista ( $M_L=4.9$ ) earthquake,
- No.4 (1974.45-1975.28), possibly associated with the Hollister ( $M_L=5.1$ ) earthquake and
- No.9 (1979.35-1979.70), possibly associated with the Coyote Lake ( $M_L=5.9$ ) earthquake.

After knowing the instant when an episodic motion may have occurred, it is possible to model the deformation in the time domain by using the episodic time function (6.25). Very short linear episodes ( $\Delta t = 0.01$  yr) were associated with each of the four earthquakes given in Table 9.1. The episode associated with the 1974 Gilroy earthquake was left out as practically no response was found for this episode (approximations No.72 and 74).

In model No.75 a time polynomial up to order 5 and with 3 linear episodic terms is employed. The space functions are the same as in approximation No.45.

| Episode<br>No. | Interval  |          | Seismic Event |          |
|----------------|-----------|----------|---------------|----------|
|                | Beginning | End      | No.           | Time     |
| 1              | 1972.754  | 1972.764 | 1             | 1972.759 |
| 2              | 1974.905  | 1974.915 | 3             | 1974.910 |
| 3              | 1979.592  | 1979.602 | 4             | 1979.597 |

Table 9.8

## Co-seismic episodes

As this episodic model was found to describe very satisfactorily the 'co-seismic' motions — the episodic model approximations yield the minimal estimate  $\hat{G}_0$  — it was selected for the final approximation No. 91. The final model and its fit to the data will be discussed in Sub-section 9.5.9.

## 9.5.8 Additional Experiments

## a) Elimination of Variable Network Scale Factors:

The program CRUSTRAIN allows the estimation of nuisance parameters for scale and orientation variations of each individual network. Unknown scale factors were introduced in approximations No.51 and 52 for all epochs except epoch No. 5 (of which the scale was adopted as a reference). The estimated scale factors were found to vary irregularly (Mod. No.52). The variations of up to 0.3 ppm relative to the

arbitrarily adopted reference scale are likely to reflect accidental as well as small systematic scale errors of the EDM-observations, rather than crustal dilatation. (Note: The magnitude of these variations is in good agreement with the a priori estimate of the scale error; cf. eqn. 9.2.) The anti-conformal complex strain element (shear) is the interesting strain quantity which is sought in a zone of active transcurrent faults. As shear does not depend on the network scales (except for second order effects), it was decided to introduce unknown scale nuisance parameters and to eliminate them in the approximation (final model No. 91).

b) Accumulation and Release of Shearing Strain Across the Faults:

The development of shear in the direction normal to the strike of a fault is particularly interesting if the accumulation and the release of shearing strain across an active strike slip fault is to be investigated. As shear in a given direction is a scalar quantity, it can be depicted by a three-dimensional surface. Figure 9.11 shows, for example, the lines of equal shear (iso-lines) in the direction perpendicular to the San Andreas fault (azimuth: 42 gon) as it is estimated from the approximation No.45 (at  $t=1975.0$ ). Note the coincidence of the zone of maximum shear-rate (in azimuth: 42 gon) with the Sargent fault trace, which indicates that minor fault creep may occur within the Sargent zone.

Since shear varies considerably in space, the display of this shear component surface by iso-lines is much easier to interpret than the

pattern of shear-rosettes. The area in which shearing strain is accumulated can very well be distinguished from the zone in which shearing strain is released. However, such plots display only one component of the anti-conformal strain, whereas the display of the shear-rosettes or the axes of maximum shear represents the full information.

#### 9.5.9 Final Approximation Model

From the experiments with continuous approximation functions in space (approximation No.2 - 6), it was found that spurious oscillations of the spatial approximation to the strain-field can be reliably avoided within the network area if the degree of the complex algebraic polynomials are not higher than 4. Only small effects towards the periphery of the network were observed when polynomials of degree 6 were used in approximation No.6.

Considering the distribution of observations in time (cf. Figure 9.4), 3rd degree polynomials in space and a 5th degree polynomial in time were selected for the final model (No.91). Spurious oscillations of the strain field in time are definitely avoided with this choice, as the network was re-observed almost completely at 11 occasions within the last decade. The discontinuities in space were modeled by the rigid block translation model introduced in 9.5.4 and the discontinuities in time by the episodic model discussed in 9.5.7.

The statistical filtering of the Fourier coefficients is based on the (a priori) variance of coefficients ( $\sigma_0^2 = 1$ , known) and a level of significance  $\alpha = 0.05$ . A total of 97 unknown parameters (48 position coordinates, 21 heights and 28 scale factors) were eliminated from the parameter vector of the simultaneous adjustment and approximation (cf. Table 9.4). The results of the final approximation are graphically presented in Figures No. 9.12 to 9.23. The estimate  $\hat{\sigma}_0$  remained larger than 2 in all approximations reported in Table 9.4. A value of  $\hat{\sigma}_0 = 2.217$  was obtained for the final model. A  $\chi^2$ -square test on the variance factor  $\sigma_0^2$  fails on the level of significance  $\alpha = 0.05$ . The reasons for this incompatibility of the observation data with the approximation model are:

- a) incomplete formulation of the approximation model (model errors)  
(Note: The approximation model in space could probably be improved if spatial discontinuities along known fault lines were also modeled.),
- b) individual, irregular motions of station marks which may be related to non-tectonic surface deformations (Savage et al., 1979) (The model is too smooth to pick up these irregularities.) and
- c) too optimistic estimates for the variance of the distance observations (cf. 9.2.1).



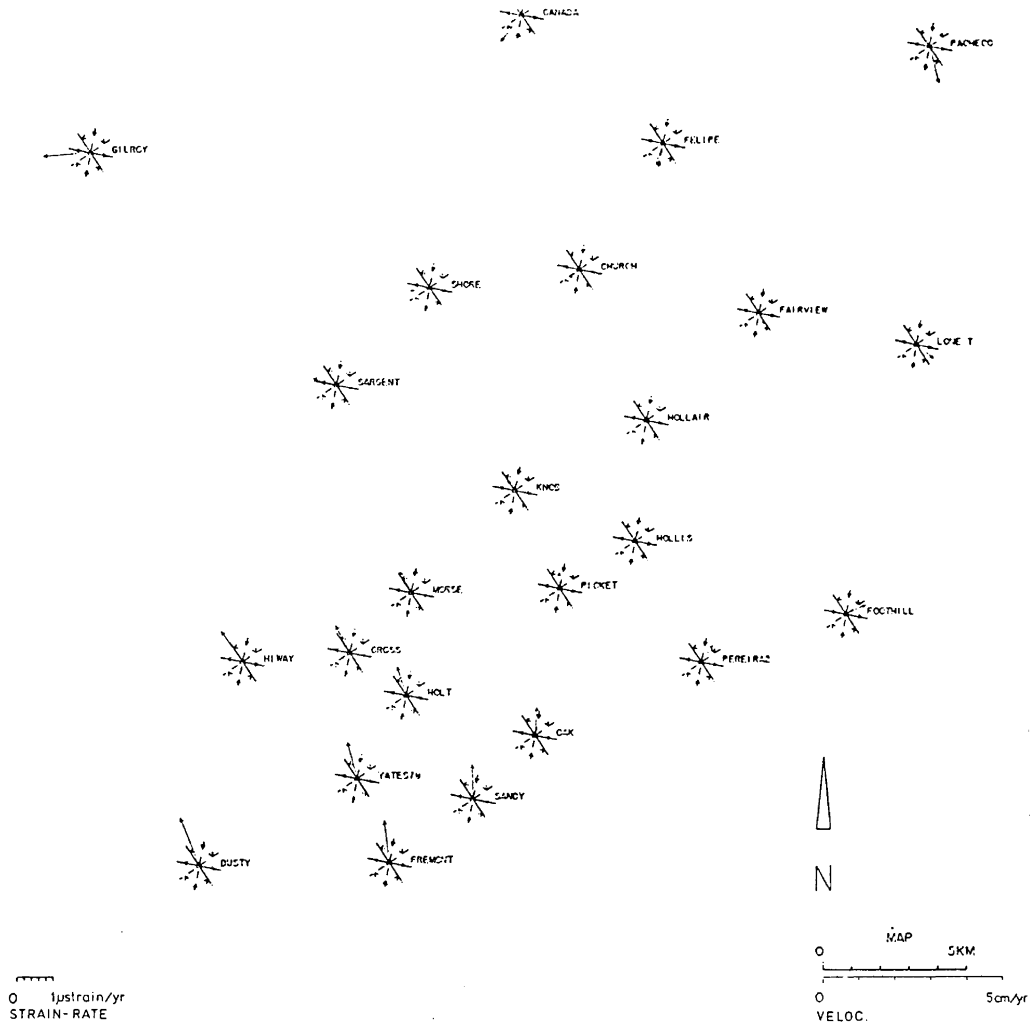


Figure 9.6

Average spatially uniform tensor shear-rate (Mod. No.2)

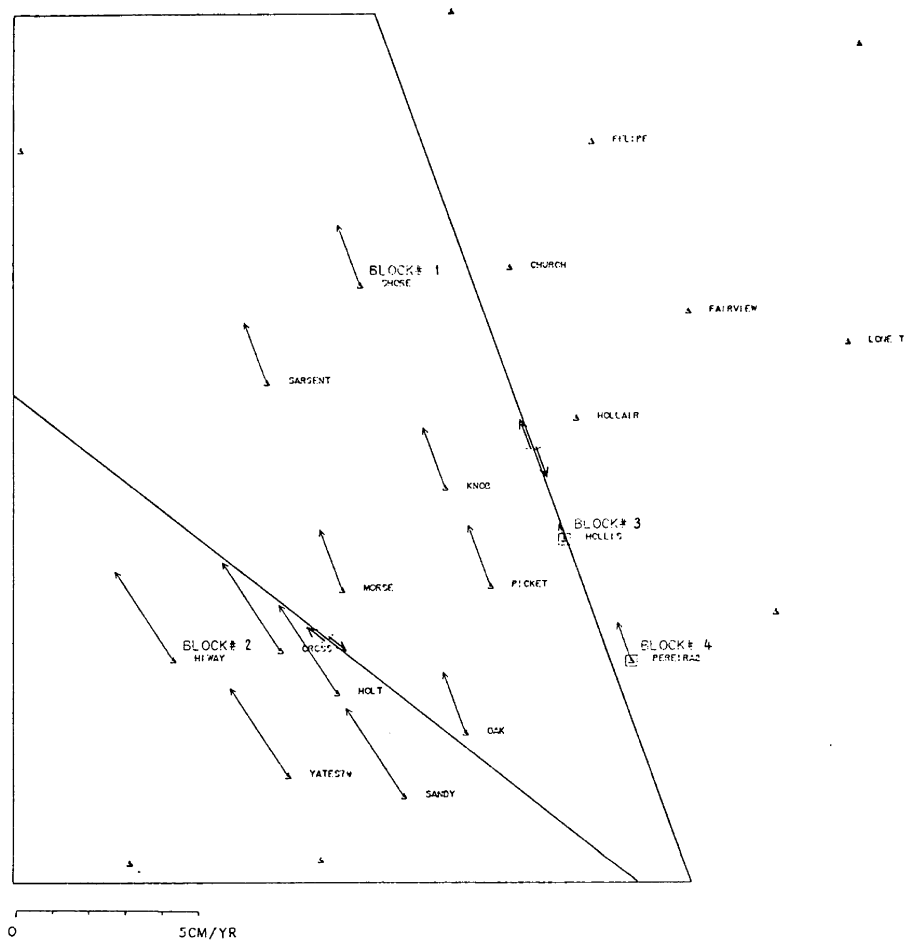


Figure 9.7

Velocity of average rigid block translation (Mod. No.21)

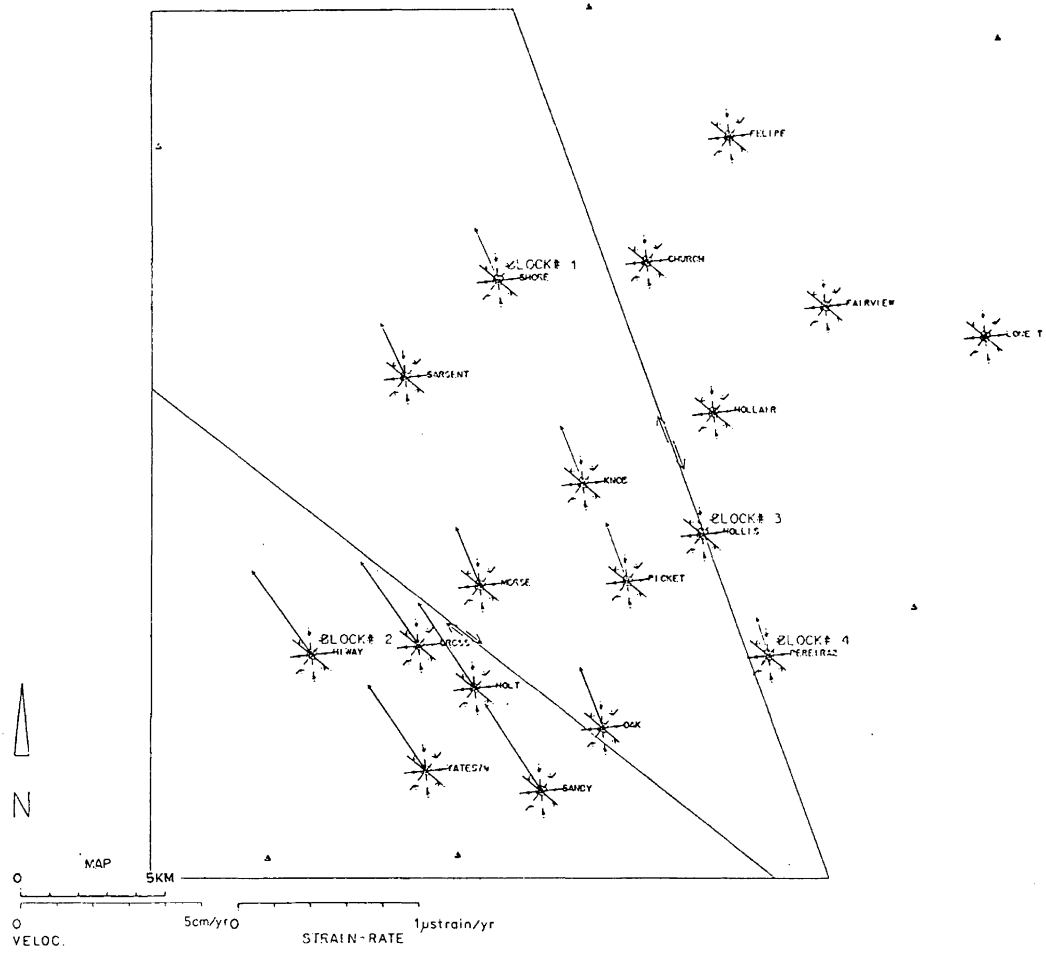


Figure 9.8

Velocity of average block translation and over-all tensor shear-rate

(Mod. No. 31)

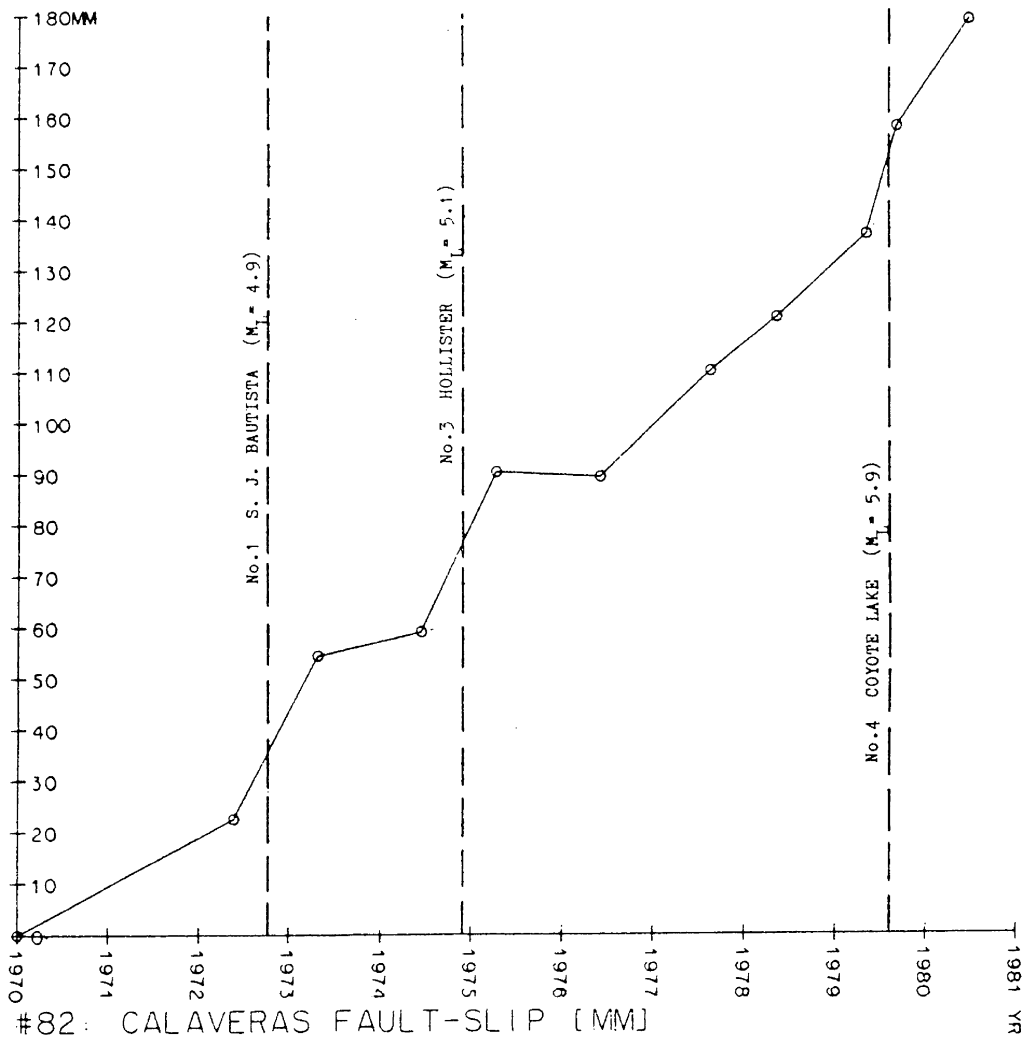


Figure 9.9

Calaveras fault-slip as estimated from the piecewise linear model No.82

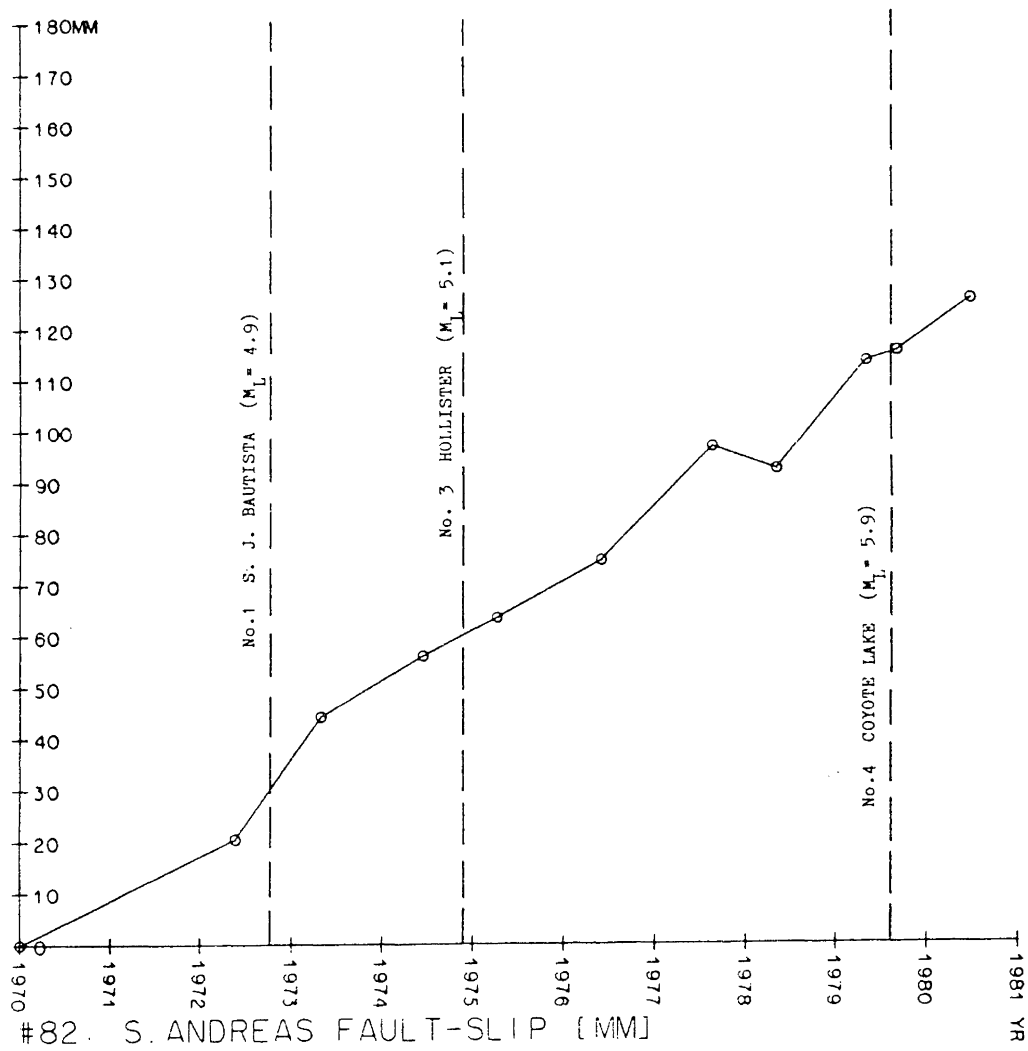


Figure 9.10

San Andreas fault-slip as estimated from the  
 piecewise linear model No.82

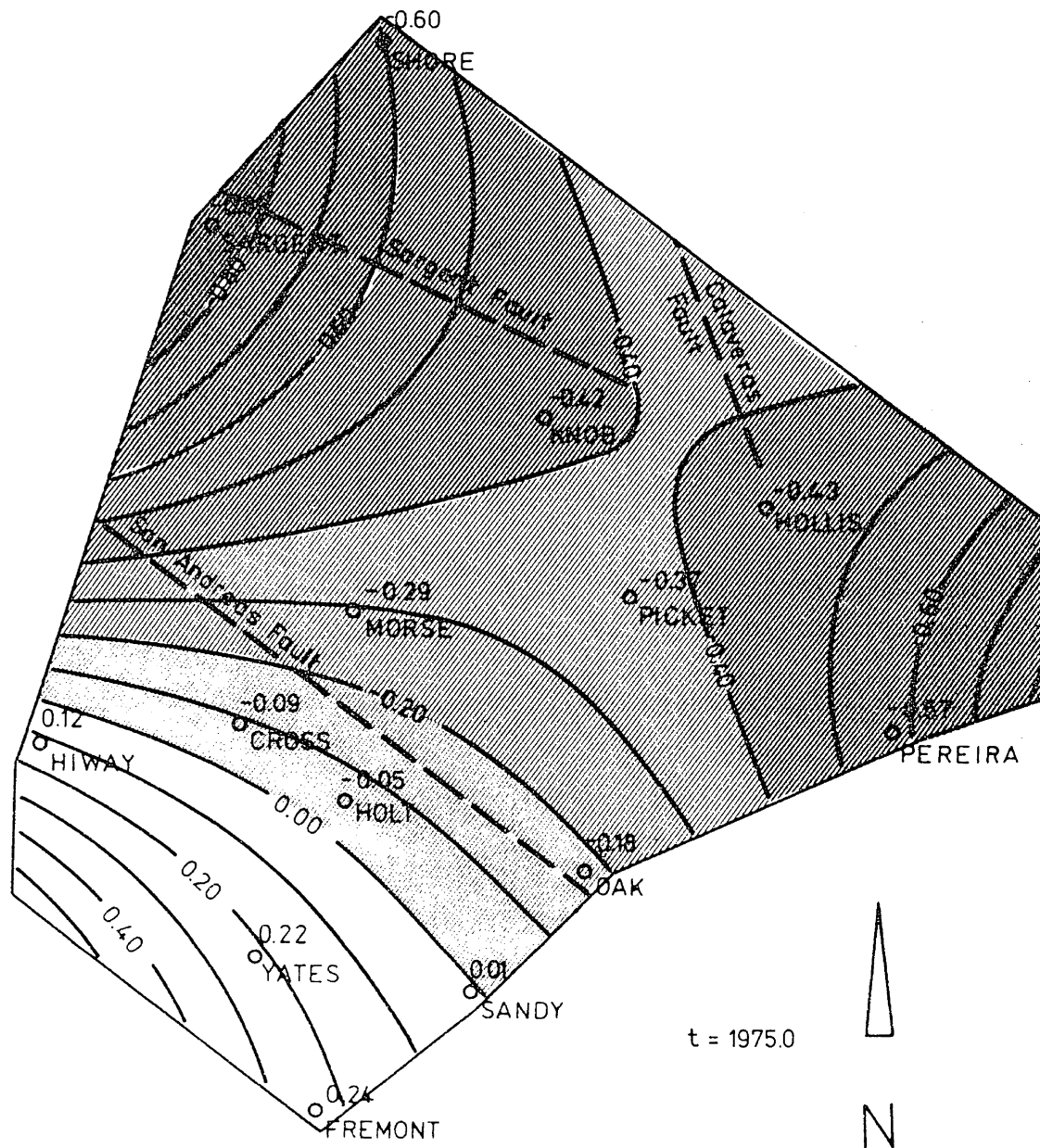


Figure 9.11

Tensor shear-rate component in the direction perpendicular to the San Andreas fault (azimuth: 42 gon)

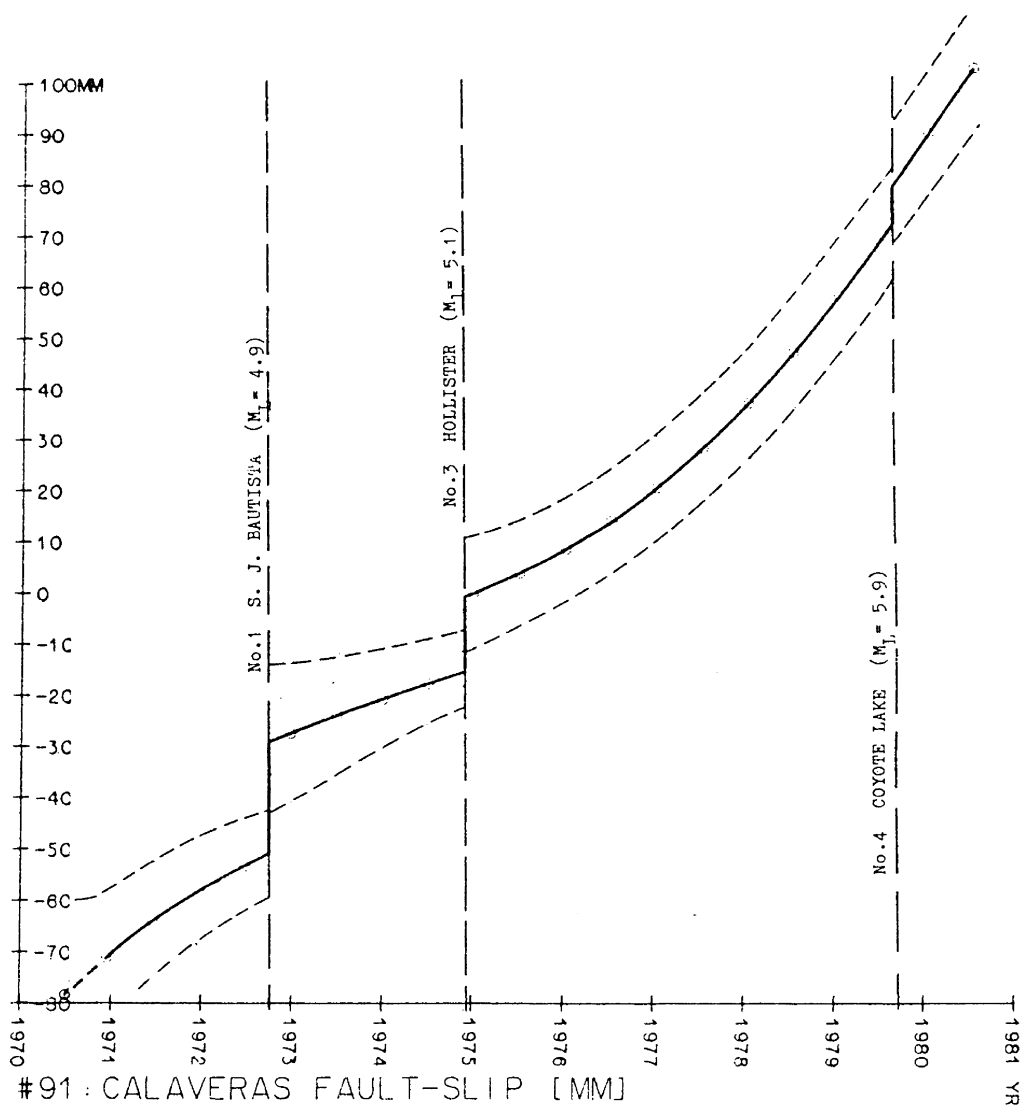


Figure 9.12

Calaveras fault-slip and its standard deviation (Mod. No.91)

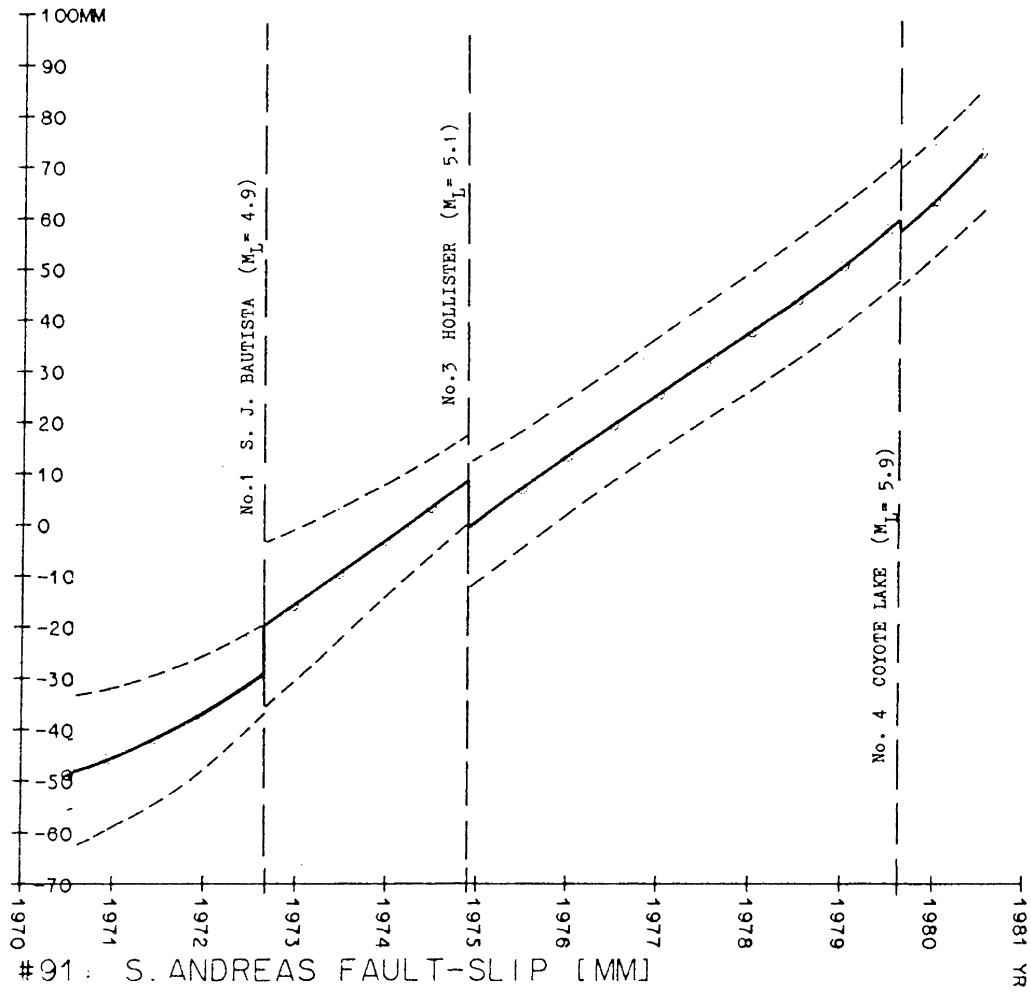


Figure 9.13

San Andreas fault-slip and its standard deviation (Mod. No.91)



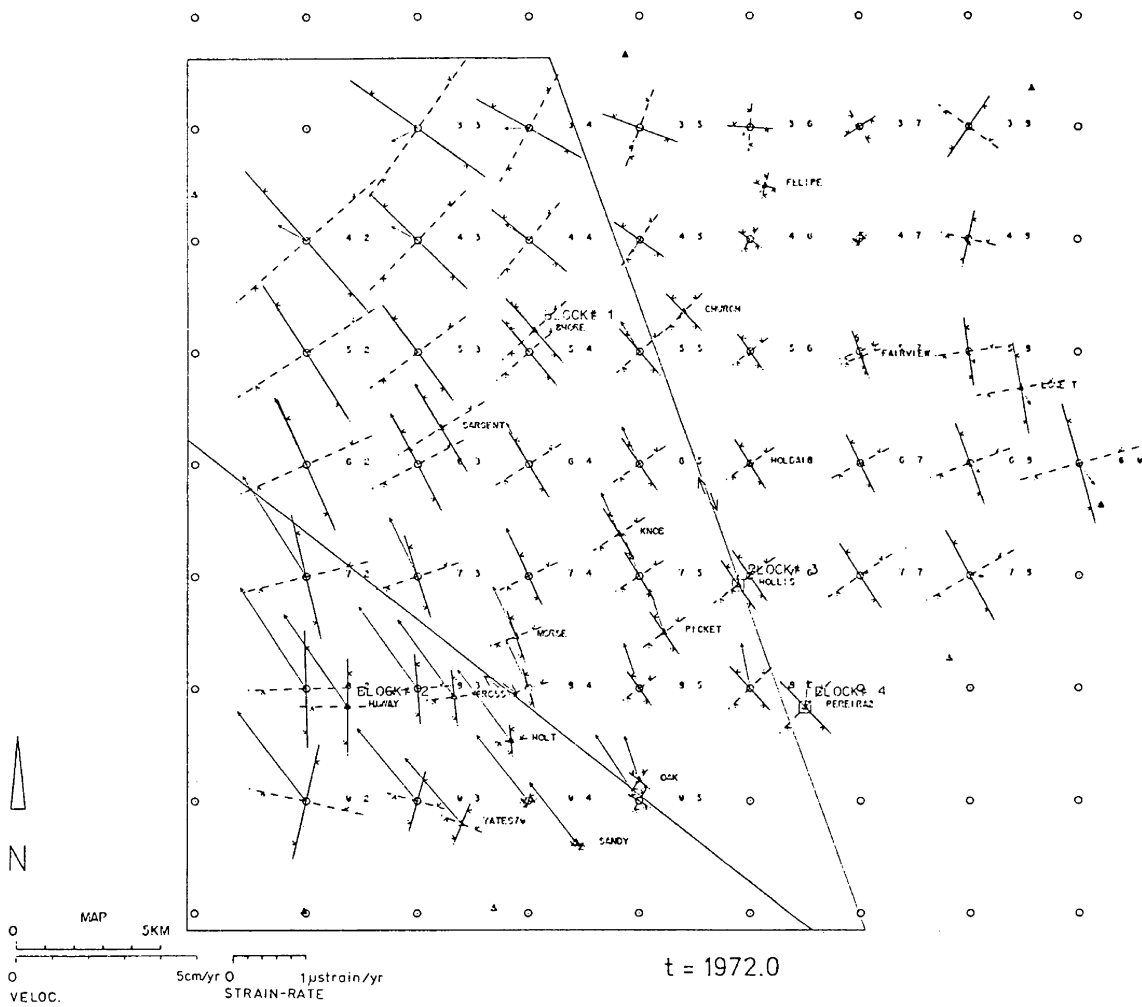


Figure 9.14

Fault slip-rates and tensor shear-rates (Mod. No.91,  $t=1972.0$ )

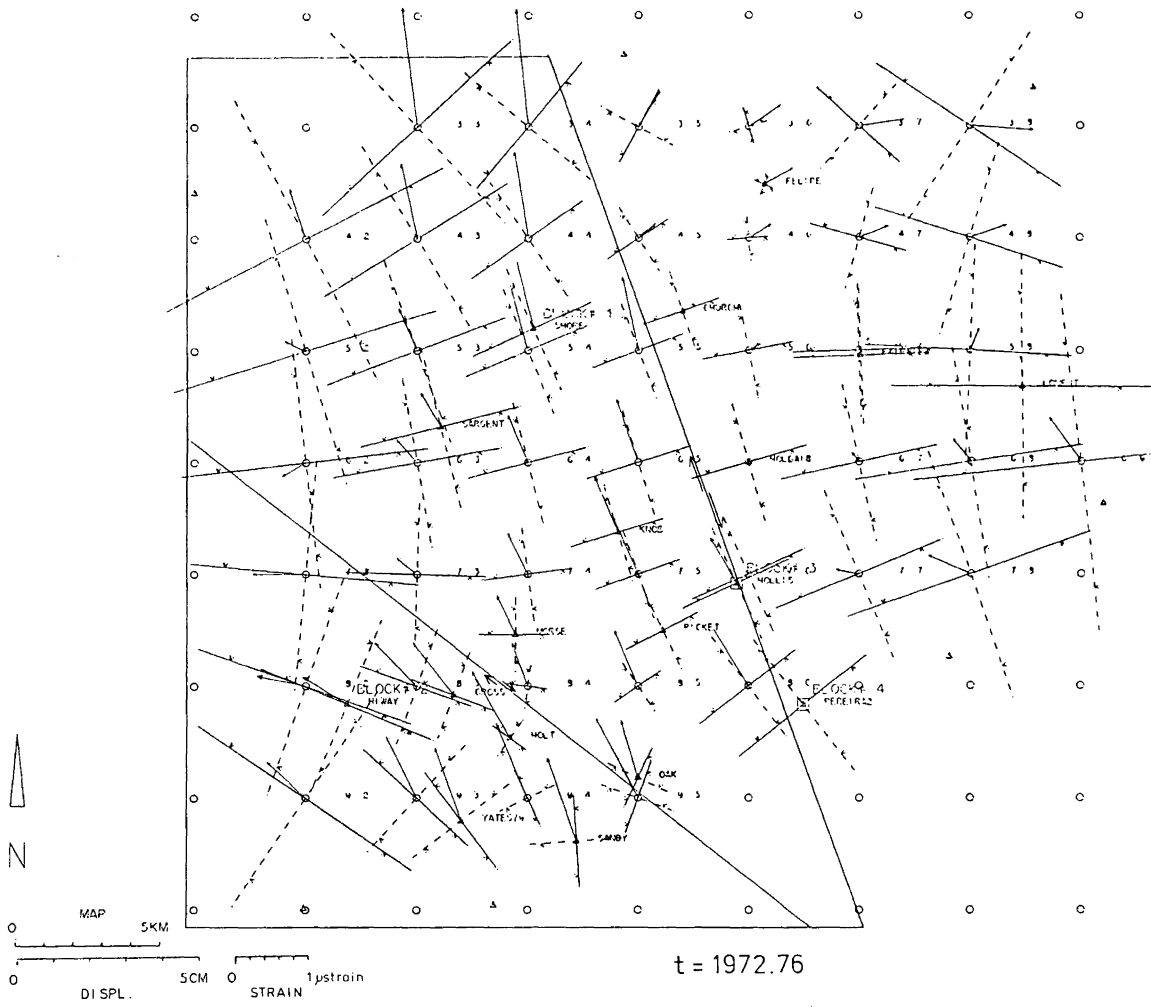


Figure 9.15

Co-seismic fault slip and tensor shear (Mod. No.91, t=1972.76)

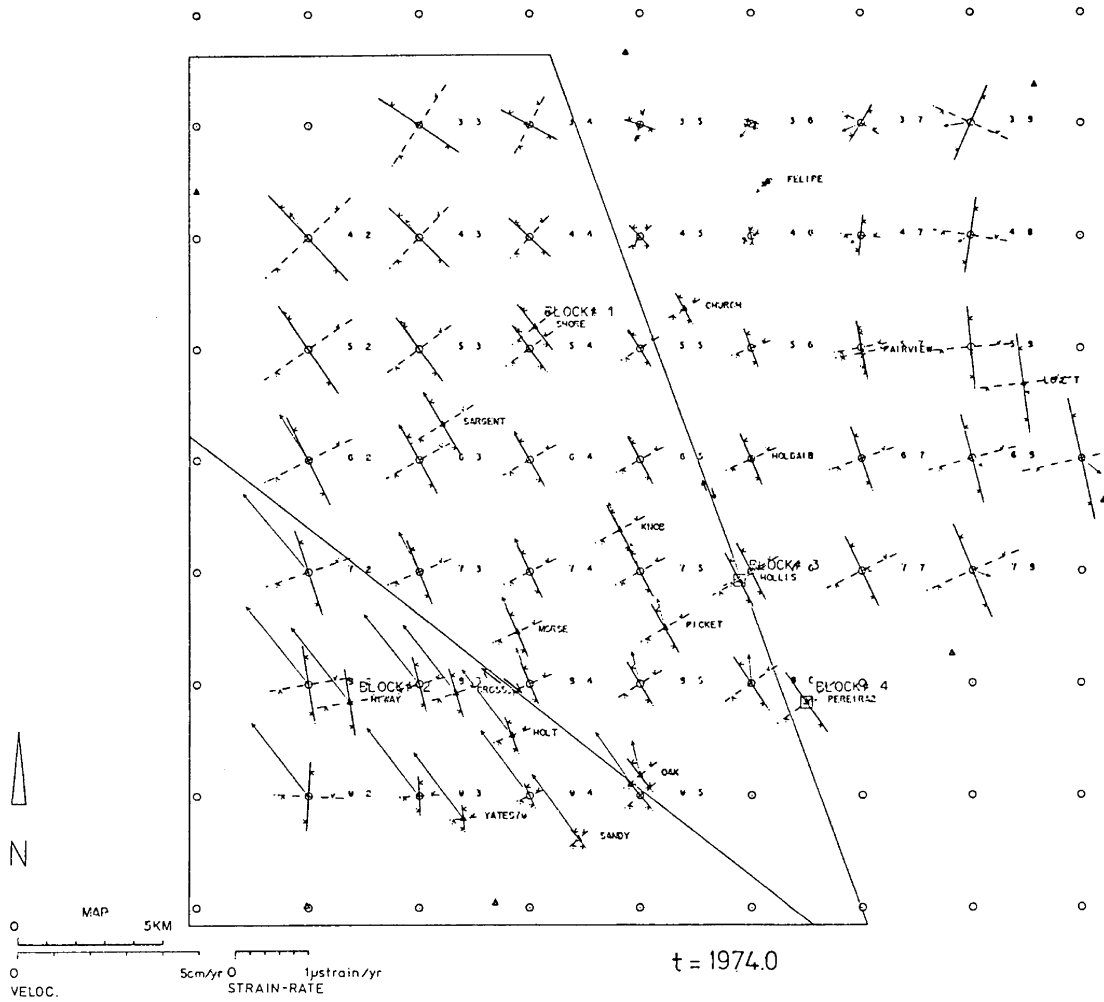


Figure 9.16

Fault slip-rates and tensor shear-rates (Mod. No.91, t=1974.0)

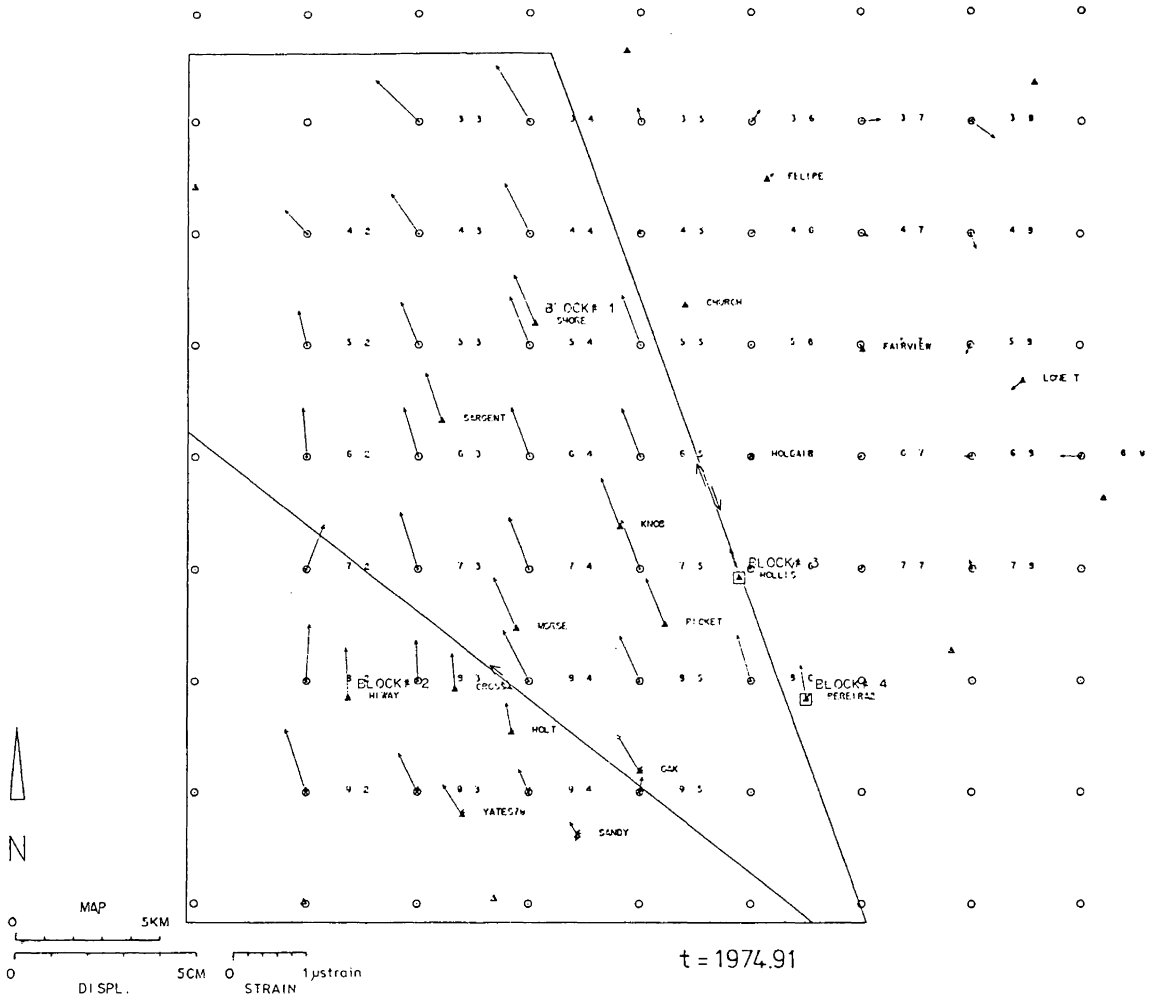


Figure 9.17

Co-seismic fault slip and tensor shear (Mod. No.91, t=1974.91)

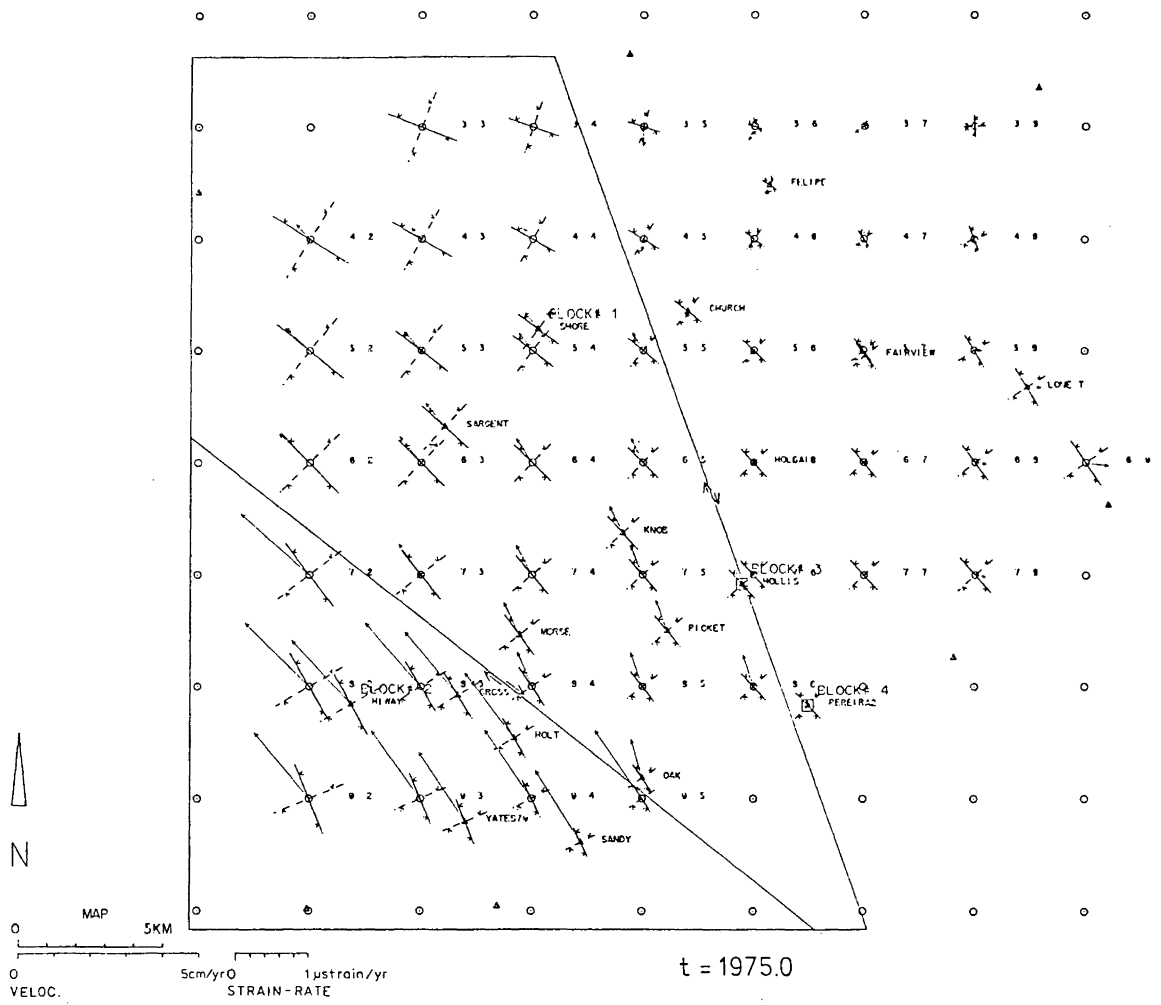


Figure 9.18

Fault slip-rates and tensor shear-rates (Mod. No.91, t=1975.0)

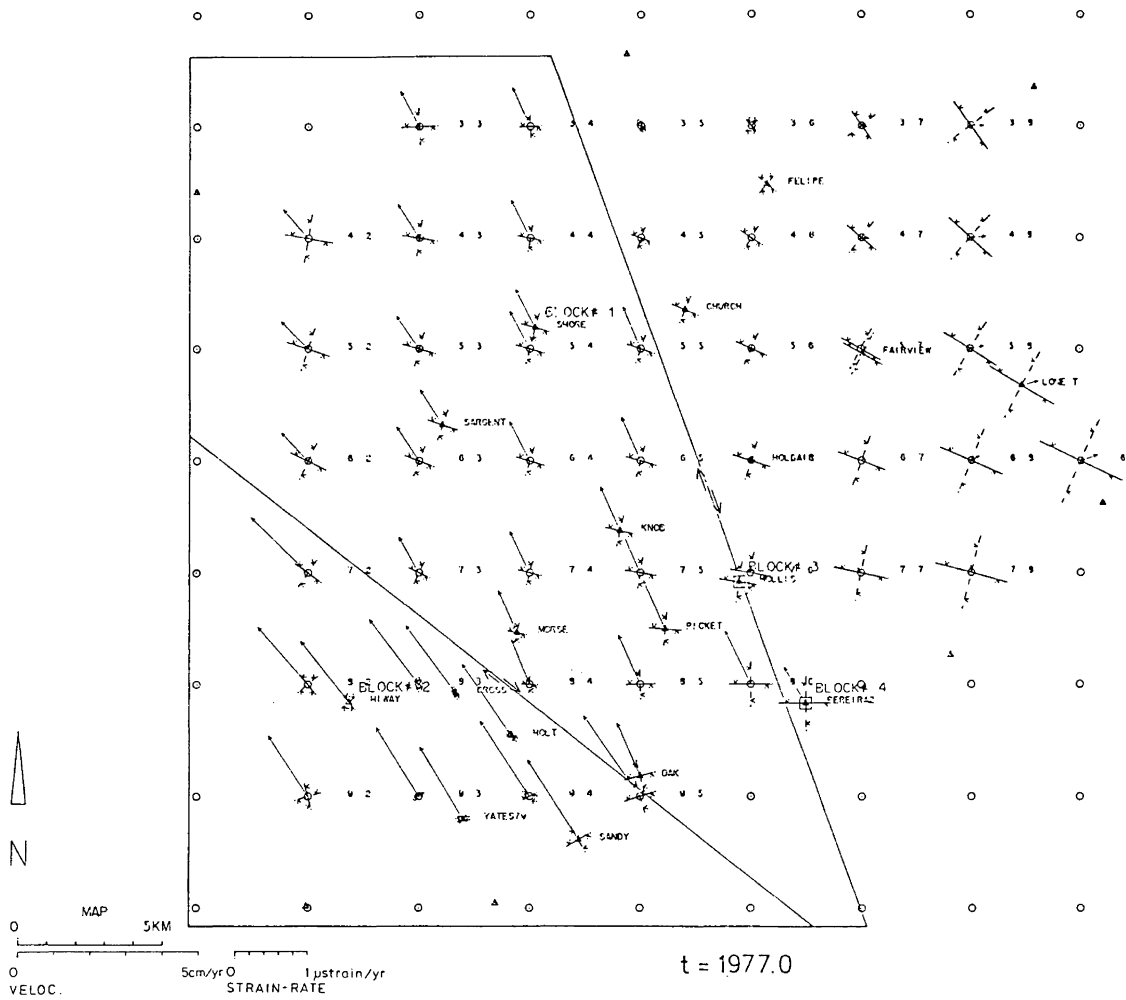


Figure 9.19

Fault slip-rates and tensor shear-rates (Mod. No.91, t=1977.0)

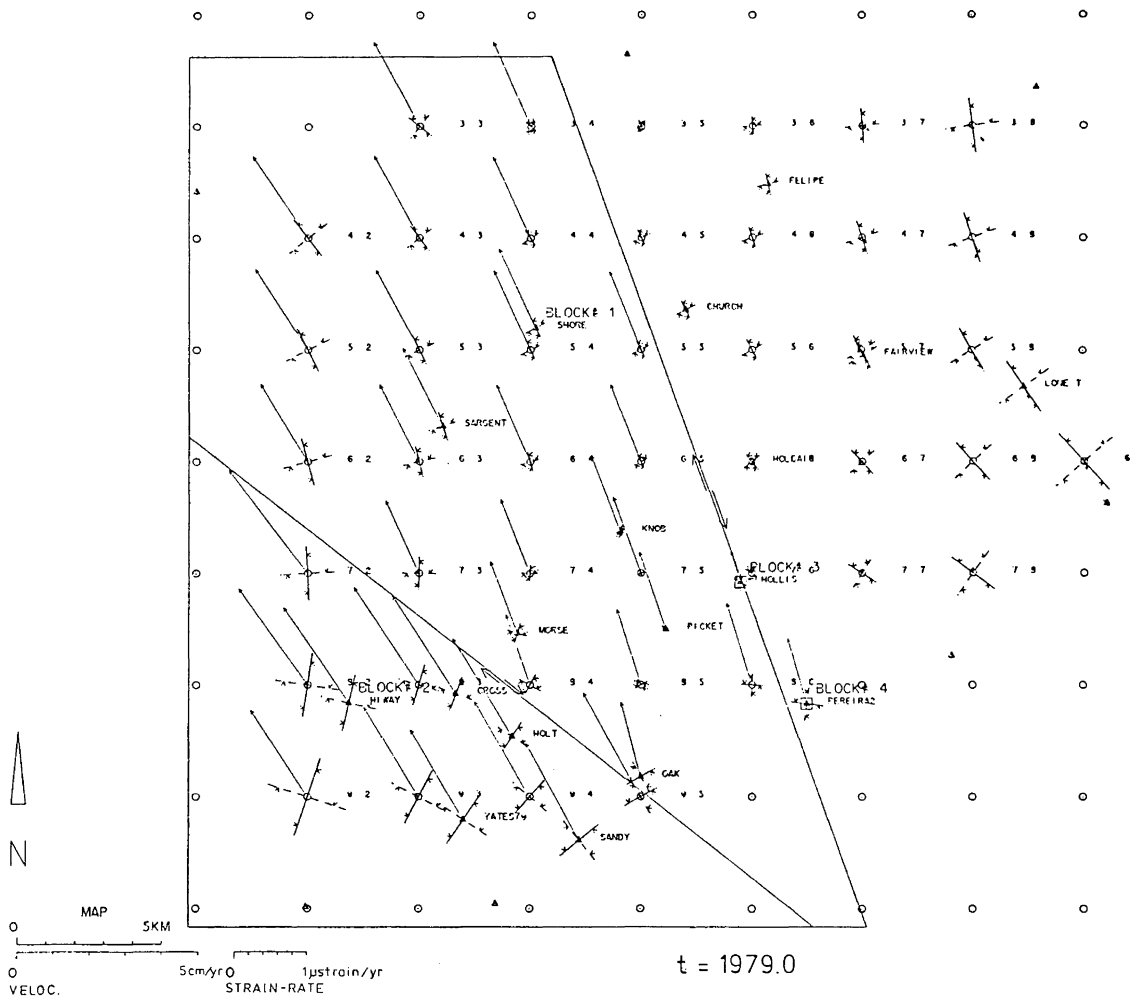


Figure 9.20

Fault slip-rates and tensor shear-rates (Mod. No.91, t=1979.0)

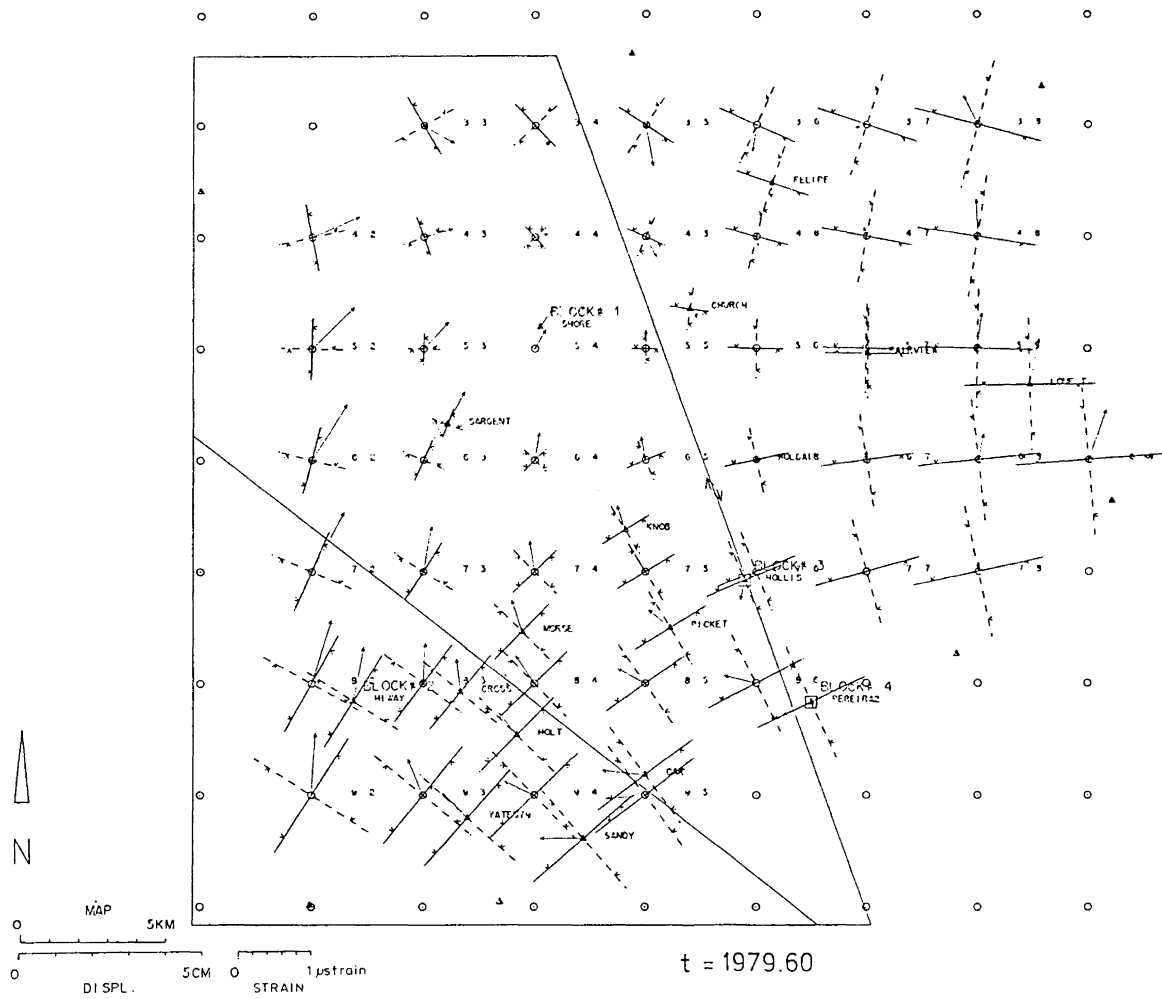


Figure 9.21

Co-seismic fault slip and tensor shear (Mod. No.91, t=1979.60)



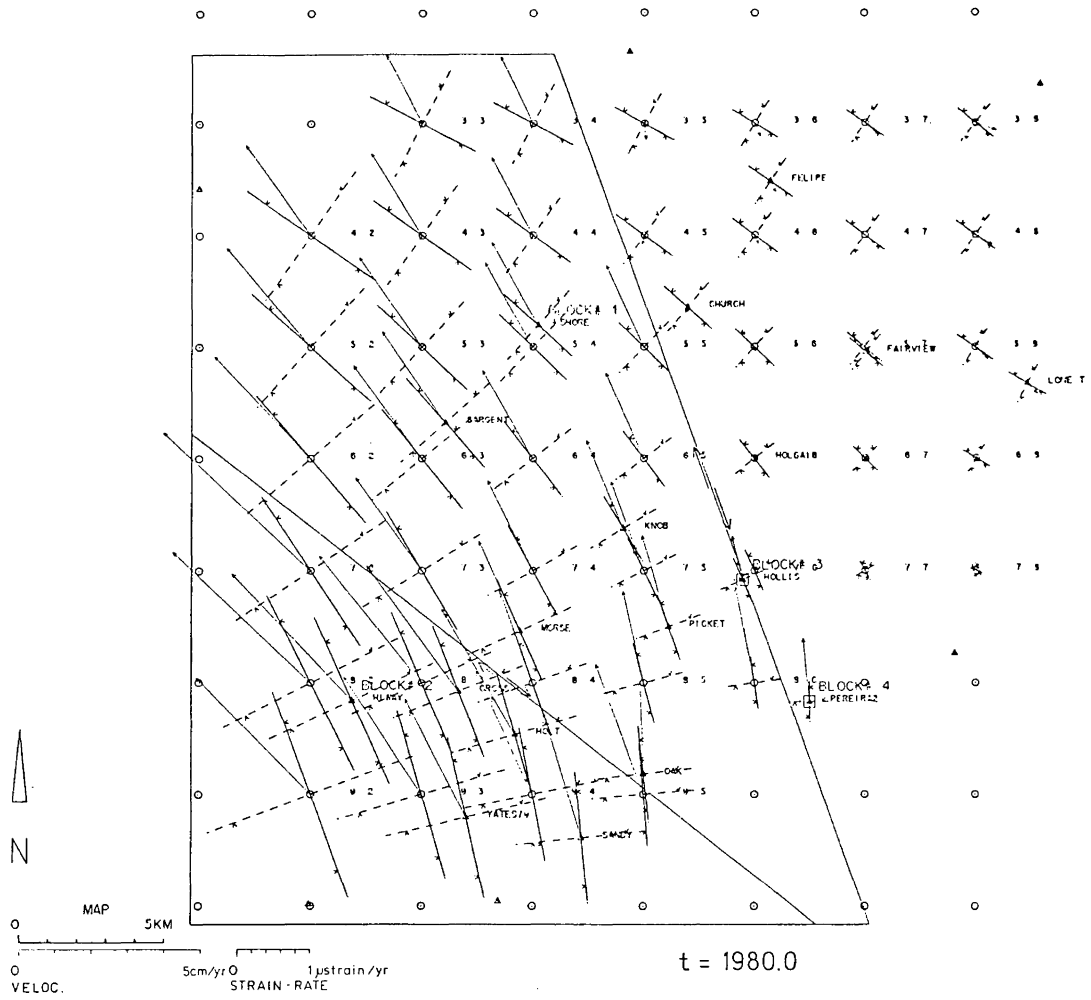


Figure 9.22

Fault slip-rate and tensor shear-rate (Mod. No.91, t=1980.0)

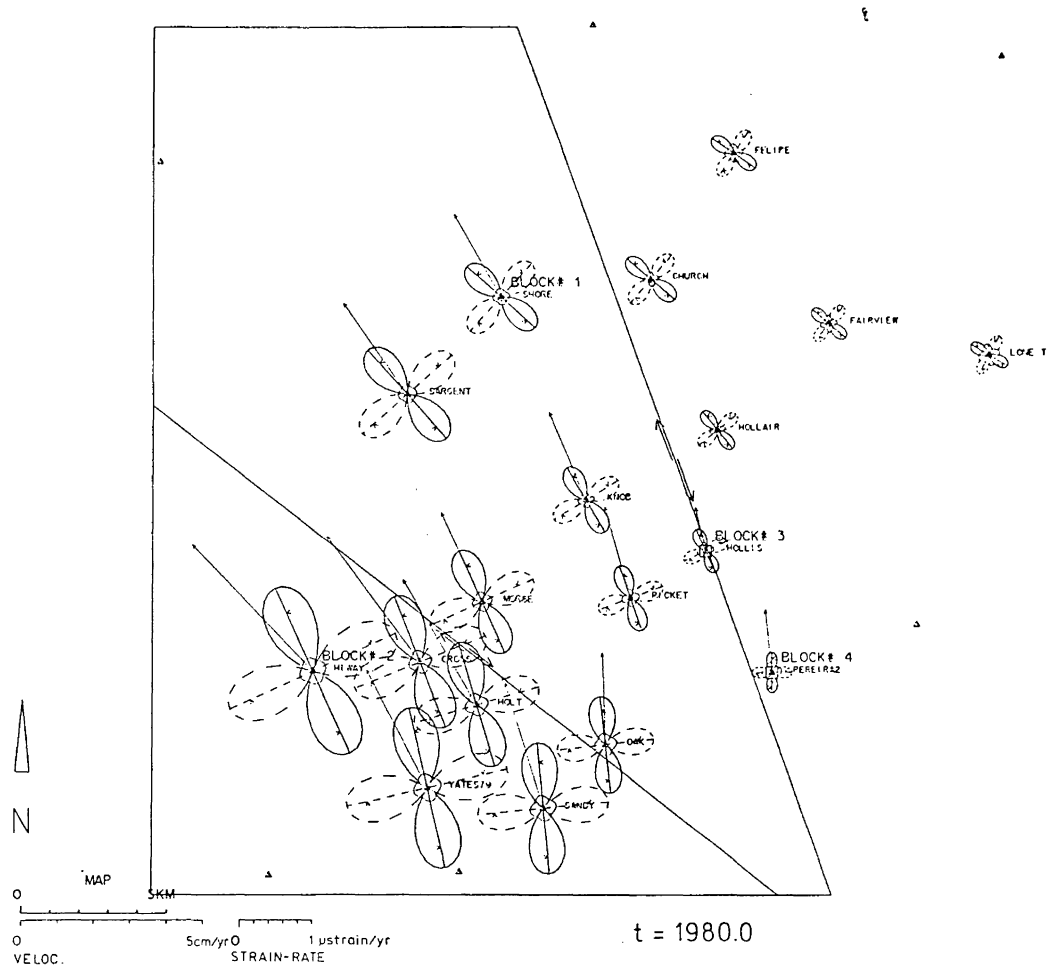


Figure 9.23

Rosettes showing the tensor shear-rate and its standard deviation  
in a given direction

## 9.6 Interpretation

The following kinematical interpretation of the results obtained from the final approximation No.91 is based on the graphical displays given in Figures 9.12 to 9.23. The development of crustal deformation between 1971 and 1980.5 is described in a sequence of seven phases. (Note: All measures of accuracy given below are standard deviations estimated from the least-squares approximation).

### Phase 1: (1971.0 to 1972.754)

Accumulation of right-lateral shear (of approximately  $0.5 \mu\text{strain/yr}$ ) along a line normal (in average) to the faults takes place. The most dominant shear-rate is found in the northern part of the Sargent wedge (cf. Figure 9.14). The Calaveras fault slip-rate decreases to  $10.3 \pm 5.0 \text{ mm/yr}$  (right-lateral,  $t=1972.0$ ), whereas the San Andreas fault slip-rate slightly increases and reaches  $10.3 \pm 4.7 \text{ mm/yr}$  (right-lateral,  $t=1972.0$ ). The estimated accumulated slip with respect to the reference time  $t_0 = 1975.0$  is shown in the Figures 9.12 and 9.13. The standard deviation of accumulated slip is represented by broken lines plotted on either side of the slip-curves.

### Phase 2: (1972.754 to 1972.764) Co-seismic motion associated with the S.J. Bautista earthquake ( $M_L = 4.9$ )

The epicenter of the earthquake is located close to the San Andreas fault trace (cf. Figure 9.3). The episode is characterized by left-lateral shear of approximately  $0.9 \mu\text{strain}$

across the Calaveras fault trace (cf. Figure 9.15). This is interpreted as a release of shearing strain associated with a larger co-seismic slip of  $21.7 \pm 7.4$  mm at the Calaveras fault and a smaller slip of  $9.6 \pm 8.7$  mm at the San Andreas fault (cf. Figures 9.12 and 9.13).

Phase 3: (1972.764 to 1974.905)

The most noticeable development in this phase is the accumulation of spatially almost uniform right-lateral shearing strain of approximately  $0.4 \mu$ strain perpendicular to the Calaveras fault trace (cf. Figure 9.16). The right-lateral Calaveras fault slip-rate reaches a minimum (at  $t=1974.0$ ) of only  $5.9 \pm 3.8$  mm/yr (cf. Figure 9.12), whereas the San Andreas right-lateral slip (cf. Figure 9.13) continues almost linearly in time with a rate of  $12.9 \pm 3.8$  mm/yr.

Phase 4: (1974.905 to 1974.915) Co-seismic motion associated with the Hollister earthquake ( $M_L=5.1$ )

The Hollister earthquake occurred upon the Busch fault, a left-lateral, conjugate fault to the Sargent fault (Savage et al., 1979; cf. Figure 9.3). The co-seismic motion is characterized by almost pure rigid block translation. A right lateral slip of  $14.4 \pm 6.0$  mm at the Calaveras fault and a reversed (left-lateral) slip of  $9.0 \pm 6.2$  mm at the San Andreas fault (cf. Figures 9.12 and 9.13) are estimated. Apparently shearing strain release in the close vicinity of the San Andreas fault is represented by left-lateral fault slip instead of local

left-lateral shear. This is probably a consequence of the selected continuous approximation function (with low degree algebraic polynomials) in space, which is too smooth to model local variations in space.

Phase 5: (1974.915 to 1979.592) Figure 9.18 shows the accumulation of right-lateral shearing strain similar to phase 3, though more pronounced in the Sargent wedge and the Gabilan block in 1975. The Calaveras fault slip-rate increases from  $6.9 \pm 2.8$  mm/yr in 1975 to  $22.7 \pm 3.0$  mm/yr in 1979 (cf. Figure 9.12), whereas the shear-rate decreases to approximately 0.1  $\mu$ strain in the Calaveras fault zone. The San Andreas fault slip-rate, on the other hand, remains almost constant in time ( $11.9 \pm 1.7$  mm/yr, right-lateral,  $t=1977.0$ ) within the whole time span. The right lateral shear (strain accumulation) in the Gabilan block in 1975 slowly diminishes and finally changes its sign (strain release) in 1979 (cf. Figures 9.18, 9.19 and 9.20).

Phase 6: (1979.592 to 1979.602) Co-seismic motion associated with the Coyote Lake earthquake ( $M_L=5.9$ )

The Coyote Lake earthquake occurred upon the Calaveras fault, approximately 30 km northwest of Hollister. The episode is marked by considerable release of shearing strain (approximately 0.7  $\mu$ strain, left-lateral, across the San Andreas fault) at the southern end of the Calaveras fault and in the Diablo block (cf. Figure 9.21). A co-seismic right-lateral slip of  $7.7 \pm 4.8$  mm is estimated at the Calaveras fault. The reverse slip of  $2.5 \pm 6.9$  mm

(left-lateral) at the San Andreas Fault may again be interpreted as an effect of local release of shearing strain (cf. Phase 4).

Phase 7: (1979.602 to 1980.5)

New accumulation of considerable right-lateral shearing strain in the Gabilan block (No.2), of approximately  $0.9 \mu\text{strain/yr}$  along a line normal (in average) to the faults, takes place (cf. Figure 9.22). Relatively high slip-rates are estimated for both the Calaveras ( $25.0 \pm 5.4 \text{ mm/yr}$ ) and San Andreas faults ( $17.2 \pm 6.2 \text{ mm/yr}$ ) for the time of prediction  $t=1980.0$ .

It should be noted that the data coverage is not sufficient for distinguishing between pre-seismic motions (of a duration of months before an earthquake), co-seismic motions and post-seismic motions (of a duration of a few months after the earthquake). All these motions are estimated together as 'co-seismic' from the approximation using the episodic time function (Mod. No. 91).

The standard deviation of the estimated shear-rates computed at the network stations for  $t = 1980.0$  is displayed together with the shear-rosettes in Figure 9.23. The displayed confidence regions of the shear in a given direction increase towards the periphery of the network. They also increase for those prediction times which differ most from the mean of the total time interval of observation (1975.5). The standard deviations of all predictions of shear-rates for  $t=1972.0$  to  $t=1979.0$  are considerably smaller than the values displayed for  $t=1980.0$  in Figure 9.23.

## SECTION 10

## CONCLUSIONS AND RECOMMENDATIONS

In this last section, the main contributions of this research will be summarized. The advantages as well as the drawbacks of the proposed method of simultaneous network adjustment and strain approximation will be critically discussed. Finally, desirable continuations of this kind of research in the future will be recommended.

- 1) Complex analysis was extensively applied to the mathematical formulation of the two-dimensional strain approximation and the graphical representation of strain-tensor fields. The elegance of this treatment is clearly demonstrated in Section 4, 5 and 6. The question, whether the complex treatment is advantageous as far as computer programming and practical computation are concerned, is somewhat more difficult to answer. Provided that programming languages such as FORTRAN are applied, allowing the use of complex variables, the complex formulation yields transparent and compact program structures. The number of real arithmetic operations which have to be carried out by the computer is the same for both the real or the complex treatment. There is also no difference between the data storage of complex numbers or real two-dimensional vectors. No considerable reduction of computing expenses can therefore be expected from the complex strain analysis as compared to a real approach.

2) The approximation model formulated in this study uses the concept of generalized polynomials. In this way, all types of functions can be prescribed to model the deformation in space and time. The functions discontinuous in space and time are of special importance to the crustal strain approximation in seismically active areas. In this study, the discontinuities in space were only incorporated for translational terms associated with prescribed blocks, bounded by generalized fault lines. This was done in the case of the Hollister network because of the scarcely distributed data in space. The continuity of the strain-field across the fault line is, however, too stringent an assumption. It would certainly be better to let the data tell us what kind of deformation is developing. The masking functions defined for the translational terms (cf. 6.3.2) can easily be extended to model spatially homogeneous or non-homogeneous strain individually in each block. The fact that the estimated variance factor remains rather high in all Hollister approximations suggests that this modeling of discontinuities in the strain-field should also have been tried. Experiments with discontinuous low order terms of the approximation function in space are recommended as a possible continuation of this research. It is to be noted that converging and diverging fault movement will occur in this case.

3) The method of simultaneous network adjustment and strain approximation proposed in this work is to be compared to other analysis techniques presently in use. The following advantages and drawbacks of our method should be considered:



- The complete set of observations available can be utilized, whereas only repeated measurements of the same observable can be used by the observation method (Frank's method).
- Near-simultaneous observations are first separately adjusted by the variation of coordinates. In this way, blunders and outliers among the observations can be detected. The statistical assumptions and the functional model of the network adjustment can be tested. However, the effect of neglected cross-correlations between repeated observations of the same observables and the low degrees of freedom of some epochs limit the value of the statistical assessment of separate position adjustment results.
- Incomplete networks of individual epochs suffering from formulation or configuration defects with respect to positions can be incorporated in the analysis. The conventional coordinate approach does not allow the analysis of such data.
- The approximated strain field is not necessarily assumed to be spatially uniform and the temporal variation of the deformation is not restricted to being linear.
- Strain parameters can simultaneously be estimated with average block translation.
- The method allows the evaluation of the best fitting model (in the least-squares sense) among a series of different approximation models in space and time.
- Nuisance parameters such as corrections to geodetic station heights as well as scale factors and orientation unknowns of individual epochs can be estimated simultaneously with the

deformation parameters.

- 4) The statistical filtering procedure applied has the clear advantage that it enables one to test uncorrelated variables. The significant trend (signal) is so estimated whereas the noise is filtered out from the observations on a prescribed level of significance.
  
- 5) The graphical representation of a strain-tensor field varying in space and in time turned out to be a difficult task. The full information on the pure deformation (symmetric strain tensor) at a given point and at a certain instant of time is completely described by the strain pedal-curve (or strain ellipse). The variation in space is visualized if the strain figures are plotted at equally spaced grid points. In addition, the variation in time is displayed if the patterns of strain figures or strain-rate figures are displayed for a series of equally spaced time intervals. Variations in the development of the deformation in time were easier to interpret from the representations of strain-rates than from accumulated strain. If the strain varies considerably in space, the pattern of strain figures becomes very busy and becomes difficult to interpret. In this case, surfaces or profiles representing the spatial variation of scalar strain quantities such as single strain components or shear in a prescribed direction are preferably plotted. However, scalar strain quantities do not provide the complete information contained in the strain matrix.
  
- 6) It is common geodetic practice to perform pre-analysis of the

network adjustments when geodetic networks are being designed. In this way, various variantes of the network design can be compared and the a priori variance of the unknown coordinates can be determined before the beginning of the actual measurements. Methods are available, by which the design of a network can be optimally chosen with respect to a certain prescribed design criterion.

There is no reason why pre-analyses and optimal design studies should not be carried out before kinematic networks are established. A priori variance estimates of the strain parameters can be computed if the network design of the individual epochs of observation and the time interval between the re-observations of a planned kinematic network are known (cf. Table 8.2, Mod. No.15). The approximation model has, in this case, to be known a priorily. The program package CRUSTRAIN provides a pre-analysis option, by which the a priori confidence regions can be displayed graphically.

- 7) Modern space geodesy techniques will provide accurate three-dimensional relative positions in the future. The method of simultaneous network adjustment and strain approximation should therefore be extended into the third dimension. The elegant complex formulation of the approximation function proposed in this study can not, however, be used in this case.

## LIST OF REFERENCES

- Aeschlimann, H. (1972) 'Der neue Sekundentheodolit KERN DKM2-A'. Vermessung- Photogrammetrie- Kulturtechnik, No. 1-1972.
- Aubert, D. (1959) 'Le décrochement de Pontarlier et l'orogénèse du Jura'. Mémoires de la Société vaudoise des Sciences naturelles, No.76, Vol.12, Fasc. 4.
- Benioff, H. (1964) 'Earthquake Source Mechanisms'. Science Vol.143, No.3613, 1399-1406.
- Bibby, H.M. (1975) 'Crustal Strain from Triangulation in Marlborough, New Zealand'. Tectonophysics 29, 529-540.
- Bibby, H.M. (1982) 'Unbiased Estimate of Strain from Triangulation Data Using the Method of Simultaneous Reduction'. Tectonophysics, Vol.82, 161-174.
- Bjerhammar, A. (1973) 'Theory of Errors and Generalized Matrix Inverses'. New York: Elsevier.
- Bomford, G. (1971) 'Geodesy'. 3rd ed., Oxford: Oxford University Press.
- Brown, R.D. and W.H.K. Lee (1971) 'Active Faults and Preliminary Earthquake Epicenters (1969-70) in the Southern Part of the San Francisco Bay Region'. Map, Menlo Park: U.S. Geological Survey.
- Brunner, F.K. (1979,I) 'On the Analysis of Geodetic Networks for the Determination of the Incremental Strain Tensor'. Survey Review 25, 192, 56-67.
- Brunner, F.K. et al. (1979,II) 'A Comparison of Computation Methods for Crustal Strains from Geodetic Measurements'. XVIIth IUGG General Assembly, Canberra, Australia.
- Brunner, F.K. et al. (1980) 'Investigation of the Significance in Incremental Strain Values near Palmdale, California'. AGU Spring Meeting, Toronto.
- Budden, F.J. (1968) 'Complex Numbers and their Applications'. Math. Topics, London, U.K.: Longman.
- CSTG (1980) 'International Activities of the Commission on International Coordination of Space Techniques for Geodesy and Geodynamics (CSTG)'. Bulletin, May 1, 1980, Dept. of Geodetic Science, Columbus, Ohio.

- Chinnery, M.A. (1961) 'The Deformation of the Ground Around Surface Faults'. Bull. Seism. Soc. Am., Vol.51, No.3, 355-372.
- Chrzanowski, A. et al. (1982,I) 'A General Approach to the Interpretation of Deformation Measurements'. Paper presented at the Centennial Convention of the Canadian Institute of Surveying, Ottawa: April 20-24, 1982.
- Chrzanowski, A. et al. (1982,II) 'On the Analysis of Deformation Surveys'. Paper presented at the Fourth Canadian Symposium on Mining Surveying and Deformation Measurements, Banff: June 7-9, 1982.
- Committee on Geodesy (1978) 'Geodesy: Trends and Prospects'. Assembly of Mathematical and Physical Sciences, U.S. Nat. Research Council, National Geodetic Information Center, Rockville.
- Dermanis, A. (1981) 'Geodetic Estimability of Crustal Deformation Parameters'. Quaterniones Geodaesiae, Vol.2, 159-169.
- Elmiger, A. and C. Siegrist, (1976) 'Praktische Versuche und Erfahrungen mit dem Mekometer'. 7. Internat. Kurs für Ingenieurvermessung, Darmstadt 1976.
- Fischer, W. (1974) 'Rezente Krustenbewegungen in der Schweiz'. Vermessung- Photogrammetrie- Kulturtechnik, Mitteilungsblatt, No.5-1974.
- Fraeijs de Veubeke, B. (1979) 'A Course in Elasticity'. Applied Mathematical Sciences Vol.29, New York: Springer-Verlag.
- Frank, F.C. (1966) 'Deduction of Earth Strains from Survey Data'. Bull. Seism. Soc. Am., Vol.56, No.1, 35-42.
- Grove, E.A. and G. Ladas (1974) 'Introduction to Complex Variables'. Boston: Houghton Mifflin Co.
- Harsh, P.W. and N. Pavoni, (1978) 'Slip on the Paicines Fault'. Bull. Seism. Soc. Am., Vol.68, No.4, 1191-1193.
- Henrici, P. and A. Huber, (1970) 'Analysis'. Vorlesungsskript, Zürich: Verlag des AMIV.
- Henrici, P. (1974) 'Applied and Computational Complex Analysis'. Vol. 1 New York: John Wiley & Sons.
- Henrici, P. and R. Jeltsch (1977) 'Komplexe Analysis für Ingenieure'. Vol.1, 1st ed. Basel, Switzerland: Birkhäuser Verlag.
- Huggett, G.R. et al. (1977) 'Fault Slip Episodes near Hollister, California: Initial Results Using a Multiwavelength Distance-Measuring Instrument'. J. Geophys. Res., Vol.82, No.23,

3361-3368.

- Huggett, G.R. and L.E. Slater (1975) 'Precision Electromagnetic Distance-Measuring Instrument for Determining Secular Strain and Fault Movement'. *Tectonophysics*, Vol.29 (1975), 19-27.
- Jaeger, J.C. (1961) 'Elasticity Fracture and Flow with Engineering and Geological Applications'. New York: John Wiley.
- Jeanrichard, F. (1974) 'Essais de mesure géodésique des mouvements horizontaux de la croûte terrestre'. *Vermessung-Photogrammetrie- Kulturtechnik*, No.3-1974.
- Jeffrey, H. (1970) 'The Earth'. Cambridge: Cambridge University Press.
- Kahle, H.-G. (1980) 'Aktuelle Probleme der Geodäsie und Geodynamik'. *Vermessung- Photogrammetrie- Kulturtechnik*, No. 7-80.
- Kasahara, K. and A. Sugimura (1964) 'Horizontal Secular Deformation of Land Deduced from Retriangulation Data'. *Bull. Earthquake Res. Inst., University of Tokyo, Japan*, Vol.35, 511-530.
- King, N.E. et al. (1980) 'Preseismic and Coseismic Deformation Associated with the Coyote Lake, California, Earthquake'. Report USGS, Menlo Park, Calif..
- Kisslinger, C. et al. (1978) 'Earthquake Precursors'. *Advances in Earth and Planetary Sciences*, Vol.2, Center for Academic Publications, Japan.
- Kovach, R.L. and A. Nur (ed.) (1973) 'Proceedings of the Conference on Tectonic Problems of the San Andreas Fault System'. *Geological Sciences*, Vol.13, Stanford: School of Earth Sciences, Stanford University.
- Krakiwsky, E.J. (1975) 'A Synthesis of Recent Advances in the Method of Least Squares'. Lecture Note No. 42, Fredericton, N.B.: Department of Surveying Engineering, University of New Brunswick.
- Lomnitz, C. (1975) 'Global Tectonics and Earthquake Risk'. *Developments in Geotectonics 5*, Amsterdam: Elsevier.
- Margrave, G.F. and E. Nyland (1980) 'Strain from Repeated Geodetic Surveys by Generalized Inverse Methods'. *Can. J. of Earth Sciences*, Vol.17, No.8, 1020-1030.
- Means, W.D. (1967) 'Stress and Strain: Basic Concepts of Continuum Mechanics for Geologists'. New York: Springer.
- Miller, R.W. et al. (1969) 'Crustal Movement Investigations -

- Triangulation, Taft-Mojave Area, Calif., 1959-60, 1967'. Operational Data Report, C&GS DR 5 and 6, Office of Geodesy and Photogrammetry, Rockville.
- NASA (1979) 'Application of Space Technology to Crustal Dynamics and Earthquake Research'. NASA Technical Paper 1464, Washington.
- NASA (1981) 'NASA Geodynamics Program: Annual Report for 1980'. NASA Technical Memorandum 84010, Washington, D.C.
- Nason, R.D. (1971) 'Investigation of Fault Creep in Northern and Central California'. Ph.D.thesis, San Diego: University of California.
- Niemeier, W. (1979) 'Zur Kongruenz mehrfach beobachteter Geodätischer Netze'. Wiss. Arbeiten der Fachrichtung Vermessungswesen No.88. Hannover: Universität Hannover.
- Pavoni, N. (1973) 'A Structural Model for the San Andreas Fault Zone Along the Northeast Side of the Gabilan Range'. Proc. of the Conference on Tectonic Problems of the San Andreas Fault System. Geological Sciences, Vol.13, 259-267. Stanford: Stanford University.
- Pavoni, N. (1979) 'A Study of Earthquake Focal Mechanisms in the Hollister Area, Southern Coast Ranges, California'. Tectonophysics, Vol.52, 363-371.
- Pavoni, N. (1961) 'Faltung durch Horizontalverschiebung'. Eclogae geol. Helv. 1961, Vol.54, 515-534, Basel 1971.
- Pavoni, N. and J.-P. Schaer (ed.) (1967) 'Kriterien zur Beurteilung der Rolle des Sockels bei der Faltung des Faltenjura'. Etages tectoniques, 307-314, La Baconnière, Neuchâtel.
- Pavoni, N. and E. Peterschmitt (1974) 'Das Erdbeben von Jeurre vom 21.Juni1971 und seine Beziehungen zur Tektonik des Faltenjura'. Approaches to Taphrogenesis, Inter-Union on Geodynamics, Sc.Rep. No.8.
- Pavoni, N. (1982) Personal communication.
- Pelzer, H. (1980) 'Geodätische Netze in Landes- und Ingenieurvermessung'. Stuttgart: Konrad Wittwer.
- Pope, A.J. (1969) 'Strain Analysis of Horizontal Crustal Movements in Alaska based on Triangulation Surveys before and after the Prince William Sound Earthquake of March 27, 1964'. Publication unknown.
- Pope, A.J. (1966) 'Strain Analysis for Repeated Triangulation for the Investigation of Crustal Movement'. M.Sc. Thesis, Columbus,

- U.S.A.: Department of Geodetic Science, The Ohio State University.
- Prescott, W.H. (1976) 'An Extension of Frank's Method for Obtaining Crustal Shear Strains from Survey Data'. Bull. Seism. Soc. Am. 66, 1847-1853.
- Prescott, W.H. et al. (1981) 'Geodetic Measurement of Crustal Deformation on the San Andreas, Hayward, and Calaveras Faults Near San Francisco, California'. J. Geophys. Res., Vol.86, No.B11, 10853-10869.
- Ramsay, J.G. (1967) 'Folding and Fracturing of Rocks'. New York: McGraw Hill.
- Rikitake, T. (1976) 'Earthquake Prediction'. Developments in Solid Earth Geophysics, Vol.9, New York: Elsevier.
- Savage, J.C. and R.O. Burford (1970) 'Accumulation of Tectonic Strain in California'. Bull. Seism. Soc. Am., Vol.60, No.6, 1877-1896.
- Savage, J.C. and R.O. Burford (1971) 'Strain Accumulation along the San Andreas Fault'. Discussion of paper by C.H. Scholz and T.J. Fitch, J. Geophys. Res., Vol. 76, 6469-6479.
- Savage, J.C. and W.H. Prescott (1973) 'Precision Geodolite Distance Measurements for Determining Fault Movements'. J. Geophys. Res. 78, 6001-6008.
- Savage, J.C. and W.H. Prescott (1976) 'Strain Accumulation on the San Jacinto Fault Near Riverside, California'. Bull. Seism. Soc. Am.66, No.5, 1749-1754.
- Savage, J.C. et al. (1976) 'Preseismic and Coseismic Deformation Associated with the Hollister, California, Earthquake of November 28, 1974'. J. Geophys. Res., Vol.81, No.20, 3567-3574.
- Savage, J.C. et al. (1979) 'Geodolite Measurements of Deformation near Hollister, California, 1971-1978'. J. Geophys. Res. 84, 7599-7615.
- Savage, J.C. (1982) Personal communication.
- Schneider, D. (1978) 'Raumnetz Thusis'. Vermessung- Photogrammetrie-Kulturtechnik, No. 4-1978.
- Scholz, C.H. and T.J. Fitch (1969) 'Strain Accumulation along the San Andreas Fault'. J. Geophys. Res., Vol.74, No.27, 6649-6666.
- Schwarz, H.R. et al. (1972) 'Numerik symmetrischer Matrizen'. Stuttgart: Teubner.



- Slater, L.E. and R.O. Burford (1979) 'A Comparison of Long-Baseline Strain Data and Fault Creep Records Obtained near Hollister, California'. *Tectonophysics*, Vol.52, 481-496.
- Slater, L.E. (1981) 'Episodic Block Motion and Convergence along the Calaveras Fault in Central California'. *Tectonophysics*, Vol.71, 87-94.
- Snay, R.A. and M.W. Cline (1980) 'Geodetically Derived Strain at Shelter Cove, California'. *Bull. Seism. Soc. Am.*, Vol.70, No.3, 893-901.
- Sokolnikoff, I.S. (1956) 'Mathematical Theory of Elasticity'. New York: McGraw Hill.
- Spiegel, M.R. (1974) 'Theory and Problems of Complex Variables with an Introduction to Conformal Mapping and its Applications'. Schaum's Outline Series, New York: McGraw Hill.
- Steeves, R.R. (1978) 'A Users Manual for Program GEOPAN, Geodetic Plane Adjustment and Analysis'. Technical Report No.54, Fredericton, N.B.: Department of Surveying Engineering, University of New Brunswick.
- Terada, T. and N. Miyabe (1929) 'Deformation of the Earth's Crust in Kwansai District and its Relation to the Orographic Feature'. *Bull. Earthquake Res. Inst., Univ. of Tokyo, Japan*, Vol.7, 223-241.
- Thapa, K. (1980) 'Strain as a Diagnostic Tool to Identify Inconsistent Observations and Constraints in Horizontal Geodetic Networks'. Technical Report No.68, Fredericton, N.B.: Department of Surveying Engineering, University of New Brunswick.
- Thatcher, W. (1979) 'Horizontal Crustal Deformation from Historic Geodetic Measurements in Southern California'. *J. Geophys. Res.*, 88, 2351-2370.
- Tsuboi, C. (1930) 'A Note on the Analytical Treatments of the Horizontal Deformation of the Earth's Crust'.
- Vaniček, P. and D.E. Wells (1972) 'The Least-Squares Approximation and Related Topics'. Lecture Notes No.22, Fredericton, N.B.: Department of Surveying Engineering, University of New Brunswick.
- Vaniček, P. et al. (1979) 'Four-Dimensional Modeling of Recent Vertical Movements in the Area of the Southern California Uplift'. *Tectonophysics*, 52, 287-300.
- Vaniček, P., K. Thapa and D. Schneider, (1981) 'The Use of Strain to Identify Incompatible Observations and Constraints in Horizontal

- Geodetic Networks'. *Manuscripta geodetica*, Vol. 6, 257-281.
- Vaniček, P. and E. Krakiwsky (1982) 'Geodesy: The Concepts'. Amsterdam: North-Holland.
- Wegener, A. (1929) 'Die Entstehung der Kontinente und Ozeane'. *Die Wissenschaft*, Vol. 66, Braunschweig: Vieweg.
- Wells, D.E. and E. Krakiwsky (1971) 'The Method of Least-Squares'. Lecture Notes No.18, Fredericton, N.B.: Department of Surveying Engineering, University of New Brunswick.
- Welsch, W.M. (1982) 'Finite Element Analysis of Strain Patterns from Geodetic Observations Across a Plate Margin'. IAG Symposium on Recent Crustal Movements and Phenomena Associated with Earthquakes and Volcanism, Tokyo, May 7-20, 1982.
- Whitten, C.A. (1960) 'Horizontal Movements in the Earth's Crust'. *J. Geophys. Res.*, Vol. 65, 2839-2844.
- Whitten, C.A. (1968) 'Geodetic Measurements for the Study of Crustal Movements'. AGU Geophys. Monograph No.12.
- Wolfrum, O. (1978) 'Die Verzerrungseigenschaften der affinen Transformation'. *Allgemeine Vermessungsnachrichten* Vol. 85 (1978), No.10, 367-374.

## APPENDIX I

## NOTATION USED FOR STRAIN-PARAMETERS

position vector:

$$\underline{r} = (x, y)$$

displacement vector:

$$\underline{d} = (u, v,)$$

strain tensors:

$$\underline{E} = \begin{bmatrix} e_{xx} & e_{xy} \\ e_{yx} & e_{yy} \end{bmatrix}$$

... infinitesimal, non-translational strain matrix

$$\underline{\xi} = \begin{bmatrix} e_{xx} & \nu \\ \nu & e_{yy} \end{bmatrix}$$

... non-rotational, symmetric strain tensor

strain components:

$$\sigma = \frac{1}{2} (e_{xx} + e_{yy})$$

... dilation or average extension

$$\omega = \frac{1}{2} (e_{yx} - e_{xy})$$

... average differential rotation

$$\tau = \frac{1}{2} (e_{xx} - e_{yy})$$

... first tensor shear component

$$\nu = \frac{1}{2} (e_{yx} + e_{xy})$$

... second tensor shear component

total shear and principal strains:

$$\gamma_r = (\tau^2 + \nu^2)^{1/2}$$

... total shear

$$\epsilon_{1,2} = \sigma \pm \gamma_r$$

... principal strains

$$\theta_{\epsilon_1} = \arctan\left(\frac{\nu}{\tau}\right)$$

... direction of major principal strain

$$\theta_l = \theta_{\epsilon_1} - \frac{\pi}{4}$$

... direction of maximum shear (left lateral)

$$\alpha_l = \frac{\pi}{2} - \theta_l$$

... azimuth of maximum shear

## APPENDIX II

## OUTLINE OF THE LEAST-SQUARES APPROXIMATION THEORY

This brief outline gives a summary of a more systematic treatment of the theory of least-squares adjustment by Vaníček and Wells (1972). The following problem of least-squares approximation will be discussed. Given a function  $F$ , defined on a finite set  $M$ , find another function of a prescribed general form that represents the given function in a specified way. The approximation function can be expressed as a generalized polynomial,

$$P_n = \sum_{i=1}^n c_i \mathcal{G}_i \quad (\text{A-1})$$

where  $c \in \mathbb{C}$  are the complex coefficients of the polynomial and

$$\underline{\Phi} = \mathcal{G}_1, \mathcal{G}_2, \dots, \mathcal{G}_n \quad (\text{A-2})$$

is the set of the prescribed functions. The individual functions  $\mathcal{G}_i$  may have certain properties depending on the desired approximation. They may be functions of one or  $n$  variables.  $G_M$  is a real vector space comprising the set of all possible functions, with pointwise addition and scalar multiplications, defined on the same set  $M$  as  $F$ . Provided that the functions  $\mathcal{G}_i$  are linearly independent in  $G_M$ ,  $\underline{\Phi}$  is said to be the base or the set of base functions.

For a given  $\underline{\Phi}$ , we must find a set of coefficients  $\{c_i\}$ , so that  $P_n$  will have the smallest distance from the given function  $F$ . The space that the distance will be measured in, is the complex vector space  $G_M$  known as functional space.

Any function

$$\rho(G, H)$$

that maps a two-tuple of function  $G, H$  from the functional space  $G_M$ , into the set of real numbers, is called a metric and can be used to measure the distance, providing it satisfies the axioms for a metric:

- i)  $\rho(G, H) \geq 0$  (non-negativeness)
- ii)  $\rho(G, H) = \rho(H, G)$  (symmetry) (A-3)
- iii)  $\rho(G, H) \leq \rho(G, E) + \rho(E, G)$  (triangle-rule)

where  $G, H, E \in G_M$ .

A norm of a vector space  $V$  is a function  $\|G\| : G \rightarrow \|G\| \in \{V \rightarrow R\}$  that maps the elements of  $G$  of  $V$  to  $R$  and satisfies the axioms,

- i)  $\|G\| \geq 0$
- ii)  $\|\lambda G\| = |\lambda| \cdot \|G\|$  ;  $\lambda \in R$  (A-4)
- iii)  $\|G + H\| \leq \|G\| + \|H\|$  ;  $G, H \in V$

A vector space  $V$  on which a norm is defined is said to be a normed space. The least squares norm is defined as:

$$\|G\| = \sqrt{\sum_{X \in M} W(X) G(X)^2} \in R^+ \quad (A-5)$$

where the real non-negative function  $W$  on  $M$  is known as the weight function.

The scalar product of two functions on the functional space  $G$  is defined as

$$[G, H] = \sum_{X \in M} W(X) G(X) H(X) \quad (A-6)$$

A functional space on which scalar products are defined is known as the Hilbert functional space. If for two functions  $G, H \in G_M$ , the scalar product is zero, they are orthogonal. Similar, if for a set of base

functions  $\underline{\Phi} \in G_M$  the equations

$$[\varphi_i, \varphi_j] = \|\varphi_i\|^2 \cdot \delta_{ij} \quad ; \quad i, j = 1, 2, \dots, n \quad (\text{A-7})$$

(where

$$\delta_{ij} = \begin{cases} 1 & \text{for } i = j \\ 0 & \text{for } i \neq j \end{cases} \quad \dots \text{Kronecker's delta)}$$

are valid, the set is known as an orthogonal set of base functions or a 'base'.

Furthermore, if the norms of all  $\varphi$ 's are

$$[\varphi_i, \varphi_j] = \delta_{ij} \quad ; \quad i, j, = 1, 2, \dots, n \quad (\text{A-8})$$

then the system  $\underline{\Phi}$  is said to be orthonormal. An orthogonal set can always be ortho-normalized, by dividing the individual base functions with their norms. Orthogonality and orthonormality depend on  $\underline{\Phi}$ , M and W. Therefore, we may have orthogonal or orthonormal systems on one M and not on another set M'.

The necessary and sufficient condition for  $\{\varphi_i\}$  to be linearly independent on  $G_M$  (to present an orthogonal base) is

$$\varphi(X) = 0 \quad \text{for all } X \in M, \quad \lambda_i \in \mathbb{R} \quad (\text{A-9})$$

if and only if all the  $\lambda$ 's are equal to zero. In this case, the so called Gram's determinant:

$$g(\underline{\Phi}) = \det [\varphi_i, \varphi_j] = \det \begin{bmatrix} |\varphi_1, \varphi_1| & |\varphi_1, \varphi_2| & \dots & |\varphi_1, \varphi_n| \\ |\varphi_2, \varphi_1| & |\varphi_2, \varphi_2| & \dots & |\varphi_2, \varphi_n| \\ \vdots & \vdots & \ddots & \vdots \\ |\varphi_n, \varphi_1| & |\varphi_n, \varphi_2| & \dots & |\varphi_n, \varphi_n| \end{bmatrix} \quad (\text{A-10})$$

is different from zero. For orthogonal sets of functions it is

$$g(\underline{\Phi}) = \prod_{i=1}^n \|\varphi_i\|^2 \quad (\text{A-11})$$

and for orthonormal functions we have

$$g(\underline{\Phi}) = \prod_{i=1}^n 1 = 1. \quad (\text{A-12})$$

The polynomial  $P_n$  is the best approximating one in the least-squares sense, if its coefficients make the distance

$$\begin{aligned} \rho &= \|F - P_n\| \\ &= \sqrt{\sum_{X \in M} W(X) (F(X) - P_n(X))^2} \end{aligned} \quad (\text{A-13})$$

the minimum. The minimization of the Euclidean distance  $\rho$  yields the normal equations

$$\sum_{i=1}^n |\mathcal{G}_i, \mathcal{G}_j| c = [F, \mathcal{G}_i] \quad ; \quad i=1,2,\dots,n. \quad (\text{A-14})$$

Let

$$\underline{N} = [\mathcal{G}_i, \mathcal{G}_j], \quad (\text{A-15})$$

$$\text{then } g(\underline{\Phi}) = \det(\underline{N}) = \det([\mathcal{G}_i, \mathcal{G}_j]) \quad (\text{A-16})$$

and the solution vector is

$$\hat{c} = \underline{N}^{-1} [F, \underline{\Phi}] \quad (\text{A-17})$$

The matrix  $N$  has an inverse  $N^{-1}$  only if  $g(\underline{\Phi}) \neq 0$ . In the case of an orthogonal base  $\underline{\Phi}$ , it follows

$$\underline{N} = \text{diag}([\mathcal{G}_i, \mathcal{G}_j]) = \text{diag}(\|\mathcal{G}_i\|^2) \quad (\text{A-18})$$

and the system of normal equations takes the form

$$\|\mathcal{G}_i\|^2 \hat{c}_i = [F, \mathcal{G}_i] \quad ; \quad i=1,2,\dots,n \quad (\text{A-19})$$

and the solution is

$$\hat{c}_i = [F, \mathcal{G}_i] / \|\mathcal{G}_i\|^2 \quad ; \quad i=1,2,\dots,n \quad (\text{A-20})$$

In the orthonormal case, the solution degenerates to

$$\hat{c}_i = [F, \mathcal{G}_i] \quad ; \quad i=1,2,\dots,n \quad (\text{A-21})$$

since  $\|\mathcal{G}_i\|^2 = 1$ .

Any system of base functions  $\underline{\Phi}$  defined on  $G_M$  can be transformed into

an orthogonal system of base functions on  $M$  with a certain metrization  $W$  using for instance the Gram-Schmidt orthogonalization process.

This process is defined as follows:

- 1) We chose  $p_i = \mathcal{P}_i$ , and then we define
- 2)  $p_i = \mathcal{P}_i + \sum_{j=1}^{i-1} \alpha_{ij} \cdot p_j$  ;  $i=1,2,\dots,n$  (A-22)

where

$$\alpha_{ij} = - \frac{[\mathcal{P}_i, p_j]}{[p_i, p_j]} .$$

We obtain an orthonormal system by dividing each element  $p_i$  by its norm  $\|p_i\|$ .

The system of normal equations (A-14) can be rewritten as follows:

$$\underline{A}^T \underline{W} \underline{A} \hat{c} = \underline{A}^T \underline{W} \underline{f} \quad (\text{A-23})$$

where:

$$\underline{A} = \begin{bmatrix} \mathcal{P}_1(X_1) & \mathcal{P}_2(X_1) & \dots & \mathcal{P}_n(X_1) \\ \mathcal{P}_1(X_2) & \mathcal{P}_2(X_2) & \dots & \mathcal{P}_n(X_2) \\ \dots & \dots & \dots & \dots \\ \mathcal{P}_1(X_m) & \mathcal{P}_2(X_m) & \dots & \mathcal{P}_n(X_m) \end{bmatrix} \quad \dots \text{ Vandermonde's} \\ \text{matrix}$$

$$\underline{f} = [F(X_1), F(X_2), \dots, F(X_m)]^T$$

$\underline{c}$  ... coefficient vector

$$\underline{W} = \text{diag}(W(X_i)) \quad ; \quad i=1,2,\dots,n .$$

Equation (A-23) can be interpreted as the system of normal equations of a parametric least-squares adjustment. This shows the equivalence of the formulations of approximation and parametric adjustment.

In the case of a unit weight matrix  $\underline{W} = \underline{I}$ , the transformation of (A-23) into an orthonormal solution space by the Gram-Schmidt process (A-22)



can be expressed by the following relations:

$$\begin{aligned}\underline{N} &= \underline{A}^T \underline{A} \\ &= \underline{R}_{ON}^T \underline{S}^T \underline{S} \underline{R}_{ON} \\ &= \underline{R}_{ON}^T \underline{R}_{ON}\end{aligned}\tag{A-24}$$

where:  $\underline{S}$  ... matrix with orthonormal column vectors

$\underline{R}_{ON}$  ... uniquely defined upper triangular matrix

from which follow the normal equations in orthonormal solution space:

$$(\underline{R}_{ON}^{-1})^T \underline{R}_{ON}^T \underline{R}_{ON} \underline{R}_{ON}^{-1} \hat{\underline{c}}_{ON} = (\underline{R}_{ON}^{-1})^T \underline{A}^T \underline{f}\tag{A-25}$$

with the solution:

$$\hat{\underline{c}}_{ON} = (\underline{R}_{ON}^{-1})^T \underline{A}^T \underline{f}\tag{A-26}$$

If the 'observed' values  $\underline{f}$  are not statistically independent,  $\underline{W}$  has non-zero off-diagonal elements. In order to orthogonalize the normal equations  $\underline{N} = \underline{A}^T \underline{W} \underline{A}$  in this more general case,  $\underline{N}$  can be transformed into the quadratic form

$$\underline{N} = \underline{R}_{CH}^T \underline{R}_{CH}\tag{A-27}$$

by the process of Cholesky Decomposition of the symmetric and positive definite matrix  $\underline{N}$  (with  $\dim(\underline{N}) = u$ ) which is defined as follows (Schwarz, et al. 1972):

$$\begin{aligned}n_{ik} &= n_{ik}^{(p-1)} - r_{pi} r_{pk} & i, k &= p+1, p+2, \dots, u \\ & & p &= 1, 2, \dots, u-1\end{aligned}\tag{A-28}$$

where:  $r_{ii} = \sqrt{n_{ii}^{(i-1)}}$   
 $r_{ik} = \frac{n_{ik}^{(i-1)}}{r_{ii}} ; k > 1 .$

With  $r_{ik} = 0$  for  $k > i$ , the coefficients  $r_{ik}$  uniquely define the upper triangular matrix:

$$\underline{R} = \{ r_{ik} \} ; i, k = 1, 2, \dots, u .\tag{A-29}$$

It is interesting to note that the Cholesky decomposition  $\underline{N} = \underline{R}_{CH}^T \underline{R}_{CH}$  is mathematically equivalent to the Gram-Schmidt ortho-normalization of the row vectors of  $\underline{A}$  in (A-24). This will become clear by comparing the two unique processes:

Cholesky Decomposition:

$$\underline{N} = \underline{R}_{CH}^T \underline{R}_{CH}$$

Gram-Schmidt Ortho-normalization:

$$\begin{aligned} \underline{N} &= \underline{A}^T \underline{A} \\ &= \underline{R}_{ON}^T \underline{R}_{ON} \end{aligned}$$

from which follows:

$$\underline{R}_{ON} = \underline{R}_{CH} = \underline{R} \quad (\text{A-30})$$

The transformation (A-25) into orthonormal solution space is therefore found from the Cholesky Decomposition (A-28 , A-29).

## APPENDIX III

## PROGRAM PACKAGE 'CRUSTRAIN'

1) General Concept

'CRUSTRAIN' (=CRUstal STRAIN Analysis) is a software package for the multi-epoch case of the crustal deformation analysis from repeated surveys of horizontal geodetic networks. The software is designed for the analysis of most horizontal kinematic networks. Repeated classical triangulations, pure trilaterations, and all kinds of combined kinematic networks with varying network design can be analyzed.

The analysis procedure is divided into three steps:

- Separate network adjustments
- Complex strain approximation
- Graphical representation of the strain tensor field

The package consists of four main programs, which are based on the theory and mathematical models presented in the first part of this thesis. All programs are written in FORTRAN IV, whereby structured programming techniques are applied. Program CRUSTRAIN and program STRAINPLOT contain interactive program blocks, which enable the user to select the options and parameters of the computation by means of a dialog at the computer terminal. Program CRUSTRAIN provides the results of the analysis in numerical form.

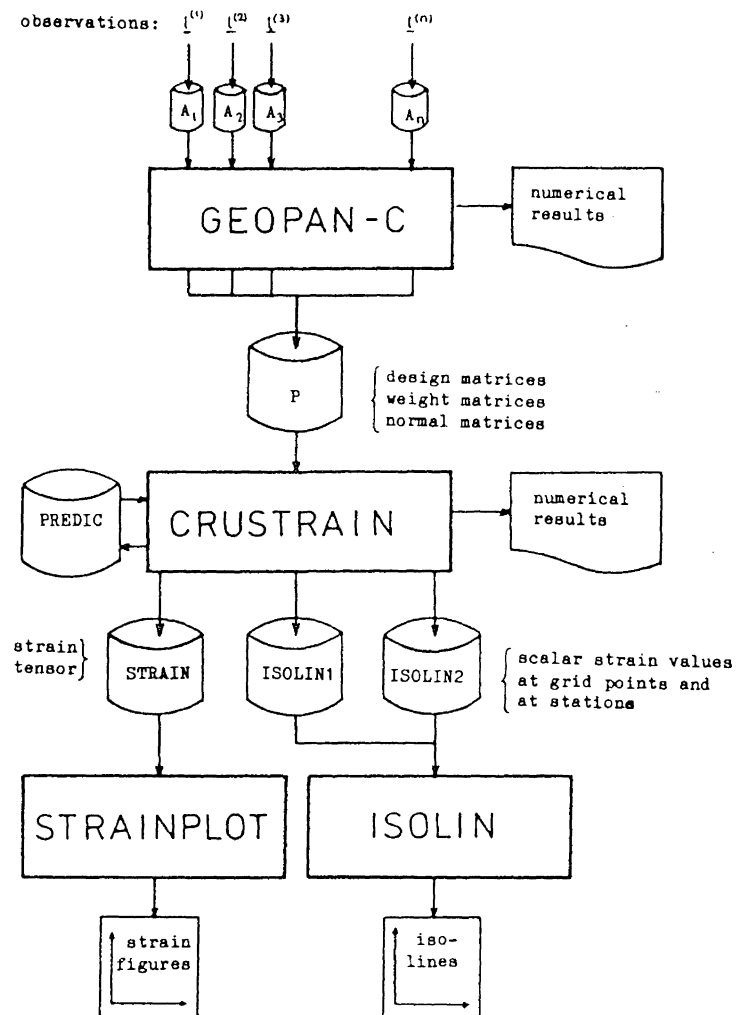


Figure A.1

Program Package 'CRUSTRAIN': Data Flow Diagram

Two plot programs containing standard CALCOMP plotting routines have been written for the graphical representation of the resulting strain-tensor field. The plot software provides the possibility of choosing from a large variety of graphical representations of the strainfield.

The basic concept of the software package and the data flow of the analysis procedure is presented in Fig. A.1 . The following chapters of this section provide short program descriptions of the four main programs. A more comprehensive description can be found in the user's short descriptions provided with the programs.

## 2) Program GEOPAN-C

GEOPAN is a computer program for the network adjustment in the mapping plane by the variation of coordinates. GEOPAN-C is an adapted three dimensional version for the crustal strain analysis. The observation equations, the weight matrix, as well as the normal equations are stored on a permanent file. This data will subsequently be read by the program CRUSTRAIN.

The original program GEOPAN was developed by R.R. Steeves at the University of New Brunswick (Steeves,1978).

|   |                                 |
|---|---------------------------------|
| Program: GEOPAN-C   | Copyright: none                 |
| Author: R.R. Steeves, 1978                                      | Modification: D.Schneider, 1981 |
| Options:  |                                 |
| - adjustment / pre-analysis                                     |                                 |
| - 2-dim. / 3-dim. adjustment                                    |                                 |
| - fixed or weighted stations                                    |                                 |
| - map projection: Transverse Mercator / UTM                     |                                 |
| - statistical tests on the variance factor and on the residuals |                                 |
| - output of various intermediate results                        |                                 |
| Limitations:  |                                 |
| - number of stations  | = 30                            |
| - number of observations  | = 1000                          |
| Library subroutines: none                                       |                                 |
| Estimated program size:   |                                 |
| - program:  | 135 kbyte                       |
| - data:   | 555 kbyte                       |

Table A.1

## Specifications of Program GEOPAN-C

3) Program CRUSTRAIN

This program performs a least-squares approximation of the relative displacement field in space and time.

## A) Approximation:

The user interactively selects the type and degree of the generalized approximation polynomial in space and time. The normal equations of the three-dimensional coordinate adjustment of each epoch are read from a permanent file. The least squares approximation of the relative

displacement field is simultaneously performed with the solution of the network normal equations. The three-dimensional coordinate unknowns with respect to an arbitrarily selected reference time are eliminated from the system of normal equations. Only the normal equations of the approximation coefficients remain. These are subsequently ortho-normalized and solved by the method of Cholesky Decomposition. A statistical filtering procedure selects those ortho-normal coefficients which differ significantly from zero. All remaining coefficients are set to zero. The ortho-normal vector of coefficients is transformed back into the original parameter vector space.

The coordinates at each time of observation are predicted by using the derived coefficients. The observation equations of the network adjustments of each epoch are read and the residuals of the original geodetic observations are computed.

#### B) Prediction:

The analytical description of the relative displacement field in space and time enables us to predict relative displacements and the strain tensor at any point and at any instant of time. The user chooses among various prediction options. Prediction in space is possible at all network stations, at grid points, or at individually chosen locations. In the time domain, regular time intervals or individual instants can be prescribed. Either relative displacement rates and accumulated strain with respect to a reference time or relative velocities and strain rates can be predicted by the program CRUSTRAIN. The predicted

strain quantities with their covariance matrices are stored on a permanent file to be subsequently graphically displayed.

C) Pre-analysis:

The standard deviations of all predicted quantities are computed by the program CRUSTRAIN. A pre-analysis of the strain approximation can be performed if the design and the approximation model of a kinematic network project are known. Only the standard deviations of all strain quantities are predicted in this way. The pre-analysis mode is useful for optimal design studies of kinematic networks.

|                         |   |            |        |
|-------------------------|---|------------|--------|
| Program:                | CRUSTRAIN   | Copyright: | none   |
| Author:                 | D. Schneider, 1981  |            |        |
| Options:                |   |            |        |
| -                       | adjustment / pre-analysis / prediction                    |            |        |
| -                       | estimate strain / relative rigid block translations       |            |        |
| -                       | estimate nuisance parameters for network scale / rotation |            |        |
| -                       | predict strain at grid points                             |            |        |
| -                       | predict relative displacements at block boundaries        |            |        |
| -                       | predict variance of estimated strain quantities           |            |        |
| Limitations:            |   |            |        |
| -                       | number of stations  | =          | 30     |
| -                       | number of observation epochs                              | =          | 50     |
| -                       | number of crustal blocks                                  | =          | 5      |
| -                       | degree of generalized complex polynomial in space         | =          | 2 x 12 |
| -                       | degree of generalized time polynomial                     | =          | 10     |
| Estimated Program Size: |   |            |        |
| -                       | program:  | 64         | kbyte  |
| -                       | data:   | 3015       | kbyte  |

Table A.2

Specifications of Program CRUSTRAIN



#### 4) Program STRAINPLOT

The plot program offers various options of graphically displaying the strain field. The user interactively chooses among the following strain figures:

- principal strains
- strain ellipses
- dilation circles
- shear rosettes
- axes of maximum shear
- strain pedal curves
- rotation sectors

Additional plotting of confidence regions of selected strain quantities can be chosen.

STRAINPLOT was originally developed by K. Thapa at the University of New Brunswick.

|  |                                  |
|--|----------------------------------|
| Program: STRAINPLOT                          | Copyright: none                  |
| Author: K. Thapa                             | Modification: D. Schneider, 1981 |
| Options:                                     |                                  |
| - plot relative displacement vectors         |                                  |
| - plot dilation circles                      |                                  |
| - plot average differential rotation sectors |                                  |
| - plot principal axes of strain              |                                  |
| - plot axes of maximum shear                 |                                  |
| - plot strain ellipses                       |                                  |
| - plot strain pedal curves                   |                                  |
| - plot shear rosettes                        |                                  |
| - plot generalized fault lines               |                                  |
| - plot relative block translation            |                                  |
| - plot confidence regions                    |                                  |
| Limitations:                                 |                                  |
| - number of points = 500                     |                                  |
| Library Subroutines:                         |                                  |
| - CALCOMP plotlib                            |                                  |
| Estimated Program Size:                      |                                  |
| - program and data: 49 kbyte                 |                                  |

Table A.3

## Specifications of Program STRAINPLOT

5) Program ISOLIN

The most appropriate way to display scalar strain quantities, for example, total shear, dilation, or average differential rotations, is to plot iso-lines. Given a discrete scalar function of two variables, ISOLIN interpolates a smooth surface and displays it by lines of equal functional values (iso-lines).

ISOLIN was developed by E. Klingel  at the Institute of Geophysics of ETH Zurich.

|  |                                     |
|--|-------------------------------------|
| Program: ISOLIN  | Copyright: Inst. für Geophysik ETHZ |
| Author: E. Klingelé  | Modification: D. Schneider, 1981    |
| Library Subroutines:<br>- CALCOMP plotlib                          |                                     |
| Estimated Program Size:<br>- Program: 35 kbyte<br>- Data: 85 kbyte |                                     |

Table A.4

Specifications of Program ISOLIN

## APPENDIX IV

A PROOF FOR THE DERIVATION OF THE NORMAL EQUATIONS  
USING GENERALIZED MATRIX INVERSION TECHNIQUES

Any generalized inverse  $\underline{A}^-$  of a matrix  $\underline{A}$  is defined by

$$\underline{A} \underline{A}^- \underline{A} = \underline{A} \quad (\text{A-31})$$

A particular choice among the generalized inverses is the transnormal inverse (Bjerhammar, 1973)

$$\underline{A}_{oi}^- = (\underline{A}^T \underline{A})^- \underline{A}^T. \quad (\text{A-32})$$

Given the equation

$$\underline{A} \underline{x} = \underline{1} \quad (\text{A-33})$$

the solution

$$\begin{aligned} \hat{\underline{x}} &= \underline{A}_{oi}^- \underline{1} \\ &= (\underline{A}^T \underline{A})^- \underline{A}^T \underline{1} \end{aligned} \quad (\text{A-34})$$

minimizes  $(\underline{A} \underline{x} - \underline{1})^T (\underline{A} \underline{x} - \underline{1})$ .

(For a proof see Bjerhammar, 1973.)

On the right-hand side of the normal equations in hypermatrix form (7.22) we encountered the product

$$\underline{N} \underline{N}^- \underline{A} \underline{1} = \underline{A}^T \underline{A} (\underline{A} \underline{A})^- \underline{A}^T \underline{1}. \quad (\text{A-35})$$

(Note: The diagonal matrix  $\underline{C}$  involved in equation (7.22) is here assumed to be the unit matrix.)

From (A-32) it follows

$$\begin{aligned} \underline{N} \underline{N}^- \underline{u} &= \underline{A}^T \underline{A} \underline{A}_{oi}^- \underline{1} \\ &= \underline{A}^T \underline{A}^{\circ} \underline{1} \end{aligned} \quad (\text{A-36})$$

where  $\underline{A}^{\circ} = \underline{A} \underline{A}^-$  is a singular unit matrix for which the following

relations are valid (Bjerhammar, 1973):

$$\underline{A}^{\circ} = (\underline{A}^{\circ})^{\top} \quad (\text{symmetry}) \quad (\text{A-37})$$

$$\underline{A}^{\circ} \underline{A} = \underline{A}$$

This yields

$$\begin{aligned} \underline{N} \underline{N}^{-1} \underline{u} &= \underline{A}^{\top} (\underline{A}^{\circ})^{\top} \underline{1} \\ &= (\underline{A}^{\circ} \underline{A})^{\top} \underline{1} \\ &= \underline{A}^{\top} \underline{1} \end{aligned} \quad (\text{A-38})$$

which means that  $\underline{N} \underline{N}^{-1}$  can be replaced by the unit matrix.

VITA

Candidate's full name: Dieter Schneider

Place and date of birth: Basel (Switzerland), April 28, 1944

Permanent address: c/o Bundesamt für Landestopographie  
CH-3084 Wabern, Switzerland

Schools attended: Elementary School  
Riehen, 1951-1955

Secondary School (Realschule)  
Riehen and Basel, 1955-1960

Professional School for Surveyors  
(Gewerbeschule)  
Zürich, 1960-64

School of Surveying Technology (HTL)  
Basel, 1965-68

Universities attended: Federal Institute of Technology (ETH)  
Zürich, 1972-76  
Diploma (dipl. Ing. ETH)  
Swiss Surveyor's License  
(Patent als Ing.-Geometer)

Publications:

'Interferometrie'. Bericht Nr. 12 aus dem Institut für Geodäsie und  
Photogrammetrie, Eidg. Technische Hochschule (ETHZ), Zürich, 1977.

'Raumnetz Thusis'. Vermessung- Photogrammetrie- Kulturtechnik, No.  
4-1978.

'Erneuerung der Landestriangulation in der Westschweiz, Netz 1. und 2.  
Ordnung 1977' (with H. Chablais). Bundesamt für Landestopographie,  
Wabern, Switzerland, 1979.

'Amtliches Vermessungswesen' (with H. Matthias and P. Kasper). Vol.1:  
Geschichte und Grundlagen (1980), Vol.2: Triangulation 4. Ordnung (in  
press), Sauerländer, Aarau.

'RAUMTRI: Dreidimensionale Netzausgleichung in einem geozentrischen  
kartesischen Koordinatensystem, Programmbeschreibung / Benutzeranlei-  
tung' (with N. Wunderlin). Bericht Nr.45 aus dem Institut für Geodäsie  
und Photogrammetrie, Eidg. Technische Hochschule (ETHZ), Zürich, 1981.

'The Use of Strain to Identify Incompatible Observations and  
Constraints in Horizontal Geodetic Networks' (with P. Vaníček and K.  
Thapa). Manuscripta geodetica, Vol. 6, 257-281, 1981.